

# On the Relation between Surface Profiles and Internal Flow Properties in Long-Wave Models

Philosophiae Doctor Thesis

Amutha Senthilkumar



Department of Mathematics  
University of Bergen  
Norway

January 2017



## Preface

This dissertation is submitted as a partial fulfillment of the requirements for the degree Doctor Philosophy (PhD) at the University of Bergen. The work in this PhD thesis is conducted at the Department of Mathematics, University of Bergen in Norway.

The work on the thesis started in August 2012, and the funding has been provided by The Research Council of Norway through the research project “ 213474/F20 FRINATEK, Nonlinear PDE in Spaces of Analytic Functions ”. The work supervised by Professor Henrik Kalisch from the University of Bergen in Norway.

## Outline

The thesis consists of two parts. Part I is devoted to background theory required for the collection of research papers given in Part II. Part II consists of 4 papers written during the work with the thesis.

## Papers included in this thesis

The following papers are included in the thesis:

**Paper A:** Kalisch, H. and Senthilkumar, A. Derivation of Boussinesq’s Shoaling Law Using a Coupled BBM System. *Nonlin. Processes Geophys.*, 2013, **20**, 213–219. <https://doi.org/10.5194/npg-20-213-2013>.

**Paper B:** Senthilkumar, A. On the Influence of Wave Reflection on Shoaling and Breaking Solitary Waves. *Proceedings of the Estonian Academy of Sciences*, 2016, **65** (4), 414–430. doi: 10.3176/proc.2016.4.06.

**Paper C:** Kalisch, H. and Senthilkumar, A. Particle Trajectories in Non-linear Waves on a Uniform Shear Flow. To be submitted.

**Paper D:** Kalisch, H. and Senthilkumar, A. Wave Breaking in the KdV Equation in a Flow with Constant Vorticity. To be submitted.

## Acknowledgements

I have been at the University of Bergen for more than six years and there are several people who have helped, advised and supported me during those years and I am very thankful to everyone. Firstly I would like to extend my sincere gratitude to my advisor professor Henrik Kalisch for all the help during my master and PhD Studies. His enthusiasm has been a considerable source of my motivation. His inspiring proposals and small pushes along the way is highly acknowledged. Throughout the work he was always ready to guide and give motivational words when needed.

A special thanks to my colleagues and friends at the department of Mathematics who supported me through out this entire progress. I am very grateful for the help and constructive discussions, both scientific and remarkably non-scientific, with Vincent Teyekpiti, Zahra Khorsand, Daulet Moldabayev and Alfatih Ali. I appreciate all our discussion. I would like also to thank my colleagues at the Nonlinear Waves group and Fluid Mechanics group for their time, interest and helpful comments.

I would like to thank the professors at the department of mathematics, University of Bergen, for all the wonderful lessons that they have taught me during the last six years of my education. Furthermore, I want to thank the administration at Mathematics department, University of Bergen. I would like to extend my appreciation to my dissertation committee.

Last but not the least, I would like to thank my family. The constant encouragement and support kept me focused and motivated. I owe my deepest gratitude to my better half for his eternal support, patience and understanding of my goals. I cannot fully express in words my gratitude to my mother Jayamani, whose unconditional love has been my greatest strength of success. The constant love and support of my sisters is surely acknowledged. Finally, I thank my son Rohit for being the joy of my life. He always try to do everything to make his presence felt and has contributed enormously to family's happiness in a special way.

## Abstract

In this work, we investigate the internal velocity field in a number of Boussinesq models in non-uniform situations. A coupled BBM-BBM type system of equations is derived in the assumption of water wave propagating over an uneven bottom. The focus is on formulating mass, momentum and energy densities and fluxes associated with the BBM-BBM system over an uneven bottom. These densities and the associated fluxes arise from establishing mechanical balance equations of the same asymptotic order as the evolution equations.

The BBM-BBM type system derived here is solved numerically by applying a Fourier collocation method coupled with a four stage Runge-Kutta time integration scheme. We look at the propagation of waves over a slope, and how the reconstruction of the flow under the surface is connected with shoaling and wave breaking. The mass conservation equations are used to quantify the role of reflection in the shoaling of solitary waves. Moreover, the principle of conservation of energy is used to develop an equation relating the waveheight and undisturbed depth to the initial undisturbed depth and the incident waveheight. Boussinesq's shoaling law is approximately recovered for waves of very small waveheight. Shoaling and breaking results for the different Boussinesq systems are plotted.

Internal properties of the flow are also in focus in the case of a background shear flow. The Boussinesq -type equations for water waves with constant vorticity are derived in the Boussinesq regime. We reduced the Boussinesq -type equations to the Korteweg-de Vries (KdV) equation in the unidirectional case. We found the approximate velocity field associated with exact solutions of KdV equation including shear flow. The influence of the shear flow on particle trajectories and breaking of surface waves are studied using the approximate velocity field.



# Contents

<b>I General Background</b>	<b>1</b>
<b>1 Introduction</b>	<b>3</b>
1.1 Boussinesq theory . . . . .	3
1.2 Wave shoaling . . . . .	5
1.3 Breaking waves . . . . .	7
<b>2 Boussinesq system over variable bottom</b>	<b>9</b>
2.1 Exact solitary wave solution in the BBM-BBM type system . .	14
2.2 Numerical scheme . . . . .	16
<b>3 Mechanical balance laws in Boussinesq theory</b>	<b>21</b>
3.1 Mass balance . . . . .	23
3.2 Momentum balance . . . . .	25
3.3 Energy balance . . . . .	27
<b>4 Shallow water equations in uniform shear flows</b>	<b>33</b>
4.1 Cnoidal wave solutions . . . . .	36
4.2 Solitary wave solutions . . . . .	38
4.3 Particle trajectories . . . . .	38
4.3.1 Particle trajectories in solitary-wave solutions . . . . .	39
4.3.2 Particle trajectories in periodic-wave solutions . . . . .	42
4.4 Breaking criterion . . . . .	45
4.5 Further work . . . . .	45
<b>Bibliography</b>	<b>47</b>
<b>II Included Papers</b>	<b>53</b>
<b>A Derivation of Boussinesq's Shoaling Law Using a Coupled BBM System</b>	<b>55</b>

<b>B On the Influence of Wave Reflection on Shoaling and Breaking Solitary Waves</b>	<b>63</b>
<b>C Particle Trajectories in Nonlinear Waves on a Uniform Shear Flow</b>	<b>81</b>
<b>D Wave Breaking in the KdV Equation in a Flow with Constant Vorticity</b>	<b>99</b>

# **Part I**

## **General Background**



# Chapter 1

## Introduction

The study of surface water waves is one of the classical problems in fluid mechanics and has practical significance in coastal dynamics. The main contribution in this thesis is the study of long waves propagating on the surface of water over an uneven bottom and on the shear flows over a flat bottom. In some sense, the thesis could be viewed as consisting of two parts. Firstly, we study the propagation of waves over a slope, and how the reconstruction of the flow under the surface is connected with shoaling and wave breaking. Secondly, the modelling of the propagation of the nonlinear water waves on the shear flows over a flat bottom is explored. In addition, we study the influence of the shear flow on particle trajectories and breaking of surface waves.

In this chapter, the fundamentals of Boussinesq-type modelling are introduced and we give an overview of the wave shoaling and wave breaking. In chapter 2, the outline for the derivation of the coupled BBM-BBM type system is given, and the numerical framework that is used in the included papers is presented. In chapter 3, the mechanical balance equations are derived. The last chapter gives a brief derivation of the family of Boussinesq system in the presence of the shear flow.

### 1.1 Boussinesq theory

Airy wave theory done by George Biddell Airy in 1841 [1] is the earliest approximate model to describe the propagation of water waves in shallow regions. The motion of gravity waves on a fluid surface is described by using a velocity potential flow approach in this theory. Airy wave theory is a linear theory and it assumes that the wave propagation only transfers energy in the propagation direction and the effect of dispersion is negligibly small.

However, there is no constraint for the effect of nonlinearity. The Airy wave model performs quite well for the shallow water waves in which the water depth is small compared to the wavelength. This theory was later extended by George Stokes in 1847 [58], to add nonlinear wave motion. However, Stokes' nonlinear theory anticipates that long waves of significant amplitude can not propagate without altering shape.

Russell (1844) [54], paid great consideration to a particular type of wave which is called the solitary wave in his interesting experimental investigations. The solitary waves could travel large distances while maintaining a constant shape and was therefore hard to accept for Airy and Stokes theory. The conflict between Airy's shallow water theory and Russell's observations was resolved by Joseph Boussinesq in 1871 [8, 9], and then again separately by Lord Rayleigh in 1876 [53]. They showed that for appropriate contribution of the vertical acceleration and the assumption of the finite amplitude, the solitary wave could be expressed with the known "sech"-profile. Moreover, they derived Russell's formula for the solitary wave speed however, no equation was given [20]. They showed that the solitary wave form is given as a function of distance  $x$  and time  $t$

$$\eta(x, t) = a \operatorname{sech}^2(k(x - ct)), \quad (1.1)$$

where  $a$  is the maximum wave height,  $c = \sqrt{g(h+a)}$  is the wave speed,  $h$  is the undisturbed depth of water,  $g$  is the acceleration of gravity and the constant  $k$  is defined by

$$k = \sqrt{\frac{3a}{4h^2(h+a)}}.$$

Despite the  $\operatorname{sech}^2$  profile, the solitary wave form is strictly correct only if  $a/h \ll 1$ .

Despite the fact that Boussinesq and Rayleigh both came up with the surface profile (1.1), they did not derive the equation for which (1.1) is a solution. This equation was derived by Korteweg and de Vries in 1895 [36]. Korteweg and de Vries derived a non-linear evolution equation

$$\frac{\partial \eta}{\partial t} = \frac{3}{2} \sqrt{\frac{g}{h}} \frac{\partial}{\partial \chi} \left( \frac{1}{2} \eta^2 + \frac{2}{3} \alpha \eta + \frac{1}{3} \sigma \frac{\partial^2 \eta}{\partial \chi^2} \right), \quad (1.2)$$

where  $\sigma = \frac{1}{3}h^3 - \frac{T_h}{\rho g}$ , governs surface gravity waves of small amplitude, and long wavelength propagating in a shallow water channel. Here  $\alpha$  is a small arbitrary constant related to the uniform motion of the liquid,  $g$  is the gravitation constant,  $\eta$  denotes the free-surface displacement of the wave above equilibrium level ' $h$ ',  $T$  represents the surface tension and  $\rho$  is the density.

The equation (1.2) is called Korteweg-de Vries (KdV) equation, and has permanent wave solutions (see [20]). The solitary wave solution of KdV equation (1.2) is

$$\eta(x, t) = a \operatorname{sech}^2 \left[ \frac{1}{2} \left( \frac{a}{\sigma} \right)^{1/2} \left\{ x - \sqrt{gh} \left( 1 + \frac{1}{2} \frac{a}{h} \right) t \right\} \right]. \quad (1.3)$$

After neglecting surface tension and assuming  $a/h \ll 1$ , the above equation (1.3) agrees with Russell's formula for wave speed  $c$ , which also shows that the wave speed has a form

$$c^2 \sim g(h+a) + O\left(\frac{a}{h}\right),$$

and the constant  $k$  is

$$k \sim \frac{1}{2} \left( \frac{3a}{h^3} \right)^{1/2}.$$

Moreover, this also coincides with the work of Boussinesq and Lord Rayleigh. Hence, Russell's solitary wave is a solution of the KdV equation. For waves of small amplitude and large wave length, the KdV equation was formerly derived for water waves [5].

## 1.2 Wave shoaling

The ocean waves, when they propagate shorewards, experience a decrease in the water depth. Closer to the shore the water waves become affected by the depth of the water, the wave height and especially the wave steepness changes. This particular phenomenon has been studied significantly, which is known as wave shoaling. The shoaling transformation and modeling of solitary wave propagation in shallow water regions is practically essential to the study of impacts of nonlinear waves on shorelines. There are several types of Boussinesq systems [5, 7, 14, 24, 31, 33, 40, 41, 42, 44, 45, 48, 52, 61, 67] available which they have included the effect of smooth and slowly varying bottom topographies in both Boussinesq and shallow water theory.

The wave shoaling is in principle caused by the wave propagation velocity. When the effect of water depth decreases, it will decrease the wave propagation velocity, which will lead to a decrease in the wave length and then the wave steepness increase. In order to maintain the constant energy flux a decrease in group speed must be balanced by an increase in waveheight.

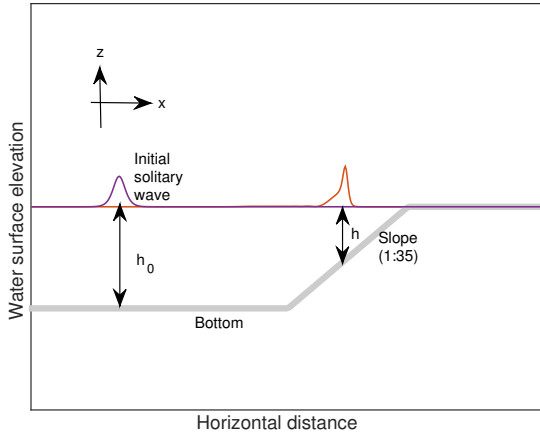


Figure 1.1: Solitary wave propagation over a sloping beach.

There are several theoretical and numerical results [12, 16, 25, 26, 27, 28, 30, 34, 35, 38, 39, 49, 50, 51, 60, 61, 66] attempting to anticipate the waveheight change of shoaling waves. They can be roughly classified as treating either solitary waves or as treating periodic waves oscillating around a mean undisturbed level. There are two classical results in the theory of long wave shoaling namely Boussinesq's law which applies to the shoaling of solitary waves and Green's law which concerns the shoaling of long periodic waves in the linear theory. Boussinesq was concerned with solitary water waves, however, his argument was quite general. In Boussinesq's case, two integral quantities, mass and energy, need to be conserved. Green's law estimates that the wave amplitude change of a long surface periodic wave as it runs up on a bottom slope is proportional to  $h^{-\frac{1}{4}}$ , where  $h$  is the local depth. Miles (1980) [44] noted that the Green's law is a better approximation for larger slopes or sufficiently small waveheight of the incident wave, however, the Boussinesq's shoaling law should be applicable for sufficiently small values of the bottom slope.

The assumption of Boussinesq theory of weakly nonlinear long waves is that the energy content of the wave is unchanged as it propagates. Boussinesq found a simple rule for the wave amplitude change of a long surface wave as it runs up on a bottom slope. Assume the initial undisturbed depth of the fluid is  $h_0$ , the initial wave amplitude is denoted by  $H_0$ , the local depth is  $h$  and the associated local wave amplitude is  $H$ , then Boussinesq's law can be written as  $H/H_0 = h_0/h$ . This Boussinesq shoaling law applies in the context of the so called Boussinesq scaling, where the wave amplitude is small and

the wavelength is long when compared to the initial undisturbed depth.

In the case where the effects on linear dispersion and of nonlinear steepening are approximately balanced, solitary waves could be found and it seems that Boussinesq's law applies primarily to the shoaling of solitary waves.

In papers A and B, numerical solutions of the BBM-BBM type system have been used in shoaling investigations. Theoretical results from Grimshaw [28] showed that for small values of initial waveheight, the shoaling rates exhibit a certain deviation from Boussinesq's law on the evolution of solitary waves over a gently sloping bottom. However, as also confirmed in paper A, the shoaling rates approach Boussinesq's law in the limit of zero waveheight [32]. In addition, the results displayed in paper B indicate that shoaling rates for small amplitude waves are closer to Boussinesq's law for very gentle slopes.

### 1.3 Breaking waves

Wave breaking is also essential in studying coastal area phenomena and for the study of tsunami propagation in nearshore area. Solitary waves are often used to model steep surface waves shoaling on coastal area. The shoaling of solitary waves over sloping bottom is one of the most important mechanisms responsible for wave breaking. As water waves approach the shoreline the wave amplitude grows larger and the wave length and phase velocity decrease. The water wave then collapses onto shore because it becomes too steep for the bottom of the wave to carry. The breaking of water waves mostly depends on wave steepness and beach slope.

Over the past two decades several authors [6, 12, 16, 17, 18, 21, 25, 26, 30, 33, 34, 43, 47, 66, 68] have been developing numerical methods able to deal with wave breaking. In [6], Boussinesq equations have been used to model the bore and derived the onset of breaking waves in bores.

The wave breaking criterion is basically classified into three different categories: namely dynamic, kinematic and geometric based on the characteristics of the wave such as particle velocity and phase speed. The kinematic breaking criterion is used often to predict wave breaking and assigns the onset for the breaking when the horizontal particle velocity at the crest  $U$  proceed the wave phase speed  $c$ . From a mathematical perspective of solitary wave dynamics, if the balance between dispersion and nonlinearity is broken, the solitary wave eventually breaks in shallow water. In the paper B, the kinematic breaking criterion is used to study the wave breaking for the solitary wave solution of the propagation of surface water waves over a slope. In the

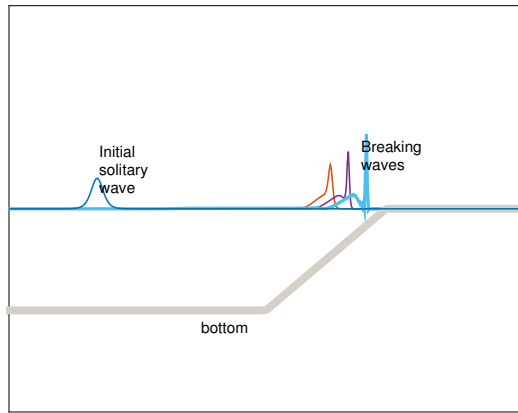


Figure 1.2: Sketch of the typical time evolution of a breaking wave, starting for instance from a solitary wave profile.

paper D, the kinematic breaking criterion is used to study the wave breaking for the solitary wave and cnoidal wave solutions of the nonlinear water waves in the presence of the shear flow.

# Chapter 2

## Boussinesq system over variable bottom

Boussinesq systems have been used in the study of long-wave models for weakly nonlinear surface water waves. The system was first developed by Boussinesq (1872) and it describes surface gravity waves of long wavelength and small amplitude, propagating in a horizontal channel of uniform depth. In [9] the Boussinesq scaling regime was defined and different types of Boussinesq systems have been used in the study of water waves. Boussinesq systems have been considered in the study of a variety of water wave phenomena in many areas because of their straightforwardness.

In the case of even bottom, the Boussinesq systems derived in their general form in [7], may be written in dimensional variables as

$$\begin{aligned} \eta_t + h_0 u_x^\theta + (\eta u^\theta)_x + \frac{1}{2}(\theta^2 - \frac{1}{3})\lambda h_0^3 u_{xxx}^\theta - \frac{1}{2}(\theta^2 - \frac{1}{3})(1 - \lambda)h_0^2 \eta_{xxt} &= 0, \\ u_t^\theta + g\eta_x + u^\theta u_x^\theta + \frac{1}{2}(1 - \theta^2)\mu g h_0^2 \eta_{xxx} &- \frac{1}{2}(1 - \theta^2)(1 - \mu)h_0^2 \tilde{u}_{xxt}^\theta = 0. \end{aligned} \quad (2.1)$$

In the system (2.1),  $t$  represents time, the independent variable  $x$  represents the position,  $u^\theta(x, t)$  represents the horizontal fluid velocity at a height  $0 < \theta h_0 < h_0$ , and  $\eta(x, t)$  describes the surface displacement from the rest position. Moreover  $h_0$  is the undisturbed depth of water and  $g$  denotes the gravitational acceleration.

The coastal surroundings are at the forefront of water wave studies. Many researchers have been interested in models which describe the changes that occur in a solitary wave as it travels over a slowly changing topography. The study of shallow water of uneven bottom in two horizontal dimensions was initiated by Peregrine [52], who used depth-averaged velocity as a de-

pendent variable and derived the system

$$\begin{aligned} \eta_t + \nabla \cdot [(h + \eta)\bar{\mathbf{u}}] &= 0, \\ \bar{\mathbf{u}}_t + \nabla \eta + (\bar{\mathbf{u}} \cdot \nabla) \bar{\mathbf{u}} - \frac{h}{2} \nabla(\nabla \cdot (h\bar{\mathbf{u}}_t)) + \frac{h^2}{6} \nabla(\nabla \cdot (\bar{\mathbf{u}}_t)) &= 0, \end{aligned} \quad (2.2)$$

where

$$\bar{\mathbf{u}} = \frac{1}{h + \eta} \int_{-h}^{\eta} \mathbf{u} dz, \quad (2.3)$$

$\eta = \eta(x, y, t)$  represents the deviation of the free surface from its rest position at time  $t$ ,  $\nabla = (\partial_x, \partial_y)^T$ ,  $\mathbf{u} = \mathbf{u}(x, y, z, t)$  denotes the horizontal velocity of the fluid at some height, while  $\bar{\mathbf{u}}$  denotes the depth-averaged velocity and the bottom is at  $z = -h(x, y)$ .

The Boussinesq equations derived here are the ones which have been used in the papers A (even bottom) and B (uneven bottom) of the thesis. The model system for surface waves propagation over an uneven bottom to be used here belongs to the family of models derived in Mitsotakis [45]. We consider a Cartesian coordinate system  $(x, z)$ , with the  $x$ - axis along the still water level and  $z$ - axis pointing vertically upwards. The fluid domain is bounded by the free surface  $z = \eta(x, t)$  and the sea bed at  $z = -h(x)$ . Then the system of Euler equations for velocity potential flow theory in the presence of a free surface is used. We write down the following system of Euler equations:

$$\Delta\phi = 0, \quad -h < z < \eta, \quad (2.4a)$$

$$\phi_z + h_x \phi_x = 0, \quad z = -h, \quad (2.4b)$$

$$\phi_t + \frac{1}{2} (\phi_x^2 + \phi_z^2) + g\eta = 0, \quad z = \eta, \quad (2.4c)$$

$$\eta_t + \phi_x \eta_x - \phi_z = 0, \quad z = \eta. \quad (2.4d)$$

Consider a characteristic water depth  $h_0$ , a typical wavelength  $l$  and a typical wave amplitude  $a$  and the variables are non-dimensionalized using following scaling:

$$\tilde{x} = \frac{x}{l}, \quad \tilde{z} = \frac{z}{h_0}, \quad \tilde{t} = \frac{\sqrt{gh_0}t}{l}, \quad (2.5a)$$

$$\tilde{h} = \frac{h}{h_0}, \quad \tilde{\eta} = \frac{\eta}{a} \quad \text{and} \quad \tilde{\phi} = \frac{h_0}{al\sqrt{gh_0}}\phi, \quad (2.5b)$$

where the tilde  $\sim$  denotes non-dimensional variables. The standard approach consists of developing the potential  $\phi$  in an asymptotic series and using (2.4a),

write the velocity potential  $\tilde{\phi}$  in the simplest form

$$\begin{aligned}\tilde{\phi} = \tilde{\phi}^{(0)} + \frac{\tilde{z}}{1!} \tilde{\phi}^{(1)} + (-\beta) & \left[ \frac{\tilde{z}^2}{2!} \frac{\partial^2}{\partial \tilde{x}^2} \tilde{\phi}^{(0)} + \frac{\tilde{z}^3}{3!} \frac{\partial^2}{\partial \tilde{x}^2} \tilde{\phi}^{(1)} \right] \\ & + (\beta^2) \left[ \frac{\tilde{z}^4}{4!} \frac{\partial^4}{\partial \tilde{x}^4} \tilde{\phi}^{(0)} + \frac{\tilde{z}^5}{5!} \frac{\partial^4}{\partial \tilde{x}^4} \tilde{\phi}^{(1)} \right] + \mathcal{O}(\beta^3),\end{aligned}\quad (2.6)$$

which is a series solution with only two unknown functions  $\tilde{\phi}^{(0)}$  and  $\tilde{\phi}^{(1)}$ . Next the velocity field can be expressed as

$$\begin{aligned}\tilde{u}(\tilde{x}, \tilde{z}, \tilde{t}) = \hat{u} + \beta & \left[ \frac{\tilde{z}}{1!} \hat{w}_{\tilde{x}} - \frac{\tilde{z}^2}{2!} \hat{u}_{\tilde{x}\tilde{x}} \right] \\ & + \beta^2 \left[ -\frac{\tilde{z}^3}{3!} \hat{w}_{\tilde{x}\tilde{x}\tilde{x}} + \frac{\tilde{z}^4}{4!} \hat{u}_{\tilde{x}\tilde{x}\tilde{x}\tilde{x}} \right] + \mathcal{O}(\beta^3),\end{aligned}\quad (2.7a)$$

$$\tilde{w}(\tilde{x}, \tilde{z}, \tilde{t}) = \beta [\hat{w} - \tilde{z} \hat{u}_{\tilde{x}}] + \beta^2 \left[ \frac{-\tilde{z}^2}{2!} \hat{w}_{\tilde{x}\tilde{x}} + \frac{\tilde{z}^3}{3!} \hat{u}_{\tilde{x}\tilde{x}\tilde{x}} \right] + \mathcal{O}(\beta^3), \quad (2.7b)$$

where  $\hat{u}$  and  $\hat{w}$  are the velocities at  $\tilde{z} = 0$ , and given by  $\hat{u} = \tilde{\phi}_{\tilde{x}}^{(0)}$  and  $\hat{w} = (1/\beta)\tilde{\phi}^{(1)}$ .

Use the bottom kinematic boundary condition (2.4b) to obtain the relation between  $\hat{u}$  and  $\hat{w}$  which has the following form after substituting the above asymptotic expressions:

$$\hat{w} = -(\tilde{h}\hat{u})_{\tilde{x}} + \beta \frac{\partial}{\partial \tilde{x}} \left( \frac{\tilde{h}^3}{3!} \hat{u}_{\tilde{x}\tilde{x}} - \frac{\tilde{h}^2}{2!} (\tilde{h}\hat{u})_{\tilde{x}\tilde{x}} \right) + \mathcal{O}(\beta^2). \quad (2.8)$$

Now insert (2.6), (2.7) and (2.8) into the free surface boundary conditions (2.4c) and (2.4d) to derive the following Boussinesq system with variable bottom

$$\hat{u}_t + \tilde{\eta}_{\tilde{x}} + \alpha \hat{u} \hat{u}_{\tilde{x}} = \mathcal{O}(\alpha\beta, \beta^2), \quad (2.9a)$$

$$\tilde{\eta}_{\tilde{t}} + \left( \alpha \tilde{\eta} \hat{u} + \tilde{h} \hat{u} \right)_{\tilde{x}} - \beta \frac{\partial}{\partial \tilde{x}} \left( \frac{\tilde{h}^3}{3!} \hat{u}_{\tilde{x}\tilde{x}} - \frac{\tilde{h}^2}{2!} (\tilde{h}\hat{u})_{\tilde{x}\tilde{x}} \right) = \mathcal{O}(\alpha\beta, \beta^2). \quad (2.9b)$$

It is accentuated that from the above system, and in terms of  $\hat{u}$ , we can extend the system in terms of other velocity variables such as the velocity at an arbitrary  $z$  location. Specify a new velocity variable  $\tilde{u}^\theta$  defined at an arbitrary water level  $\tilde{z}^\theta = -\tilde{h} + \theta(\alpha\tilde{\eta} + \tilde{h})$ , with  $0 \leq \theta \leq 1$ . Applying the standard techniques of inversion to derive the following expression as an

asymptotic formula for  $\hat{u}$  in terms of  $\tilde{u}^\theta$ :

$$\begin{aligned}
\hat{u} &= \tilde{u}^\theta + \beta \left( \tilde{h}(\theta - 1)(\tilde{h}\tilde{u}^\theta)_{\tilde{x}\tilde{x}} + (\tilde{h}(\theta - 1))^2 \frac{1}{2!} (\tilde{u}^\theta)_{\tilde{x}\tilde{x}} \right) \\
&+ \alpha\beta \left( \tilde{\eta}\theta(\tilde{h}\tilde{u}^\theta)_{\tilde{x}\tilde{x}} + \tilde{h}(\theta - 1)\theta\tilde{\eta}(\tilde{u}^\theta)_{\tilde{x}\tilde{x}} \right) \\
&- \beta^2 \tilde{h}(\theta - 1) \left( \frac{\tilde{h}^3}{3!} \tilde{u}_{\tilde{x}\tilde{x}}^\theta - \frac{\tilde{h}^2}{2!} (\tilde{h}\tilde{u}^\theta)_{\tilde{x}\tilde{x}} \right)_{\tilde{x}\tilde{x}} \\
&- \beta^2 \left( \frac{(\tilde{h}(\theta - 1))^3}{3!} (\tilde{h}\tilde{u}^\theta)_{\tilde{x}\tilde{x}\tilde{x}\tilde{x}} + \frac{(\tilde{h}(\theta - 1))^4}{4!} (\tilde{u}^\theta)_{\tilde{x}\tilde{x}\tilde{x}\tilde{x}} \right) \\
&+ \beta^2 \left( \tilde{h}(\theta - 1)(\tilde{h}\tilde{u}^\theta)_{\tilde{x}\tilde{x}} + (\tilde{h}(\theta - 1))^2 \frac{1}{2!} (\tilde{u}^\theta)_{\tilde{x}\tilde{x}} \right)^2 + \mathcal{O}(\beta^3). \quad (2.10)
\end{aligned}$$

Then the velocity field can be expressed in terms of  $\tilde{u}^\theta$  as

$$\begin{aligned}
\tilde{u} &= \tilde{u}^\theta + \beta \left( \tilde{h}(\theta - 1)(\tilde{h}\tilde{u}^\theta)_{\tilde{x}\tilde{x}} + (\tilde{h}(\theta - 1))^2 \frac{1}{2!} (\tilde{u}^\theta)_{\tilde{x}\tilde{x}} \right) \\
&+ \alpha\beta \left( \tilde{\eta}\theta(\tilde{h}\tilde{u}^\theta)_{\tilde{x}\tilde{x}} + (\tilde{h}(\theta - 1)\theta\tilde{\eta})(\tilde{u}^\theta)_{\tilde{x}\tilde{x}} \right) - \beta^2 \tilde{h}(\theta - 1) \left( \frac{\tilde{h}^3}{3!} \tilde{u}_{\tilde{x}\tilde{x}}^\theta - \frac{\tilde{h}^2}{2!} (\tilde{h}\tilde{u}^\theta)_{\tilde{x}\tilde{x}} \right)_{\tilde{x}\tilde{x}} \\
&- \beta^2 \left( \frac{(\tilde{h}(\theta - 1))^3}{3!} (\tilde{h}\tilde{u}^\theta)_{\tilde{x}\tilde{x}\tilde{x}\tilde{x}} + \frac{(\tilde{h}(\theta - 1))^4}{4!} (\tilde{u}^\theta)_{\tilde{x}\tilde{x}\tilde{x}\tilde{x}} \right) \\
&+ \beta^2 \left( \tilde{h}(\theta - 1)(\tilde{h}\tilde{u}^\theta)_{\tilde{x}\tilde{x}} + (\tilde{h}(\theta - 1))^2 \frac{1}{2!} (\tilde{u}^\theta)_{\tilde{x}\tilde{x}} \right)^2 + \beta^2 \frac{\tilde{z}}{1!} \left( \frac{\tilde{h}^3}{3!} \tilde{u}_{\tilde{x}\tilde{x}}^\theta - \frac{\tilde{h}^2}{2!} (\tilde{h}\tilde{u}^\theta)_{\tilde{x}\tilde{x}} \right)_{\tilde{x}\tilde{x}} \\
&+ \beta \left[ \frac{\tilde{z}}{1!} (-\tilde{h}\tilde{u}^\theta)_{\tilde{x}\tilde{x}} - \frac{\tilde{z}^2}{2!} \tilde{u}_{\tilde{x}\tilde{x}}^\theta \right] + \beta^2 \left[ \frac{\tilde{z}^3}{3!} (\tilde{h}\tilde{u}^\theta)_{\tilde{x}\tilde{x}\tilde{x}\tilde{x}} + \frac{\tilde{z}^4}{4!} \tilde{u}_{\tilde{x}\tilde{x}\tilde{x}\tilde{x}}^\theta \right] \\
&+ \beta^2 \left[ -\frac{\tilde{z}}{1!} \left\{ \tilde{h} \left( \tilde{h}(\theta - 1)(\tilde{h}\tilde{u}^\theta)_{\tilde{x}\tilde{x}} + (\tilde{h}(\theta - 1))^2 \frac{1}{2!} (\tilde{u}^\theta)_{\tilde{x}\tilde{x}} \right) \right\}_{\tilde{x}\tilde{x}} \right] \\
&+ \beta^2 \left[ -\frac{\tilde{z}^2}{2!} \left( \tilde{h}(\theta - 1)(\tilde{h}\tilde{u}^\theta)_{\tilde{x}\tilde{x}} + (\tilde{h}(\theta - 1))^2 \frac{1}{2!} (\tilde{u}^\theta)_{\tilde{x}\tilde{x}} \right)_{\tilde{x}\tilde{x}} \right] + \mathcal{O}(\beta^3, \alpha\beta^2), \\
\tilde{w} &= \beta \left[ -(\tilde{h}\tilde{u}^\theta)_{\tilde{x}} - \tilde{z}\tilde{u}_{\tilde{x}}^\theta \right] - \beta^2 \left\{ \tilde{h} \left( \tilde{h}(\theta - 1)(\tilde{h}\tilde{u}^\theta)_{\tilde{x}\tilde{x}} + (\tilde{h}(\theta - 1))^2 \frac{1}{2!} (\tilde{u}^\theta)_{\tilde{x}\tilde{x}} \right) \right\}_{\tilde{x}} \\
&+ \beta^2 \left( \frac{\tilde{h}^3}{3!} \tilde{u}_{\tilde{x}\tilde{x}}^\theta - \frac{\tilde{h}^2}{2!} (\tilde{h}\tilde{u}^\theta)_{\tilde{x}\tilde{x}} \right)_{\tilde{x}} + \beta^2 \left[ -\frac{\tilde{z}^2}{2!} (-\tilde{h}\tilde{u}^\theta)_{\tilde{x}\tilde{x}\tilde{x}} + \frac{\tilde{z}^3}{3!} \tilde{u}_{\tilde{x}\tilde{x}\tilde{x}}^\theta \right] \\
&- \beta^2 \tilde{z} \left( \tilde{h}(\theta - 1)(\tilde{h}\tilde{u}^\theta)_{\tilde{x}\tilde{x}} + (\tilde{h}(\theta - 1))^2 \frac{1}{2!} (\tilde{u}^\theta)_{\tilde{x}\tilde{x}} \right)_{\tilde{x}} + \mathcal{O}(\beta^3, \alpha\beta^2).
\end{aligned}$$

Switching to the variable  $\tilde{u}^\theta$  yields the following system:

$$\begin{aligned} \tilde{u}_t^\theta + \tilde{\eta}_{\tilde{x}} + \alpha \tilde{u}^\theta \tilde{u}_{\tilde{x}}^\theta \\ + \beta \left[ (\theta - 1) \tilde{h} (\tilde{h} \tilde{u}_t^\theta)_{\tilde{x}\tilde{x}} + \frac{\tilde{h}^2}{2!} (\theta - 1)^2 \tilde{u}_{\tilde{x}\tilde{x}\tilde{t}}^\theta \right] = \mathcal{O}(\alpha\beta, \beta^2) \end{aligned} \quad (2.12)$$

$$\begin{aligned} \tilde{\eta}_{\tilde{t}} + \left( \alpha \tilde{\eta} \tilde{u}^\theta + \tilde{h} \tilde{u}^\theta \right)_{\tilde{x}} \\ + \beta \frac{\partial}{\partial \tilde{x}} \left[ (\theta - \frac{1}{2}) \tilde{h}^2 (\tilde{h} \tilde{u}^\theta)_{\tilde{x}\tilde{x}} + \tilde{h}^3 (\frac{(\theta-1)^2}{2} - \frac{1}{6}) (\tilde{u}^\theta)_{\tilde{x}\tilde{x}} \right] = \mathcal{O}(\alpha\beta, \beta^2) \end{aligned} \quad (2.13)$$

From these equations we obtain

$$\tilde{\eta}_{\tilde{t}} = - \left( \tilde{h} \tilde{u}^\theta \right)_{\tilde{x}} + \mathcal{O}(\alpha, \beta), \quad \tilde{u}_t^\theta = - \tilde{\eta}_{\tilde{x}} + \mathcal{O}(\alpha, \beta). \quad (2.14)$$

For arbitrary  $\mu, \nu \in \mathbb{R}$  and using (2.14), the following equations are derived

$$(\tilde{h} \tilde{u}^\theta)_{\tilde{x}\tilde{x}} = \mu (\tilde{h} \tilde{u}^\theta)_{\tilde{x}\tilde{x}} - (1 - \mu) \tilde{\eta}_{\tilde{t}\tilde{x}} + \mathcal{O}(\alpha, \beta), \quad (2.15a)$$

$$\tilde{u}_{\tilde{t}\tilde{x}\tilde{x}}^\theta = (1 - \nu) \tilde{u}_{\tilde{t}\tilde{x}\tilde{x}}^\theta - \nu \tilde{\eta}_{\tilde{x}\tilde{x}\tilde{x}} + \mathcal{O}(\alpha, \beta). \quad (2.15b)$$

Using equations (2.9)-(2.15) and appropriate mathematical expansions, the following system is derived:

$$\begin{aligned} \tilde{u}_t^\theta + \tilde{\eta}_{\tilde{x}} + \alpha \tilde{u}^\theta \tilde{u}_{\tilde{x}}^\theta + \beta \left\{ B \tilde{h} \left[ (\tilde{h}_{\tilde{x}} \tilde{\eta}_{\tilde{x}})_{\tilde{x}} + \tilde{h}_{\tilde{x}} \tilde{\eta}_{\tilde{x}\tilde{x}} \right] \right. \\ \left. + c \tilde{h}^2 \tilde{\eta}_{\tilde{x}\tilde{x}\tilde{x}} - d \tilde{h}^2 \tilde{u}_{\tilde{x}\tilde{x}\tilde{t}}^\theta \right\} = \mathcal{O}(\alpha\beta, \beta^2), \end{aligned} \quad (2.16a)$$

$$\begin{aligned} \tilde{\eta}_{\tilde{t}} + \left( \alpha \tilde{\eta} \tilde{u}^\theta + \tilde{h} \tilde{u}^\theta \right)_{\tilde{x}} + \beta \frac{\partial}{\partial \tilde{x}} \left\{ A \tilde{h}^2 \left[ (\tilde{h}_{\tilde{x}} \tilde{u}^\theta)_{\tilde{x}} + \tilde{h}_{\tilde{x}} \tilde{u}_{\tilde{x}}^\theta \right] \right. \\ \left. + a \tilde{h}^2 (\tilde{h} \tilde{u}^\theta)_{\tilde{x}\tilde{x}} - b \tilde{h}^2 \tilde{\eta}_{\tilde{x}\tilde{t}} \right\} = \mathcal{O}(\alpha\beta, \beta^2). \end{aligned} \quad (2.16b)$$

It is noted that the parameters  $a, b, c$  and  $d$  are those of the class of Boussinesq system derived in [7], where

$$\begin{aligned} A &= \frac{1}{2} \left[ \frac{1}{3} - (\theta - 1)^2 \right], & B &= 1 - \theta, \\ a &= \frac{1}{2} \left( \theta^2 - \frac{1}{3} \right) \mu, & b &= \frac{1}{2} \left( \theta^2 - \frac{1}{3} \right) (1 - \mu), \\ c &= \frac{1}{2} (1 - \theta^2) \nu, & d &= \frac{1}{2} (1 - \theta^2) (1 - \nu). \end{aligned} \quad (2.17)$$

Assuming a constant depth  $h$ , the above system reduces to the original coupled BBM system derived in [7]. By choosing  $\mu = 0$  and  $\nu = 0$ , the coupled

BBM-BBM type system is derived from (2.16). Neglecting terms of order  $\mathcal{O}(\alpha\beta, \beta^2)$  and dropping the superscript  $\theta$ , the system takes the following form in dimensional variables

$$u_t + g\eta_x + uu_x + 2Bghh_x\eta_{xx} + Bghh_{xx}\eta_x - dh^2u_{xxt} = 0, \quad (2.18a)$$

$$\eta_t + (\eta u + hu)_x + \frac{\partial}{\partial x} \left\{ 2Ah^2h_xu_x + Ah^2h_{xx}u - bh^2\eta_{xt} \right\} = 0. \quad (2.18b)$$

## 2.1 Exact solitary wave solution in the BBM-BBM type system

Boussinesq systems have exact solitary wave solutions under some parameter conditions. Boussinesq was the first who gave a scientific explanation of the existence of traveling wave solutions. In this section, we derive the exact solitary wave solutions following an approach formulated recently in [13]. For the case of constant water depth  $h = h_0$ , the system takes the following form in dimensional variables

$$u_t + g\eta_x + uu_x - \frac{1}{2}(1 - \theta^2)h_0^2u_{xxt} = 0, \quad (2.19a)$$

$$\eta_t + (\eta u + h_0u)_x - \frac{1}{2}\left(\theta^2 - \frac{1}{3}\right)h_0^2\eta_{xxt} = 0. \quad (2.19b)$$

We consider the solutions depending only on the moving coordinate  $\xi = x - x_0 - c_s t$  as

$$\eta(x, t) = \eta(x - x_0 - c_s t) = \eta(\xi), \quad (2.20a)$$

$$u(x, t) = u(x - x_0 - c_s t) = u(\xi). \quad (2.20b)$$

It shows that the traveling-waves initially centered at  $x_0$  propagate with steady velocity  $c_s$ . Using (2.20) and (2.19), we obtain the third order nonlinear system of ordinary differential equations

$$-c_s u' + g\eta' + uu' + c_s \frac{1}{2}(1 - \theta^2)h_0^2 u''' = 0, \quad (2.21a)$$

$$-c_s \eta' + (\eta u + h_0u)' + c_s \frac{1}{2}\left(\theta^2 - \frac{1}{3}\right)h_0^2 \eta''' = 0, \quad (2.21b)$$

where the derivatives are executed with respect to the  $\xi$  coordinate. It is worth mentioning that the solitary wave solutions are localized in space. Hence the solution and its derivatives with respect to the  $\xi$  coordinate at long distance from the pulse are remarkably small and vanish asymptotically.

Integrating once with respect to the  $\xi$  coordinate and using zero boundary conditions at infinity, it follows that

$$-c_s u + g\eta + \frac{1}{2}u^2 + c_s \frac{1}{2}(1 - \theta^2) h_0^2 u'' = 0, \quad (2.22a)$$

$$-c_s \eta + (\eta u + h_0 u) + c_s \frac{1}{2} \left( \theta^2 - \frac{1}{3} \right) h_0^2 \eta'' = 0. \quad (2.22b)$$

Now we seeking functions  $\eta(\xi)$  and  $u(\xi)$  that are proportional

$$u(\xi) = A\eta(\xi). \quad (2.23)$$

Use the relation (2.23) and multiply equation (2.22b) by  $A$ , to have

$$-c_s A\eta + g\eta + \frac{A}{2}\eta^2 + c_s \frac{1}{2}(1 - \theta^2) h_0^2 A\eta'' = 0, \quad (2.24a)$$

$$-\frac{A}{2}c_s \eta + \frac{A^2}{2}\eta h_0 + \frac{A}{2}\eta^2 + c_s \frac{A}{4} \left( \theta^2 - \frac{1}{3} \right) h_0^2 \eta'' = 0. \quad (2.24b)$$

If the equations (2.24a) and (2.24b) are identical, then the system (2.19) has nontrivial solitary-wave solutions

$$-\frac{A}{2}c_s + \frac{A^2}{2}h_0 = -c_s A + g, \quad (2.25a)$$

$$c_s \frac{1}{2}(1 - \theta^2) h_0^2 A = c_s \frac{A}{4} \left( \theta^2 - \frac{1}{3} \right) h_0^2. \quad (2.25b)$$

The unique solution of the system (2.19) is given by

$$g = \frac{A^2}{2}h_0 + \frac{A}{2}c_s, \quad (2.26)$$

$$\theta^2 = \frac{7}{9}. \quad (2.27)$$

From (2.24a), (2.24b) and (2.25), we immediately find that the function  $\eta(\xi)$  satisfies

$$\frac{d\eta}{\eta \sqrt{\frac{-A}{3}\eta + \frac{c_s - Ah_0}{2}}} = \frac{3}{h_0 \sqrt{c_s}} d\xi. \quad (2.28)$$

It is easy to find that equation (2.28) has exact solitary wave solutions of the form

$$\eta(x, t) = \eta_0 \operatorname{sech}^2(\kappa_0(x - x_0 - c_s t)), \quad (2.29)$$

and the constants  $c_s$  and  $\kappa_0$  are given by

$$c_s = \frac{3h_0 + 2\eta_0}{\sqrt{3h_0(\eta_0 + 3h_0)}} \sqrt{gh_0} \quad \text{and} \quad \kappa_0 = \frac{3}{2h_0} \sqrt{\frac{\eta_0}{2\eta_0 + 3h_0}},$$

where  $h_0$  is the undisturbed depth and  $\eta_0$  is the wave amplitude. The horizontal velocity  $u(x, t)$  is given by

$$u(x, t) = W_0 \operatorname{sech}^2(\kappa_0(x - x_0 - c_s t)), \quad (2.30)$$

where

$$W_0 = A\eta_0 = \sqrt{\frac{3g}{3h_0 + \eta_0}} \eta_0. \quad (2.31)$$

The BBM-BBM type Boussinesq system (2.18) has been used in the papers A and B. In those papers, solitary wave solutions, like ( 2.29) and ( 2.30), have been used to confirm our numerical implementation, and especially to confirm the rate of convergence of the numerical scheme.

## 2.2 Numerical scheme

When attempting to solve partial differential equations (PDEs), it is not always possible to obtain analytical solution. Alternatively, a numerical method must be used to find an approximate solution. There are several numerical simulation methods to solve PDEs. The right method to choose depends on the properties of the model equations and the characters are required in the approximate solution. The most commonly used methods for numerically solving PDEs are the finite element method (FEM), finite difference method (FDM), and spectral method.

The FEM uses variational formulation to approximate the differential equation and then seek a solution in a finite dimensional space which normally consists of locally supported piecewise linear functions. However, the convergence of this method is not always sufficient.

The FDM on the other hand, replaces the derivatives appearing in the differential equations with finite difference approximations in terms of discrete quantities of dependent and independent variables. This procedure results in a system of equation of the variable at nodal points for the entire domain which is easily solved for one-dimensional domains. However, the accuracy is in general not good.

In contrast, the spectral method approximates the solution as linear combination of continuous functions that are generally non-zero over the domain of the solution. It has excellent error properties in the form of an

exponential convergence rate. Hence the spectral method takes on a global approach while the finite element method is a local approach. The convergence rate of spectral approximations depends only on the smoothness of the solution, which gives the ability to achieve high precision with a small number of materials. When compared to FEM and FDM, spectral methods have been used widely for the numerical solution of PDEs due to their better accuracy. The following introduction of spectral methods is based on the book by Trefethen [63] and paper by Hussaini, Kopriva and Patera [29].

We consider spectral collocation method for the solution of our given BBM-BBM system which are characterized by the expansion of the solution in terms of global basis functions. This method form an efficient and highly accurate class of techniques for the solution. The expansion coefficients are computed so that the differential equation is satisfied exactly at a set of collocation points. We approximate the solution  $u(x)$  by a sum of  $(N+1)$  basis functions  $\phi_i(x)$  that span the space where the approximate solution exists

$$u(x) \approx u_N(x) = \sum_{i=0}^N \hat{u}_i \phi_i(x), \quad (2.32)$$

where  $\phi_j$ ,  $j = 0,..N$  is a finite set of trial functions. This series is then substituted into the differential equation

$$\begin{cases} Lu(x) = f(x) & \text{if } x \in V, \\ Bu(y) = 0 & \text{if } y \in \partial V. \end{cases} \quad (2.33)$$

Here  $L$  is a spatial differential operator,  $B$  is a linear boundary operator and  $V$  is a spatial domain with boundary  $\partial V$ . We seek the numerical solution  $u_N(x)$  with the coefficients  $\hat{u}_i$  such that the residual  $R$  defined by

$$R(x) = Lu_N(x) - f(x),$$

is minimized. To minimize the residual  $R$ , we choose a set of test functions  $\chi_n = \delta(x - x_n)$ ,  $n = 0, 1, 2, ...N$  and demand that

$$(\chi_n, R) = 0 = Lu_N(x_n) - s(x_n), \text{ for } n = 0, 1, 2, ...N, \quad (2.34)$$

where the  $x_n$  ( $n=0,1,2,...N$ ) are the spacial points, called the collocation points. That is

$$\sum_{i=0}^N \hat{u}_i L\phi_i(x_n) - f(x_n) = 0, \quad n = 0, 1, ...N.$$

The unknown  $N+1$  coefficients  $\hat{u}_i$  are determined by using  $N+1$  equations which gives the approximated solution  $u_N$  in the nodes  $x_i$ .

The system (2.18) has been solved numerically using a Fourier collocation method coupled with a 4-stage Runge-Kutta time integration scheme. For our numerical computations, we assume periodic boundary conditions on the domain  $[0, L]$  and the problem is translated to the interval  $[0, 2\pi]$  using the suitable scaling  $u(\lambda x, t) = v(x, t)$ ,  $\eta(\lambda x, t) = \xi(x, t)$  and  $h(\lambda x) = h_1(x)$ , where  $\lambda = \frac{L}{2\pi}$ . Then the BBM-BBM system (2.18) becomes

$$\begin{aligned} & \lambda^3 v_t + \lambda^2 g \xi_x + \lambda^2 v v_x + 2Bgh_1 h_{1x} \xi_{xx} \\ & + Bgh_1 h_{1xx} \xi_x - \lambda d h_1^2 v_{xxt} = 0, \quad x \in [0, 2\pi], \\ & \lambda^3 \xi_t + \lambda^2 (\xi v + h_1 v)_x + \frac{\partial}{\partial x} \{ 2Ah_1^2 h_{1x} v_x \\ & + Ah_1^2 h_{1xx} v - \lambda b h_1^2 \xi_{xt} \} = 0, \quad x \in [0, 2\pi], \\ & v(x, 0) = u(\lambda x, 0), \quad \xi(x, 0) = \eta(\lambda x, 0), \\ & v(0, t) = v(2\pi, t), \quad \xi(0, t) = \xi(2\pi, t), \quad \text{for } t \geq 0. \end{aligned} \quad (2.35)$$

The set of  $N$  evenly spaced grid points  $x_j = \frac{2\pi j}{N}$ ,  $j = 1, \dots, N$  in the interval  $[0, 2\pi]$  is referred to as collocation nodes.

The spectral-collocation method is used in the physical space by seeking approximate solutions through a global periodic interpolation polynomial of the form

$$v_N(x) = \sum_{j=1}^N v_N(x_j) g_j(x), \quad \xi_N(x) = \sum_{j=1}^N \xi_N(x_j) g_j(x), \quad (2.36)$$

where  $g_j(x) = \frac{1}{N} \sin \left( \frac{N(x-x_j)}{2} \right) \cot \left( \frac{1}{2}(x-x_j) \right)$  and  $v_N(x)$ ,  $\xi_N(x)$  is an interpolation of the functions  $v(x)$ ,  $\xi(x)$  respectively, i.e.,  $v_N(x_j) = v(x_j)$ ,  $\xi_N(x_j) = \xi(x_j)$  (see [23], [63]). The corresponding Fourier collocation differentiation matrices  $D_x$  and  $D_{xx}$  are given by

$$D_{ij}^{(1)} = \frac{dg_j}{dx}(x_i) = \begin{cases} \frac{1}{2}(-1)^j \cot(\frac{x_i-x_j}{2}), & i \neq j, \\ 0, & i = j, \end{cases} \quad (2.37a)$$

$$D_{ij}^{(2)} = \frac{d^2 g_j}{dx^2}(x_i) = \begin{cases} -\frac{(-1)^j}{2 \sin^2((x_i-x_j)/2)}, & i \neq j, \\ \frac{-\pi^2}{3h^2} - \frac{1}{6}, & i = j. \end{cases} \quad (2.37b)$$

Then at the collocation points  $x = x_j$ , the system becomes

$$\begin{aligned} [\lambda^3 I_N - \lambda b D_N \text{diag}(h_1^2) D_N] \xi_{Nt} &= -\lambda^2 D_N(\text{diag}(h_1)v_N) \\ -\lambda^2 D_N(\xi_N v_N) - D_N(2Ah_1^2 h_{1x} D_N(v_N)) + Ah_{1xx} h_1^2 v_N, \end{aligned} \quad (2.38a)$$

$$\begin{aligned} [\lambda^3 I_N - \lambda d \text{diag}(h_1^2) D_N^{(2)}] v_{Nt} &= -\lambda^2 g D_N(\xi_N) \\ -\lambda^2 (0.5) D_N(v_N^2) - 2Bgh_1 h_{1x} D_N^{(2)}(\xi_N) - Bgh_1 h_{1xx} D_N(\xi_N), \end{aligned} \quad (2.38b)$$

where  $I_N$  is the unit  $N \times N$  matrix and  $D_N$  and  $D_N^{(2)}$  are square matrices of dimensions  $N \times N$  following from (2.37a) and (2.37b) respectively and  $\text{diag}(h_1)$  and  $\text{diag}(h_1^2)$  are the diagonal matrices of  $h_1$  and  $h_1^2$ , respectively. This is a system of  $N$  ordinary differential equations for  $\xi_N$  and also  $v_N$ .

We use a four-stage explicit Runge-Kutta method (RK-4) to solve the system because this method is quite accurate, stable and easy to program. The truncation error in RK-4 method is  $O(\Delta t)^5$  and the global error is  $O(\Delta t)^4$ . When we halve the time step the error will be  $O\left(\frac{(\Delta t)^4}{16}\right)$ . Hence, halving the time step results in 16 times protection of error in RK-4 method.

In paper B, the coupled BBM-BBM type system (2.18) is solved numerically and the convergence of the the numerical scheme is verified.



# Chapter 3

## Mechanical balance laws in Boussinesq theory

In this section mass, momentum and energy conservation properties of the system (2.16) are explored in terms of the velocity potential  $\phi$ . If non-dimensional mass density  $\tilde{M}(\tilde{\eta})$  and mass flux  $\tilde{q}_{\tilde{M}}(\tilde{\eta})$ , momentum density  $\tilde{I}(\tilde{\eta})$  and momentum flux  $\tilde{q}_{\tilde{I}}(\tilde{\eta})$  and energy density  $\tilde{E}(\tilde{\eta})$  and energy flux  $\tilde{q}_{\tilde{E}}(\tilde{\eta})$  are defined appropriately in terms of  $\tilde{\eta}$  and its derivatives, then the mechanical balance law relations

$$\frac{\partial}{\partial \tilde{t}} \tilde{M}(\tilde{\eta}) + \frac{\partial}{\partial \tilde{x}} \tilde{q}_{\tilde{M}}(\tilde{\eta}) = \mathcal{O}(\alpha\beta, \beta^2), \quad (3.1a)$$

$$\frac{\partial}{\partial \tilde{t}} \tilde{I}(\tilde{\eta}) + \frac{\partial}{\partial \tilde{x}} \tilde{q}_{\tilde{I}}(\tilde{\eta}) = \mathcal{O}(\alpha\beta, \beta^2), \quad (3.1b)$$

$$\frac{\partial}{\partial \tilde{t}} \tilde{E}(\tilde{\eta}) + \frac{\partial}{\partial \tilde{x}} \tilde{q}_{\tilde{E}}(\tilde{\eta}) = \mathcal{O}(\alpha\beta, \beta^2), \quad (3.1c)$$

will hold. The mechanical balance laws of these physical quantities to the system (2.16) are correct to the same order as the evolution equations. To convert the non-dimensional variables, the corresponding non-dimensional densities are given as

$$\tilde{M} = \frac{M}{\rho h_0}, \quad \tilde{I} = \frac{M}{\rho c_0 h_0}, \quad \tilde{E} = \frac{M}{\rho c_0^2 h_0}, \quad (3.2)$$

and the non-dimensional fluxes are defined as

$$\tilde{q}_{\tilde{M}} = \frac{q_M}{\rho c_0 h_0}, \quad \tilde{q}_{\tilde{I}} = \frac{q_I}{\rho c_0^2 h_0}, \quad \tilde{q}_{\tilde{E}} = \frac{q_E}{\rho c_0^3 h_0}, \quad (3.3)$$

where  $c_0 = \sqrt{gh_0}$ . Although it is fascinating for various applications to be able to reconstruct the pressure from the primary dependent variables of the

equation of motion, an approximate expression for the pressure is also useful for computation of the momentum and energy conservations.

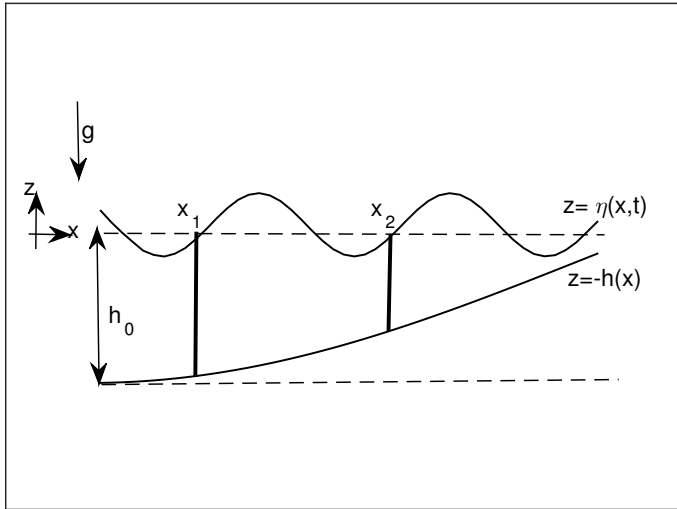


Figure 3.1: The figure describes a typical control volume used for conservation properties of the Boussinesq theory. The bottom ( $-h(x)$ ) and lateral boundary are held fixed while the upper boundary  $\eta(x, t)$  moves with the fluid free surface.

The following mechanical balance derivations are based on the work in [2, 3]. Let us consider the fluid is running in a narrow channel of total depth  $h(x, t) = -h(x) + \eta(x, t)$  and choose a control volume of unit width, bounded by the lateral sides of the interval  $[x_1, x_2]$ , the free surface and the bottom as shown in Fig. 3.1.

The Bernoulli equation (3.4) for unsteady potential flow is used to find the pressure field in the theory of ocean surface waves.

$$\frac{p}{\rho} + gz + \frac{\partial \phi}{\partial t} + \frac{1}{2} |\nabla \phi|^2 = f(t) \quad (3.4)$$

Furthermore,  $f(t)$  can be obtained by imposing asymptotic conditions and approximate this Bernoulli equation at free surface. At the free surface  $p \rightarrow p_{atm}$  (atmospheric pressure) and

$$\eta \rightarrow 0, \quad \phi \rightarrow \text{constant} \quad \text{as } x \rightarrow \infty. \quad (3.5)$$

Therefore  $f(t)$  is given by

$$f(t) = \frac{p_{atm}}{\rho}. \quad (3.6)$$

Let us define the dynamic pressure by  $p' = p - p_{atm} + \rho g z$  (see [2]) and scale it by  $p' = \tilde{p}' \rho g a$ . Then

$$\tilde{p}' = -\tilde{\phi}_{\tilde{t}} - \frac{1}{2}\alpha(\tilde{\phi}_{\tilde{x}})^2 - \frac{1}{2}\frac{\alpha}{\beta}(\tilde{\phi}_{\tilde{z}})^2. \quad (3.7)$$

Inserting the expression for  $\tilde{\phi}$  into (3.7) and performing some simplifications yield

$$\tilde{p}' = -\tilde{\phi}_{\tilde{t}}^{(0)} - \frac{\tilde{z}}{1!}\beta\hat{w}_{\tilde{t}} + \beta\frac{\tilde{z}^2}{2!}\hat{u}_{\tilde{x}\tilde{t}} - \alpha\hat{u}\hat{u}_{\tilde{x}} + \mathcal{O}(\alpha\beta, \beta^2). \quad (3.8)$$

On the other hand, it is easy to obtain the following equation from (2.6), (2.7), (2.8) and (2.16):

$$\tilde{\eta} = -\tilde{\phi}_{\tilde{t}}^{(0)} - \alpha\hat{u}\hat{u}_{\tilde{x}} + \mathcal{O}(\alpha\beta, \beta^2). \quad (3.9)$$

From equation (3.8) and (3.9) one immediately concludes that

$$\tilde{p}' = \tilde{\eta} + \frac{\tilde{z}}{1!}\beta(\tilde{h}\hat{u})_{\tilde{x}\tilde{t}} + \beta\frac{\tilde{z}^2}{2!}\hat{u}_{\tilde{x}\tilde{t}} + \mathcal{O}(\alpha\beta, \beta^2). \quad (3.10)$$

Then the total pressure in terms of dimensional variables is given by

$$p = \rho g(\eta - z) + p_{atm} + \rho\frac{z}{1!}(hu)_{xt} + \rho\frac{z^2}{2!}(u)_{xt}. \quad (3.11)$$

If the above pressure expression is evaluated at the free surface, then the pressure is not equal to atmospheric pressure.

## 3.1 Mass balance

Let us assume that the mass particles pass through a control volume of unit width, delimited by the interval  $[x_1, x_2]$  at the lateral sides,  $h(x)$  at the bottom and  $\eta(x, t)$  at the free surface. The mass balance says that the mass cannot disappear, i.e., the rate of change of the total mass per unit time is equal to the net mass flux into the control volume. The integral form of the equation of mass conservation is

$$\frac{d}{dt} \int_{x_1}^{x_2} \int_{-h(x)}^{\eta} \rho dz dx = \left[ \int_{-h(x)}^{\eta} \rho \phi_x dz \right]_{x_2}^{x_1}, \quad (3.12)$$

since there is no mass flux through the bottom or through the free surface. In non-dimensional variables the above relation becomes

$$\frac{d}{d\tilde{t}} \int_{\tilde{x}_1}^{\tilde{x}_2} \int_{-\tilde{h}}^{\alpha\tilde{\eta}} d\tilde{z} d\tilde{x} = \left[ \int_{-\tilde{h}}^{\alpha\tilde{\eta}} \alpha\tilde{\phi}_{\tilde{x}} d\tilde{z} \right]_{\tilde{x}_2}^{\tilde{x}_1}. \quad (3.13)$$

After integration with respect to  $\tilde{z}$  and use of asymptotic expansion of  $\tilde{\phi}$ , we obtain

$$\int_{\tilde{x}_1}^{\tilde{x}_2} (\alpha\tilde{\eta} + \tilde{h})_{\tilde{t}} d\tilde{x} = \alpha \left[ \hat{u}(\tilde{h} + \alpha\tilde{\eta}) + \frac{\tilde{h}^2}{2!} \beta(\hat{u}\tilde{h})_{\tilde{x}\tilde{x}} - \frac{\tilde{h}^3}{3!} \beta(\hat{u})_{\tilde{x}\tilde{x}} \right]_{\tilde{x}_2}^{\tilde{x}_1} + \mathcal{O}(\alpha\beta, \beta^2). \quad (3.14)$$

If we take the limit  $\tilde{x}_2 \rightarrow \tilde{x}_1$ , where  $\tilde{x}_2 = x_2/l$  and  $\tilde{x}_1 = x_1/l$ , then we obtain the balance equation (2.9b). i.e,

$$\frac{\partial}{\partial \tilde{t}} \tilde{M} + \frac{\partial}{\partial \tilde{x}} \tilde{q}_M = \mathcal{O}(\alpha\beta, \beta^2), \quad (3.15)$$

where

$$\begin{aligned} \tilde{M} &= \alpha\tilde{\eta} + \tilde{h}, \\ \tilde{q}_M &= \alpha \left[ \left( \alpha\tilde{\eta}\tilde{u}^\theta + \tilde{h}\tilde{u}^\theta \right) + \beta(\theta - \frac{1}{2})\tilde{h}^2(\tilde{h}\tilde{u}^\theta)_{\tilde{x}\tilde{x}} + \beta\tilde{h}^3(\frac{1}{2}(\theta - 1)^2 - \frac{1}{6})(\tilde{u}^\theta)_{\tilde{x}\tilde{x}} \right]. \end{aligned} \quad (3.16)$$

If we use the scalings  $M = \rho h_0 \tilde{M}$  and  $q_M = \rho h_o \sqrt{(gh_0)} \tilde{q}_M$ , then the dimensional form of these quantities are

$$\begin{aligned} M &= \rho(\eta + h(x)), \\ q_M &= \rho \left[ u(h + \eta) + h^2(\theta - \frac{1}{2})(hu)_{xx} + \frac{1}{2}h^3((\theta - 1)^2 - \frac{1}{3})u_{xx} \right]. \end{aligned} \quad (3.17)$$

Eq. (3.15) represents the approximate mass balance equation. The net mass transfer to or from a control volume during a time interval  $\Delta t$  is equal to the net change (increase or decrease) in the total mass in the control volume during  $\Delta t$ .

In paper B, mass conservation is used to quantify the role of reflection in the shoaling of solitary waves. It has been shown in paper B [56] that this approximate mass conservation relation is reasonably accurate and the ratio of mass reflection to mass influx approaches zero as the difference in flow depths becomes small.

## 3.2 Momentum balance

The integral form of the equation of momentum conservation is

$$\frac{d}{dt} \int_{x_1}^{x_2} \int_{-h(x)}^{\eta} \rho \phi_x dz dx = \left[ \int_{-h(x)}^{\eta} \rho \phi_x^2 dz + \int_{-h(x)}^{\eta} p dz \right]_{x_2}^{x_1}. \quad (3.18)$$

In non-dimensional variables the above relation becomes

$$\alpha \frac{d}{d\tilde{t}} \int_{\tilde{x}_1}^{\tilde{x}_2} \int_{-\tilde{h}}^{\alpha\tilde{\eta}} \alpha \tilde{\phi}_{\tilde{x}} d\tilde{z} d\tilde{x} = \left[ \int_{-\tilde{h}}^{\alpha\tilde{\eta}} \alpha^2 \tilde{\phi}_{\tilde{x}}^2 d\tilde{z} + \int_{-\tilde{h}}^{\alpha\tilde{\eta}} (\alpha \tilde{p} - \tilde{z}) d\tilde{z} \right]_{\tilde{x}_2}^{\tilde{x}_1}. \quad (3.19)$$

After integration with respect to  $\tilde{z}$  and use of asymptotic expansion of  $\tilde{\phi}$ , we obtain

$$\begin{aligned} & \alpha \int_{\tilde{x}_1}^{\tilde{x}_2} \left\{ \{ \tilde{u}^\theta (\alpha \tilde{\eta} + \tilde{h}) + \beta \tilde{h}^2 (\theta - 1) (\tilde{h} \tilde{u}^\theta)_{\tilde{x}\tilde{x}} \} \right\}_{\tilde{t}} d\tilde{x} \\ & + \alpha \int_{\tilde{x}_1}^{\tilde{x}_2} \left\{ \{ \beta \frac{\tilde{h}^3}{2} (\theta - 1)^2 \tilde{u}^\theta_{\tilde{x}\tilde{x}} + \beta \frac{\tilde{h}^2}{2!} (\tilde{h} \tilde{u}^\theta)_{\tilde{x}\tilde{x}} - \beta \frac{\tilde{h}^3}{3!} \tilde{u}^\theta_{\tilde{x}\tilde{x}} \} \right\}_{\tilde{t}} d\tilde{x} \\ & = \alpha \left[ \alpha \tilde{h} \tilde{u}^\theta_{\tilde{x}\tilde{x}} + \tilde{h} \tilde{\eta} + \frac{1}{\alpha} \frac{\tilde{h}^2}{2} + \alpha \frac{\tilde{\eta}^2}{2} - \beta \frac{\tilde{h}^2}{2} (\tilde{h} \tilde{u}^\theta)_{\tilde{x}\tilde{t}} + \beta \frac{\tilde{h}^3}{3!} (\tilde{u}^\theta)_{\tilde{x}\tilde{t}} \right]_{\tilde{x}_2}^{\tilde{x}_1} \\ & + \mathcal{O}(\alpha^3, \alpha^2 \beta, \beta^3). \end{aligned} \quad (3.20)$$

If we use the scalings  $I = \rho c_0 h_0 \tilde{I}$  and  $q_I = \rho c_0^2 h_o \tilde{q}_I$ , then the dimensional form of these quantities are

$$\begin{aligned} I &= \rho(\eta + h)u^\theta + \rho((\theta - 1)h^2(h^\theta u^\theta)_{xx} + \frac{h^3}{2}(\theta - 1)^2 u_{xx}^\theta \\ &\quad + \frac{h^2}{2}(hu^\theta)_{xx} - \frac{h^3}{3!}u_{xx}^\theta)), \\ q_I &= \rho u^{\theta 2} h + \frac{\rho g}{2}(h + \eta)^2 - \rho \frac{h^2}{2}(hu_t^\theta)_x + \rho \frac{h^3}{6}u_{xt}^\theta. \end{aligned} \quad (3.21)$$

We now find the horizontal component of the force acting on unit width of the sloping bottom D, which is defined by

$$D = \int_{h_1}^{h_2} ph'(x) dx. \quad (3.22)$$

Now the momentum balance law derived above are examined in a concrete situation. In all the numerical results of this section we use the

exact solitary wave solutions (2.29) and (2.30). Consider a control volume delimited by the interval [50 m, 150 m] on the  $x$ -axis. The momentum per unit width contained in this interval is defined by  $\int_{50}^{150} I(x, t) dx$  and the momentum flux through the boundaries of the control volume is defined by  $q_I(50, t)$  and  $q_I(150, t)$ , where  $I$  and  $q_I$  are given in (3.21). The quantities  $I$  and  $q_I$  during the passage of solitary wave are computed and they are averaged over time from  $t = 0$  s to  $t = 200$  s. It is observed that the momentum flux difference is approximately equal to the pressure integral  $D$  which is defined in (3.22).

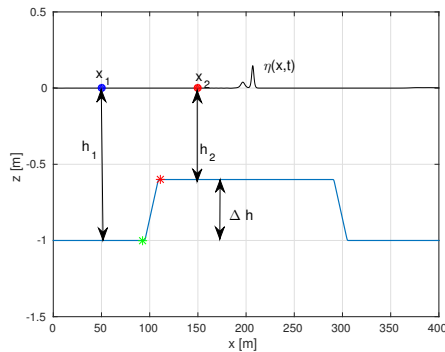


Figure 3.2: The left panel shows a solitary wave solution for the system (2.18) with initial amplitude 0.2 m at time  $t = 60$  s.

$\Delta h$	Influx	Outflux	Flux difference	Pressure integral D
0.1	0.5040	0.4087	-0.0954	-0.0954
0.2	0.5041	0.3234	-0.1807	-0.1808
0.3	0.5043	0.2562	-0.2561	-0.2561
0.4	0.5044	0.1828	-0.3216	-0.3216

Table 3.1: This table gives the conservation of momentum of a solitary wave with initial amplitude 0.1 m on a slope 1:35 for different  $\Delta h$ .

Amplitude	Influx	Outflux	Flux difference	Pressure integral D
0.05	0.5028	0.4075	-0.0953	- 0.0953
0.1	0.5040	0.4087	-0.0954	-0.0954
0.2	0.5061	0.4106	-0.0955	- 0.0955
0.3	0.5079	0.4123	-0.0956	-0.0956
0.4	0.5096	0.4139	-0.0958	-0.0957

Table 3.2: This table gives the momentum conservation for different wave-heights on a slope 1:35 and  $\Delta h = h_0 - h = 0.1$  m.

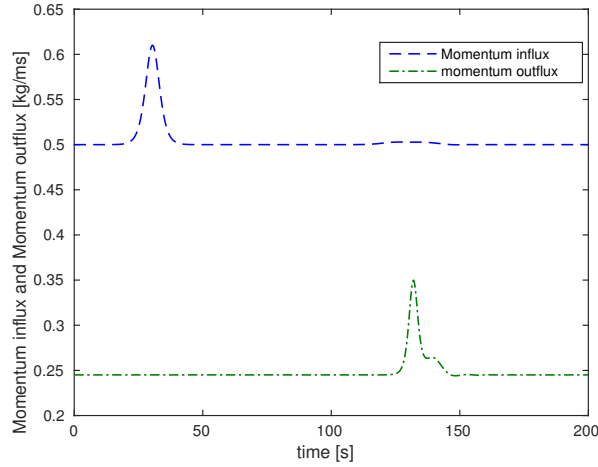


Figure 3.3: The figure shows plots of time series of the momentum influx at  $x = 50$  m (blue dashed curve) and momentum outflux at  $x = 150$  m (green dash-dotted curve), per unit span. The fluxes during the passage of solitary wave of amplitude 0.1 m and  $\Delta h = 0.3$  m are computed and they are averaged over time from  $t = 0$  s to  $t = 200$  s.

### 3.3 Energy balance

In this section, we examine energy balance of the BBM-BBM type system (2.18). If we assume that the potential energy of a particle is zero at the undisturbed free surface and the potential energy is zero when no wave motion is present, then the total energy inside a control volume of unit width, delimited by the interval  $[x_1, x_2]$  on the lateral sides, the bottom and the free surface can be written as

$$E = \frac{1}{2} \int_{x_1}^{x_2} \int_{-h(x)}^{\eta} \rho |\nabla \phi|^2 dz dx + \int_{x_1}^{x_2} \int_{-h(x)}^{\eta} \rho g z dz dx, \quad (3.23)$$

where the first term represents the kinetic energy and the second term represents potential energy. The conservation of total mechanical energy is written

as

$$\begin{aligned} & \frac{d}{dt} \frac{1}{2} \int_{x_1}^{x_2} \int_{-h(x)}^{\eta} \rho |\nabla \phi|^2 dz dx + \frac{d}{dt} \int_{x_1}^{x_2} \int_{-h(x)}^{\eta} \rho g z dz dx \\ &= \left[ \int_{-h(x)}^{\eta} \left\{ \frac{\rho}{2} |\nabla \phi|^2 + \rho g z + P \right\} \phi_x dz \right]_{x_2}^{x_1}. \end{aligned} \quad (3.24)$$

Expressing the above relation in non-dimensional variables gives

$$\begin{aligned} & \frac{d}{dt} \frac{1}{2} \int_{\tilde{x}_1}^{\tilde{x}_2} \int_{-\tilde{h}}^{\alpha \tilde{\eta}} \left\{ \alpha^2 \left( \tilde{\phi}_{\tilde{x}}^2 + \frac{1}{\beta} \tilde{\phi}_{\tilde{z}}^2 \right) + 2\tilde{z} \right\} d\tilde{z} d\tilde{x} \\ &= \left[ \int_{-\tilde{h}}^{\alpha \tilde{\eta}} \left\{ \frac{\alpha^3}{2} \tilde{\phi}_{\tilde{x}}^3 + \frac{1}{\beta} \tilde{\phi}_{\tilde{z}}^2 \tilde{\phi}_{\tilde{x}} + \alpha^2 \tilde{p}' \tilde{\phi}_{\tilde{x}} \right\} d\tilde{z} \right]_{\tilde{x}_2}^{\tilde{x}_1} \end{aligned}$$

If we substitute the expressions for  $\tilde{\phi}_{\tilde{x}}$ ,  $\tilde{\phi}_{\tilde{z}}$  and  $\tilde{p}'$  found in (2.7), (2.10), (2.8) and (3.10) respectively, and integrate with respect to  $\tilde{z}$ , then we obtain

$$\begin{aligned} & \frac{d}{dt} \int_{\tilde{x}_1}^{\tilde{x}_2} \left\{ \frac{\alpha^2 (\tilde{u}^\theta)^2 \tilde{h} + \tilde{\eta}^2}{2} + \frac{\alpha^2 \beta}{2} ((\theta - 1)^2 - \frac{1}{3}) \tilde{h}^3 \tilde{u}^\theta \tilde{u}^\theta_{\tilde{x}\tilde{x}} \right\} d\tilde{x} \\ &+ \frac{d}{dt} \int_{\tilde{x}_1}^{\tilde{x}_2} \left\{ \frac{\alpha^2 \beta}{2} (2(\theta - 1) + 1) \tilde{h}^2 \tilde{u}^\theta (\tilde{h} \tilde{u}^\theta)_{\tilde{x}\tilde{x}} + \frac{\alpha^2 \beta}{6} \tilde{h}^3 (\tilde{u}^\theta_{\tilde{x}})^2 \right\} d\tilde{x} \\ &+ \frac{d}{dt} \int_{\tilde{x}_1}^{\tilde{x}_2} \left\{ \frac{\alpha^2 \beta}{2} \tilde{h} ((\tilde{h} \tilde{u}^\theta)_{\tilde{x}})^2 - \frac{\alpha^2 \beta}{2} (\tilde{h})^2 (\tilde{h} \tilde{u}^\theta)_{\tilde{x}} \tilde{u}^\theta_{\tilde{x}} + \frac{\alpha^3 (\tilde{u}^\theta)^2}{2} \tilde{\eta} - \frac{\tilde{h}^2}{2} \right\} d\tilde{x} \\ &= \left[ \frac{\alpha^3}{2} \tilde{u}^\theta \tilde{h}^3 + \alpha^2 \tilde{\eta} \tilde{u}^\theta \tilde{h} + \alpha^3 \tilde{\eta}^2 \tilde{u}^\theta + (\frac{-1}{6} + \frac{(\theta-1)^2}{2}) \alpha^2 \beta \tilde{\eta} \tilde{u}^\theta \tilde{u}^\theta_{\tilde{x}\tilde{x}} \tilde{h}^3 \right]_{x_2/l}^{x_1/l} \\ &+ \left[ (\theta - \frac{1}{2}) \alpha^2 \beta \tilde{\eta} (\tilde{h} \tilde{u}^\theta)_{\tilde{x}\tilde{x}} \tilde{h}^2 - (\frac{\tilde{h}^2}{2}) \alpha^2 \beta \tilde{u}^\theta (\tilde{h} \tilde{u}^\theta)_{\tilde{x}\tilde{t}} + (\frac{\tilde{h}^3}{6}) \alpha^2 \beta \tilde{u}^\theta (\tilde{u}^\theta)_{\tilde{x}\tilde{t}} \right]_{x_2/l}^{x_1/l} \\ &\quad + \mathcal{O}(\alpha^2 \beta^2, \alpha^3 \beta, \alpha^4). \end{aligned} \quad (3.25)$$

Taking the limit as  $x_2 \rightarrow x_1$ , and omitting the common factor  $\alpha^2$ , we obtain the differential energy balance equation

$$\begin{aligned} & \frac{d}{d\tilde{t}} \left[ \frac{(\tilde{u}^\theta)^2 \tilde{h} + \tilde{\eta}^2}{2} + \frac{\beta}{2} ((\theta - 1)^2 - \frac{1}{3}) \tilde{h}^3 \tilde{u}^\theta \tilde{u}^\theta_{\tilde{x}\tilde{x}} \right] \\ & + \frac{d}{d\tilde{t}} \left[ +\frac{\beta}{2} (2\theta - 1) \tilde{h}^2 \tilde{u}^\theta (\tilde{h} \tilde{u}^\theta)_{\tilde{x}\tilde{x}} - \beta (\tilde{h})^2 (\tilde{h} \tilde{u}^\theta)_{\tilde{x}} \tilde{u}^\theta_{\tilde{x}} \frac{\alpha \tilde{u}^\theta}{2} \tilde{\eta} + \frac{\beta}{6} \tilde{h}^3 (\tilde{u}^\theta_{\tilde{x}})^2 \right] \\ & + \frac{d}{d\tilde{t}} \left[ \frac{\beta}{2} \tilde{h} ((\tilde{h} \tilde{u}^\theta)_{\tilde{x}})^2 - \frac{\beta}{2} (\tilde{h})^2 (\tilde{h} \tilde{u}^\theta)_{\tilde{x}} \tilde{u}^\theta_{\tilde{x}} + \frac{\alpha \tilde{u}^\theta}{2} \tilde{\eta} - \frac{\tilde{h}^2}{2} \right] \\ & + \frac{d}{d\tilde{x}} \left[ \frac{\alpha}{2} \tilde{u}^\theta \tilde{h}^3 + \tilde{\eta} \tilde{u} \tilde{h} + \alpha \tilde{\eta}^2 \tilde{u}^\theta + (\frac{(\theta-1)^2}{2} - \frac{1}{6}) \beta \tilde{\eta} \tilde{u}^\theta_{\tilde{x}\tilde{x}} \tilde{h}^3 + (\theta - \frac{1}{2}) \beta \tilde{\eta} (\tilde{h} \tilde{u}^\theta)_{\tilde{x}\tilde{x}} \tilde{h}^2 \right] \\ & + \frac{d}{d\tilde{x}} \left[ -(\frac{\tilde{h}^2}{2}) \beta \tilde{u}^\theta (\tilde{h} \tilde{u}^\theta)_{\tilde{x}\tilde{t}} + (\frac{\tilde{h}^3}{6}) \beta \tilde{u}^\theta (\tilde{u}^\theta)_{\tilde{x}\tilde{t}} \right] = \mathcal{O}(\beta^2, \alpha\beta, \alpha^2). \end{aligned}$$

The dimensional versions of the equations are given by

$$\begin{aligned} E &= \frac{\rho}{2} u^2 h + \frac{\rho}{2} h^3 ((\theta - 1)^2 - \frac{1}{3}) u u_{xx} + \frac{\rho}{2} h^2 u (2\theta - 1) (h u)_{xx} - \frac{\rho}{2} g h^2 \\ &+ \frac{\rho}{2} u^2 \eta + \frac{\rho}{6} h^3 (u_x)^2 + \frac{\rho}{2} h ((h u)_x)^2 - \frac{\rho}{2} h^2 u_x (h u)_x + \frac{\rho}{2} g \eta^2 \quad (3.26) \end{aligned}$$

and

$$\begin{aligned} q_E &= \frac{\rho}{2} u^3 h + \rho g \eta h u + \rho (\frac{(\theta-1)^2}{2} - \frac{1}{6}) g h^3 \eta u_{xx} \\ &+ \frac{\rho}{6} h^3 u u_{xt} - \frac{\rho}{2} h^2 u (h u)_{xt} + \rho g u \eta^2 + \rho (\theta - \frac{1}{2}) g h^2 \eta (h u)_{xx}. \quad (3.27) \end{aligned}$$

To test the energy conservation, we consider a control volume delimited by the interval [50 m, 150 m] on the  $x$ -axis. The energy per unit width contained in this interval is defined by  $\int_{50}^{150} E(x, t) dx$  and the energy flux through the boundaries of the control volume is defined by  $q_E(50, t)$  and  $q_E(150, t)$ , where  $E$  and  $q_E$  are given in (3.26) and (3.27). The quantities  $E$  and  $q_E$  during the passage of solitary wave are computed and they are averaged over time from  $t = 0$  s to  $t = 200$  s. Tables 3.3 and 3.4 suggest that energy conservation has a negligible error.

In the paper A, we use the expression for  $E$  and evaluate the integral  $\mathbb{E} = \int E dx$  for the total energy at two different instances in time; one at which the wave is located over the initial depth  $h_0$  and one at which the wave is located above a different depth  $h$  and obtained an equation relating the waveheights  $H_0$  and  $H$  at the two different depths. Now given  $H_0$ ,  $h_0$  and  $h$ , it is possible to find the wave height  $H$  at the depth  $h$ . Since the pressure

$\Delta h$	Energy influx	Energy outflux	Energy flux difference
0.1	2.5606e-4	2.5706e-4	-5.8565e-07
0.2	2.5606e-4	2.5706e-4	-1.0633e-06
0.3	2.5556e-4	2.5706e-4	-1.4085e-06
0.4	2.5506e-4	2.5706e-4	-1.5991e-06

Table 3.3: This table gives the the conservation of energy of a solitary wave with initial amplitude 0.1 m on a slope 1:35 for different  $\Delta h$ .

Amplitude	Energy influx	Energy outflux	Energy flux difference
0.05	8.8339e-05	8.8481e-05	-7.0548e-10
0.1	2.5606e-04	2.5706e-04	-5.8565e-07
0.2	7.6069e-04	2.5606e-04	-2.6727e-06
0.3	1.4614e-03	1.4684e-03	-7.0018e-06
0.4	2.3461e-03	2.3606e-03	-1.4004e-05

Table 3.4: This table gives conservation of energy for different wave heights on a slope 1:35 and  $\Delta h = h_0 - h = 0.1$  m.

force acting on the fluid at the sloping bottom is perpendicular to the fluid velocity, the energy is conserved. From the conservation of energy and the exponential decay of  $\eta$  and  $w$ , we have

$$\int_{-\infty}^{\infty} E(\eta_0, w_0) dx = \int_{-\infty}^{\infty} E(\eta, w) dx, \quad (3.28)$$

where  $E$  is the energy density, and  $\eta$  and  $w$  are given in (2.29) and (2.30) with the constants  $W$ ,  $c_s$  and  $\kappa$  given in terms of  $h$  and  $H$  instead of  $h_0$  and  $H_0$ .

We have computed wave shoaling for initial undisturbed depth  $h_0 = 1$  m and initial waveheights  $H_0$  equal to 0.05 m, 0.1 m and 0.2 m, and for a ratio of undisturbed to initial depth of up to 0.5 m. It is shown in paper A that the computed curves  $H/H_0$  get close to the line  $h^{-1}$  for decreasing initial waveheight.

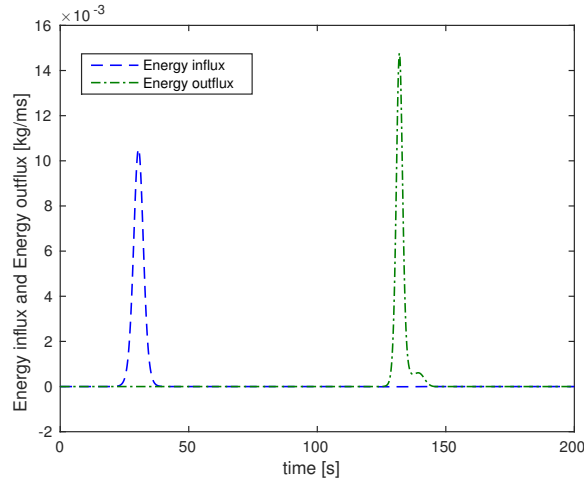


Figure 3.4: The figure shows plots of time series of the energy influx at  $x = 50$  m (blue dashed curve) and energy outflux at  $x = 150$  m (green dash-dotted curve), per unit span. The quantities, energy influx and outflux, during the passage of solitary wave of amplitude 0.1 m and  $\Delta h = 0.3$  m are computed and they are averaged over time from  $t = 0$  s to  $t = 200$  s.

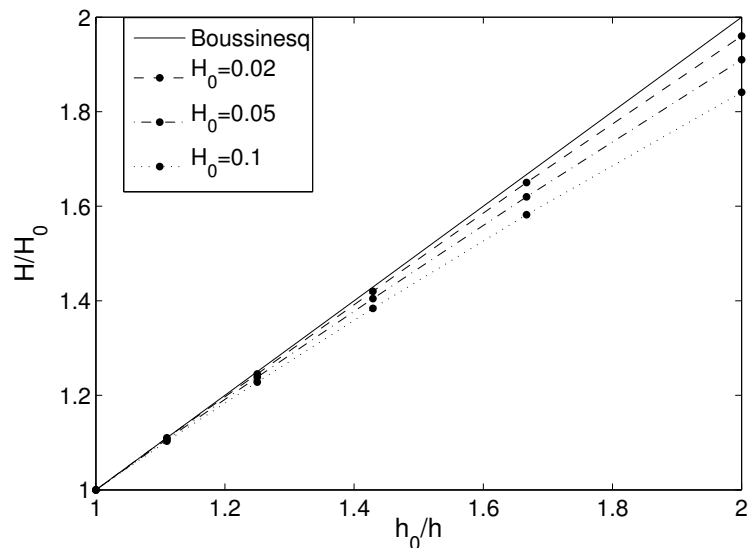


Figure 3.5: Computations for the shoaling of solitary waves with different amplitudes using relation equation. The solid line depicts the shoaling relation according to Boussinesq's law. As the amplitude of the incident solitary waves decreases, the shoaling relation approaches Boussinesq's result.



# Chapter 4

## Shallow water equations in uniform shear flows

With the assumption of null vorticity, Boussinesq-type models have been used for calculation of the transformation of nonlinear and dispersive waves in coastal areas. The water flows include shear flows in nature, it is no longer relevant to use the assumption of irrotational flows when gravity waves propagate on the surface of shear flows. So in this study we consider the effect of vorticity on the motion of a long-wave models for weakly nonlinear surface water waves. Recently, several authors [4, 11, 15, 22, 46, 65, 69] have added the influence of horizontal vorticity on the waves in their works. To avoid mathematical complexity and to confine the consequence of background vorticity, a simple case of constant vorticity has been considered. Let the spatial coordinates be  $(x, z)$  and the  $x$ -axis be oriented in the horizontal direction. Assume that the motion is uniform in the direction perpendicular to the  $xz$ -plane (long-crested waves). The gravitational acceleration  $g$  is in the negative  $z$ -direction. Let  $\eta(x, t)$  denote the surface elevation. Assuming  $a$  is a typical amplitude and  $l$  is a typical wavelength of the waves to be described, the parameter  $\alpha = a/h_0$  represents the waveheight to depth ratio and the parameter  $\beta = h_0^2/l^2$  represents a water depth to wavelength ratio.

The vorticity of the water flow is defined by  $\omega = v_x - u_y$ . Here  $\omega$  is constant. A shear flow with constant vorticity is described by a velocity vector field  $\mathbf{u} = (U, W) = (u + z\Gamma, w) = (\frac{\partial \phi}{\partial x} + z\Gamma, \frac{\partial \phi}{\partial z})$ , where  $\phi(x, z, t)$  is the velocity potential of the disturbances. For  $\Gamma > 0$  we have a current in the opposite wave-propagation direction, while for  $\Gamma < 0$  it is in a favorable direction.

In paper D, a corresponding system was derived to second-order ac-

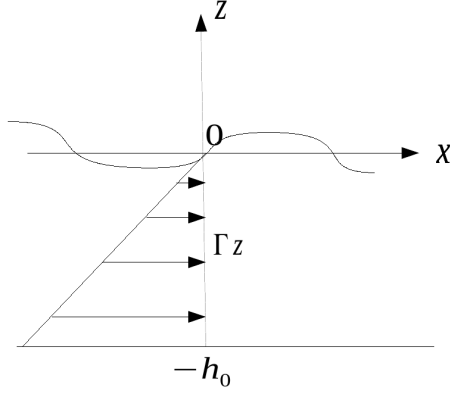


Figure 4.1: This figure shows the background uniform shear flow  $U = z\Gamma$ . In the figure  $\Gamma$  is negative, the waves which are superposed onto this background current propagate to the right.

curacy in  $\alpha$  and  $\beta$  (see also [65]). In dimensional variables this becomes

$$\begin{aligned}\tilde{\eta}_{\tilde{t}} + \tilde{v}_{\tilde{x}} + \alpha\tilde{\Gamma}\tilde{\eta}\tilde{\eta}_{\tilde{x}} + \alpha(\tilde{\eta}\tilde{v})_{\tilde{x}} - \frac{\beta}{6}\frac{\partial^3\tilde{v}}{\partial\tilde{x}^3} &= \mathcal{O}(\alpha\beta, \beta^2), \\ \tilde{v}_{\tilde{t}} + \tilde{\eta}_{\tilde{x}} + \alpha\tilde{v}\tilde{v}_{\tilde{x}} - \tilde{\Gamma}\tilde{v}_{\tilde{x}} - \frac{\beta}{2}\frac{\partial^3\tilde{v}}{\partial\tilde{x}^2\partial\tilde{t}} + \frac{\beta}{6}\tilde{\Gamma}\frac{\partial^3\tilde{v}}{\partial\tilde{x}^3} &= \mathcal{O}(\alpha\beta, \beta^2),\end{aligned}\quad (4.1)$$

where  $\tilde{v}$  denotes horizontal velocity at the bottom of the channel and the velocity potential is given by

$$\tilde{\phi} = \phi_0 - \frac{\beta}{2}(1 + \tilde{z})^2\frac{\partial^2\phi_0}{\partial\tilde{x}^2} + \frac{\beta^2}{24}(1 + \tilde{z})^4\frac{\partial^4\phi_0}{\partial\tilde{x}^4} + \mathcal{O}(\beta^3). \quad (4.2)$$

Now if we let  $\tilde{u}^\theta$  be the non-dimensional velocity at a non-dimensional height  $\tilde{z}_\theta = -1 + \theta(\alpha\tilde{\eta} + 1)$ , with  $0 \leq \theta \leq 1$ , the system Eq. (4.1) yields

$$\begin{aligned}\tilde{\eta}_{\tilde{t}} + \tilde{u}_{\tilde{x}}^\theta + \alpha\tilde{\Gamma}\tilde{\eta}\tilde{\eta}_{\tilde{x}} + \alpha(\tilde{\eta}\tilde{u}^\theta)_{\tilde{x}} + \frac{\beta}{2}(\theta^2 - \frac{1}{3})\frac{\partial^3\tilde{u}^\theta}{\partial\tilde{x}^3} &= \mathcal{O}(\alpha\beta, \beta^2), \\ \tilde{u}_{\tilde{t}}^\theta + \tilde{\eta}_{\tilde{x}} + \alpha\tilde{u}^\theta\tilde{u}_{\tilde{x}}^\theta - \tilde{\Gamma}\tilde{u}_{\tilde{x}}^\theta + \frac{\beta}{2}(\theta^2 - 1)\frac{\partial^3\tilde{u}^\theta}{\partial\tilde{x}^2\partial\tilde{t}} - \frac{\beta}{2}(\theta^2 - \frac{1}{3})\tilde{\Gamma}\frac{\partial^3\tilde{u}^\theta}{\partial\tilde{x}^3} &= \mathcal{O}(\alpha\beta, \beta^2).\end{aligned}\quad (4.3)$$

Now for any real  $\lambda$  and  $\mu$ , the above system is a special case of the more

general system

$$\begin{aligned} \tilde{\eta}_{\tilde{t}} + \tilde{u}_{\tilde{x}}^\theta + \alpha \tilde{\Gamma} \tilde{\eta} \tilde{\eta}_{\tilde{x}} + \alpha (\tilde{\eta} \tilde{u}^\theta)_{\tilde{x}} + \frac{\beta}{2} (\theta^2 - \frac{1}{3}) \lambda \tilde{u}_{\tilde{x}\tilde{x}\tilde{x}}^\theta \\ - \frac{\beta}{2} (\theta^2 - \frac{1}{3}) (1 - \lambda) \tilde{\eta}_{\tilde{x}\tilde{x}\tilde{t}} = \mathcal{O}(\alpha\beta, \beta^2), \\ \tilde{u}_{\tilde{t}}^\theta + \tilde{\eta}_{\tilde{x}} - \tilde{\Gamma} \tilde{u}_{\tilde{x}}^\theta + \alpha \tilde{u}^\theta \tilde{u}_{\tilde{x}}^\theta - \frac{\beta}{2} (\theta^2 - \frac{1}{3}) \tilde{\Gamma} \frac{\partial^3 \tilde{u}^\theta}{\partial \tilde{x}^3} + \frac{\beta}{2} (\theta^2 - 1) \mu \tilde{\Gamma} \frac{\partial^3 \tilde{u}^\theta}{\partial \tilde{x}^3} \\ - \frac{\beta}{2} (\theta^2 - 1) \mu \frac{\partial^3 \tilde{\eta}}{\partial \tilde{x}^3} + \frac{\beta}{2} (\theta^2 - 1) (1 - \mu) \frac{\partial^3 \tilde{u}^\theta}{\partial \tilde{x}^2 \partial \tilde{t}} = \mathcal{O}(\alpha\beta, \beta^2). \end{aligned} \quad (4.4)$$

The functions  $\tilde{v}$  and  $\tilde{u}^\theta$  are related by

$$\tilde{v} = \tilde{u}^\theta + \frac{\beta}{2} \theta^2 \frac{\partial^2 \tilde{u}^\theta}{\partial \tilde{x}^2} + \mathcal{O}(\alpha\beta, \beta^2). \quad (4.5)$$

As shown in paper D, the KdV equation can be derived from (4.3) by assuming a certain relationship between  $\tilde{v}$  and  $\eta$  which determines waves that mainly travel in the direction of increasing values of  $x$ . Differentiating the equation for  $\phi$  gives horizontal and vertical velocities at an arbitrary level in fluid. After neglecting the second-order term, the dimensional form of the velocities are given by

$$\begin{aligned} u &= \frac{\sqrt{gh_0}}{h_0} \left\{ \tilde{c}_+ \eta + \frac{-1}{2(2\tilde{c}_+ + \tilde{\Gamma})} \frac{\eta^2}{h_0} + \frac{1 + 3\tilde{c}_+^2}{6(2\tilde{c}_+ + \tilde{\Gamma})} h_0^2 \eta_{xx} \right. \\ &\quad \left. - \frac{\tilde{c}_+}{2} h_0^2 (1 + \frac{z}{h_0})^2 \eta_{xx} \right\}, \\ w &= -\sqrt{gh_0} \tilde{c}_+ \eta_x \left\{ 1 + \frac{z}{h_0} \right\}, \end{aligned} \quad (4.6)$$

where  $\tilde{c}_+ = \frac{-\tilde{\Gamma}}{2} + \sqrt{\frac{\tilde{\Gamma}^2}{4} + 1}$ , and  $\tilde{c}_- = \frac{-\tilde{\Gamma}}{2} - \sqrt{\frac{\tilde{\Gamma}^2}{4} + 1}$  as the conjugate of  $\tilde{c}_+$ . This approximate velocity field is valid to the same order as the KdV equation describing the excursion of the free surface with constant vorticity. The new non-dimensional variables are defined by

$$\begin{aligned} x &= h_0 x, \quad z = h_0 z, \quad \eta = h_0 \eta, \quad t = \frac{h_0}{\sqrt{gh_0}} t, \quad u = \sqrt{gh_0} u \\ \text{and} \quad \Gamma &= \frac{\Gamma \sqrt{gh_0}}{h_0}. \end{aligned} \quad (4.7)$$

Then Eq. (4.6) can be rewritten in terms of new variables as

$$\begin{aligned} u &= c_+ \eta + \frac{-1}{2(2c_+ + \Gamma)} \eta^2 + \frac{1 + 3c_+^2}{6(2c_+ + \Gamma)} \eta_{xx} - c_+ \frac{1}{2} (1 + z)^2 \eta_{xx}, \\ w &= -c_+ \eta_x (1 + z). \end{aligned} \quad (4.8)$$

The KdV equation in the presence of shear flow can then be rewritten in terms of new variables as

$$\eta_t + c_+ \eta_x + \frac{c_+(3 + \Gamma^2)}{(1 + c_+^2)} \eta \eta_x + \frac{c_+^3}{3(1 + c_+^2)} \eta_{xxx} = 0, \quad (4.9)$$

where  $c_+ = \frac{-\Gamma}{2} + \sqrt{\frac{\Gamma^2}{4} + 1}$ .

The expression for the horizontal velocity of a fluid particle in the presence of the shear flow is given in non-dimensional variables as

$$\begin{aligned} U(x, z, t) = c_+ \eta + \frac{-1}{2(2c_+ + \Gamma)} \eta^2 + \frac{1 + 3c_+^2}{6(2c_+ + \Gamma)} \eta_{xx} \\ - c_+ \frac{1}{2} (1 + z)^2 \eta_{xx} + z\Gamma. \end{aligned} \quad (4.10)$$

Since the horizontal component of the particle velocity has been found approximately, it may be compared to the local phase velocity of the wave. As we mentioned already this leads to one of the most fundamental breaking criteria used in the literature, thus, kinematic breaking criterion. It is shown in paper D that for both the solitary wave and the periodic travelling waves, there are critical wave heights for which the horizontal component of the particle velocity matches the phase velocity of the wave.

## 4.1 Cnoidal wave solutions

In this subsection, the cnoidal wave solution of the KdV equation (4.9) is derived. A cnoidal wave is an exact periodic traveling-wave solution of the KdV equation, first derived by Korteweg and de Vries in 1895 [36]. Such a wave describes a surface wave whose wavelength is large compared to the water depth.

We seek for a solution of Eq. (4.9) in the form of a single-phase travelling wave of a permanent shape,

$$\eta(x, t) = \eta(\xi), \quad (4.11)$$

where  $\xi = x - ct$  is the travelling phase and  $c$  is the phase velocity. Using these solutions in the KdV equation (4.9), the following ordinary differential equation is obtained:

$$-c\eta_\xi + c_+ \eta_\xi + \frac{c_+(3 + \Gamma^2)}{(1 + c_+^2)} \eta \eta_\xi + \frac{c_+^3}{3(1 + c_+^2)} \eta_{\xi\xi\xi} = 0. \quad (4.12)$$

We then integrate once:

$$(-c + c_+) \eta + \frac{c_+(3 + \Gamma^2)}{(1 + c_+^2)} \frac{\eta^2}{2} + \frac{c_+^3}{3(1 + c_+^2)} \eta \xi \xi = D_1, \quad (4.13)$$

where  $D_1$  is an integration constant. We multiply by  $\eta_\xi$  and integrate again:

$$(-c + c_+) \frac{\eta^2}{2} + \frac{c_+(3 + \Gamma^2)}{(1 + c_+^2)} \frac{\eta^3}{6} + \frac{c_+^3}{3(1 + c_+^2)} \frac{\eta_\xi^2}{2} = D_1 \eta + D_2, \quad (4.14)$$

where  $D_2$  is a second integration constant. Introducing a function  $f(\eta)$  leads to:

$$\begin{aligned} \frac{c_+^2}{(3 + \Gamma^2)} \eta_\xi^2 &= -\eta^3 + 3(c - c_+) \eta^2 \frac{(2c_+ + \Gamma)}{(3 + \Gamma^2)} \\ &\quad + \frac{6(1 + c_+^2)}{c_+(3 + \Gamma^2)} (D_1 \eta + D_2) = f(\eta). \end{aligned} \quad (4.15)$$

First, we consider the case with  $\eta(\xi)$  in Eq. (4.15) having three real distinct roots  $\eta_1, \eta_2$  and  $\eta_3$  which are arranged in the order  $\eta_3 < \eta_2 < \eta_1$ . Then  $f(\eta)$  can be written as:

$$f(\eta) = -(\eta - \eta_1)(\eta - \eta_2)(\eta - \eta_3). \quad (4.16)$$

It follows from equation (4.15) that only real values for the slope exist if  $f(\eta)$  is positive. Since  $f(\eta)$  is positive,  $\eta$  oscillates between the endpoints  $\eta_1$  and  $\eta_2$  and the period of oscillations is

$$\xi = \pm \sqrt{\frac{4(1 - \Gamma c_+)}{3 + \Gamma^2}} \frac{1}{\eta_1 - \eta_3} \int_0^\psi \frac{d\hat{\psi}}{\sqrt{1 - m \sin^2 \hat{\psi}}}, \quad (4.17)$$

where

$$m = \frac{\eta_1 - \eta_2}{\eta_1 - \eta_3}, \quad 0 \leq m \leq 1. \quad (4.18)$$

Equation (4.15) is integrated in terms of the Jacobian elliptic cosine function  $\text{cn}$  to give

$$\eta = \eta_2 + (\eta_1 - \eta_2) \text{cn}^2(\mathcal{B}). \quad (4.19)$$

The argument  $\mathcal{B} = \sqrt{\frac{(3 + \Gamma^2)}{4(1 - c_+ \Gamma)}} (\eta_1 - \eta_3)^{1/2} (x - ct)$ ,  $\text{cn}$  is one of the Jacobian elliptic functions defined by the incomplete elliptic integral of the first kind [37]. The phase speed of the wave is

$$c = c_+ + \frac{(3 + \Gamma^2)}{3(2c_+ + \Gamma)} (\eta_1 + \eta_2 + \eta_3), \quad (4.20)$$

and the wavelength is given by

$$\lambda = 4 \sqrt{\frac{(1 - c_+ \Gamma)}{(3 + \Gamma^2)}} K(m) \frac{1}{\sqrt{\eta_1 - \eta_3}}, \quad (4.21)$$

where  $K(m)$  is the complete elliptic integral of the first kind.

## 4.2 Solitary wave solutions

To get solitary wave solutions, we introduce boundary conditions as follows

$$\eta, \eta', \eta'' \rightarrow 0 \quad \text{as } \xi \rightarrow \infty, \quad (4.22)$$

which lead to  $D_1 = D_2 = 0$ . Hence, Eq. (4.15) becomes:

$$\eta_\xi = \eta \sqrt{\left( c - c_+ \right) \frac{3(2c_+ + \Gamma)}{(1 - c_+ \Gamma)} - \frac{(3 + \Gamma^2)}{(1 - c_+ \Gamma)} \eta}. \quad (4.23)$$

By separation of variables we may write

$$\int \frac{d\eta}{\eta \sqrt{\left( c - c_+ \right) \frac{3(2c_+ + \Gamma)}{(1 - c_+ \Gamma)} - \frac{(3 + \Gamma^2)}{(1 - c_+ \Gamma)} \eta}} = \pm \int d\xi. \quad (4.24)$$

Then the solitary wave solution is given by:

$$\eta = H \operatorname{sech}^2 \left( \sqrt{\frac{(3 + \Gamma^2)H}{4(1 - c_+ \Gamma)}} (x - ct) \right), \quad (4.25)$$

where  $H$  is the wave amplitude, and

$$c = c_+ + \frac{(3 + \Gamma^2)H}{3(\Gamma + 2c_+)}, \quad (4.26)$$

is the phase velocity. In order to have a real solution the quantity  $c$  must be a positive number. As it is easily seen from (4.26) for  $c > 0$ , the solitary wave moves to the right.

## 4.3 Particle trajectories

Take the functions  $\xi(t)$  and  $\zeta(t)$  to describe the  $x$  and  $z$ -coordinates, respectively, of a particle originally located at the point  $(x, z) = (\xi_0, \zeta_0)$ . Then

dynamical system is recast in the form

$$\begin{aligned}\frac{\partial \xi}{\partial t} &= u(\xi(t), \zeta(t), t) + \zeta \Gamma, \\ \frac{\partial \zeta}{\partial t} &= w(\xi(t), \zeta(t), t), \\ (\xi(0), \zeta(0)) &= (\xi_0, \zeta_0),\end{aligned}\tag{4.27}$$

where now the effect of an underlying shear-flow has been added. Finally, the particle trajectories are found by numerically integrating the dynamical system (4.27) using the fourth-order Runge-Kutta method.

### 4.3.1 Particle trajectories in solitary-wave solutions

For the solitary wave solution of the equation (4.9), the relation (4.8) gives the horizontal and vertical velocities at an arbitrary point  $(x, z)$  in the fluid, at a time  $t$  as

$$\begin{aligned}u &= \eta_0 \operatorname{sech}^2 \mathcal{A} \left\{ c_+ - \frac{1}{2(2c_+ + \Gamma)} \eta_0 \operatorname{sech}^2 \mathcal{A} \right. \\ &\quad \left. + \frac{(3 + \Gamma^2)\eta_0}{4(1 - c_+\Gamma)} \left( \frac{1 + 3c_+^2}{6(2c_+ + \Gamma)} - \frac{c_+}{2}(1 + z)^2 \right) (4 - 6 \operatorname{sech}^2 \mathcal{A}) \right\}, \\ w &= c_+(\eta_0)^{3/2} \sqrt{\frac{(3 + \Gamma^2)}{1 - (c_+\Gamma)}} (1 + z) \operatorname{sech}^2 \mathcal{A} \tanh \mathcal{A},\end{aligned}\tag{4.28}$$

where the argument  $\mathcal{A}(x, t) = \sqrt{\frac{(3 + \Gamma^2)\eta_0}{4(1 - c_+\Gamma)}} (x - ct)$ .

In Figs. 4.2 and 4.3, examples of particle trajectories are shown during the propagation of a surface solitary wave of amplitude 0.2. The particle paths illustrated in Figs. 4.2 and 4.3 are approximate numerical solutions of the dynamical system (4.27), where the vector fields is given in Eq. (4.28), obtained with the fourth-order Runge-Kutta method. The fluid particle locations at the three different times where the wave profile and the particle locations are color coded in Figs. 4.2 and 4.3; the light-gray curve indicates the particle positions at the initial time  $t = 0$ ; the dark-gray curve indicates the particle positions at the middle time; the black curve indicates the particle positions at the final time. The fluid particles move to the right and upwards for the case of favorable vorticity ( $\Gamma \leq 0$ ). For  $\Gamma > 0$ , the fluid particles close to the bottom move to the left and upwards, since close to the bottom the particles have lower vertical movement and only have shear influence.

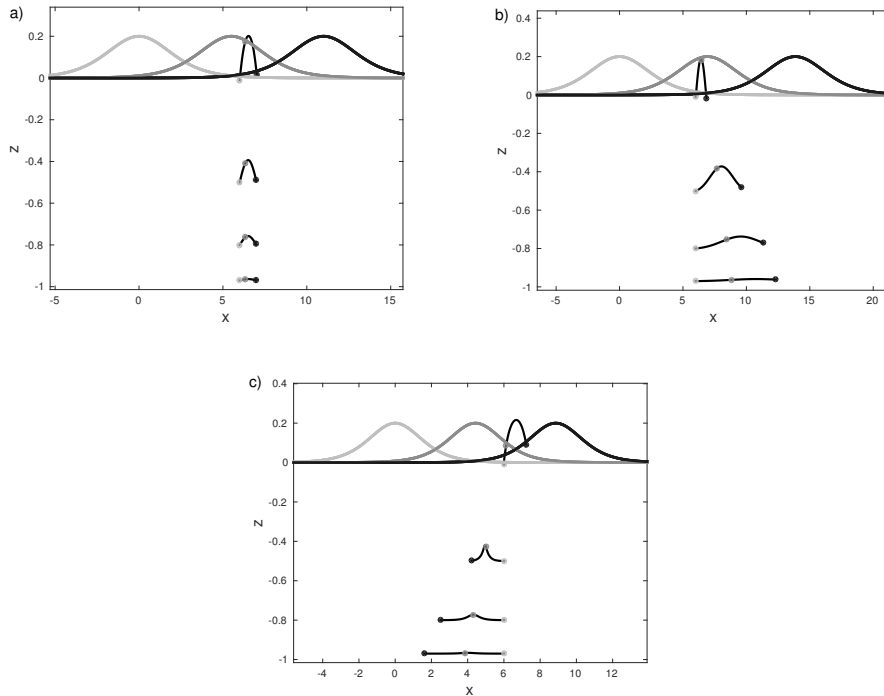


Figure 4.2: The waves of amplitude 0.2 are shown at time  $t = 0$  (light-gray),  $t = 5$  (dark-gray),  $t = 10$  (black). The wave crest is initially located at  $x = 0$ . The path of the fluid particles  $(\xi(t), \zeta(t))$  of (4.27) initially located at  $(6, -0.97)$ ,  $(6, -0.8)$ ,  $(6, -0.5)$  and  $(6, -0.01)$  are shown different cases (a) $\Gamma = 0$  ; (b)  $\Gamma = -0.5$  ; (c)  $\Gamma = 0.5$ . The particle locations at three instances where the wave profile is shown are color coded. The light-gray dot indicates the particle positions at time  $t = 0$ . The dark-gray dot indicates the particle positions at time  $t = 5$ . The black dot indicates the particle positions at time  $t = 10$ .

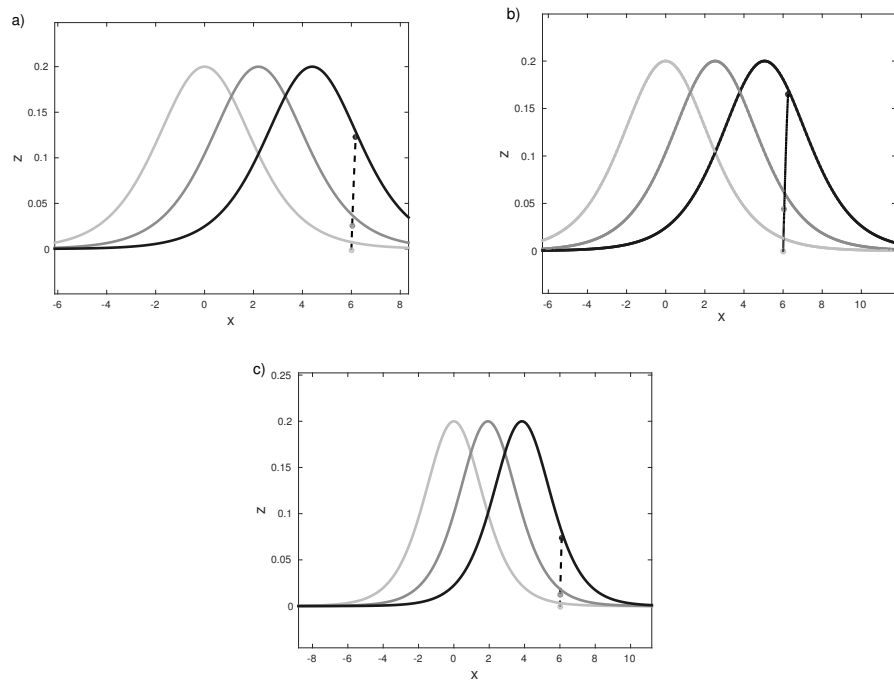


Figure 4.3: The waves of amplitude 0.2 are shown at time  $t = 0$  (light-gray),  $t = 2$  (dark-gray),  $t = 4$  (black). The wave crest is initially located at  $x = 0$ . The path of the fluid particles  $(\xi(t), \zeta(t))$  of (4.27) initially located at  $(6, -0.01)$  for different cases of vorticity (a)  $\Gamma = 0$ ; (b)  $\Gamma = -0.3$ ; (c)  $\Gamma = 0.3$  are shown. The particle locations at three instances where the wave profile is shown are color coded. The light-gray curve indicates the particle positions at time  $t = 0$ . The dark-gray curve indicates the particle positions at time  $t = 2$ . The black curve indicates the particle positions at time  $t = 4$ .

### 4.3.2 Particle trajectories in periodic-wave solutions

We now consider the particle paths in the fluid flow due to the propagation of periodic travelling waves at the surface. The KdV equation (4.9) admits the following solution in terms of cnoidal functions:

$$\eta = \eta_2 + (\eta_1 - \eta_2) \operatorname{cn}^2(\mathcal{B}), \quad (4.29)$$

where the solution is defined by the three constants  $\eta_1, \eta_2$  and  $\eta_3$  which are arranged in the order  $\eta_3 < \eta_2 < \eta_1$ . The argument  $\mathcal{B} = \sqrt{\frac{(3+\Gamma^2)}{4(1-c_+\Gamma)}}(\eta_1 - \eta_3)^{1/2}(x-ct)$ ,  $\operatorname{cn}$  is one of the Jacobian elliptic functions defined by the incomplete elliptic integral of the first kind [37] and the modulus of  $\operatorname{cn}$  is given by  $m = (\eta_1 - \eta_2)/(\eta_1 - \eta_3)$ . The phase speed of the wave is  $c = c_+ + \frac{(3+\Gamma^2)}{3(\Gamma+2c_+)}(\eta_1 + \eta_2 + \eta_3)$  and the wavelength is given by  $\lambda = 4\sqrt{\frac{(1-c_+\Gamma)}{(3+\Gamma^2)}}K(m)\frac{1}{\sqrt{\eta_1 - \eta_3}}$ , where  $K(m)$  is the complete elliptic integral of the first kind. Using the relation (4.8), the horizontal and vertical velocities may be written in terms of the Jacobian elliptic functions  $\operatorname{cn}$ ,  $\operatorname{sn}$  and  $\operatorname{dn}$  as

$$\begin{aligned} u &= c_+(\eta_2 + (\eta_1 - \eta_2)\operatorname{cn}^2(\mathcal{B})) + \frac{-1}{2(2c_+ + \Gamma)}(\eta_2 + (\eta_1 - \eta_2)\operatorname{cn}^2(\mathcal{B}))^2 \\ &\quad + \frac{(3 + \Gamma^2)}{2(1 - c_+\Gamma)}(\eta_1 - \eta_3)(\eta_1 - \eta_2) \left( \frac{1 + 3c_+^2}{6(2c_+ + \Gamma)} - \frac{c_+}{2}(1 + z)^2 \right), \\ &\quad (\operatorname{sn}^2(\mathcal{B})\operatorname{dn}^2(\mathcal{B}) - \operatorname{cn}^2(\mathcal{B})\operatorname{dn}^2(\mathcal{B}) + m\operatorname{sn}^2(\mathcal{B})\operatorname{cn}^2(\mathcal{B})) \\ w &= c_+(1 + z)\sqrt{\frac{(3 + \Gamma^2)}{(1 - c_+\Gamma)}}(\eta_1 - \eta_2)(\eta_1 - \eta_3)^{1/2}\operatorname{cn}(\mathcal{B})\operatorname{sn}(\mathcal{B})\operatorname{dn}(\mathcal{B}). \end{aligned} \quad (4.30)$$

Some examples of particle trajectories during the propagation of a cnoidal wave are presented in Figs. 4.5 and 4.4. The particle paths with different vorticity values are shown for different depths in Fig. 4.4. It is noted that from the lower panel of Fig. 4.4 that for particles closer to the bottom the wave effect diminishes and therefore, the effect due to the vorticity become dominant. This result is similar to the results of particle paths beneath solitary waves.

The particle trajectories during one complete periodic cnoidal wave cycle with  $m = 0.99$  (nearly solitary) and  $H = \eta_1 - \eta_2 = 0.2$  for different vorticity values  $\Gamma = 0, -0.1$  and  $0.1$  are plotted in Fig. 4.5. The fluid particles are located initially below the trough and the crest and the crest of the wave is centered at  $x = 0$ . The particle paths are not closed in the presence of the vorticity  $\Gamma \leq 0$ . For  $\Gamma > 0$  the particle paths are orbit loops.

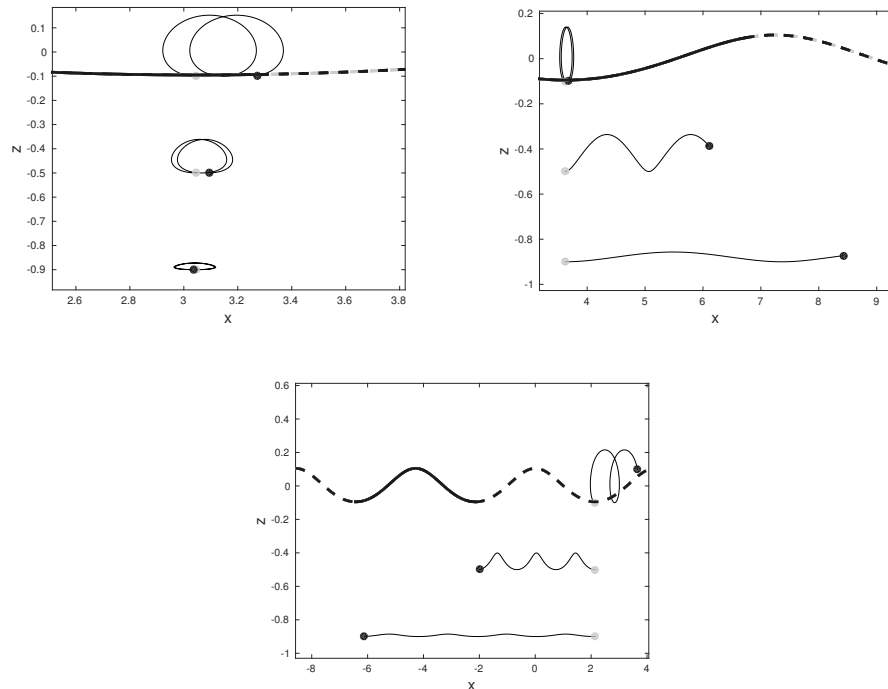


Figure 4.4: The left upper panel shows the periodic wave with amplitude 0.2, wavelength 6.0926, period 7.3850, phase speed 0.825 and  $\Gamma = 0$  at  $t = 0$  (light-gray) and  $t = 14.77$  (black). The right upper panel shows the periodic wave with amplitude 0.2, wavelength 7.2412, period 6.9691, phase speed 1.0391 and  $\Gamma = -0.4$  at  $t = 0$  (light-gray) and  $t = 13.9381$  (black). The lower panel shows the periodic wave with amplitude 0.2, wavelength 4.2834, period 7.6998, phase speed 0.5563 and  $\Gamma = 0.6$  at  $t = 0$  (light-gray) and  $t = 15.3996$  (black). The initial particle locations at the three cases are shown in light-gray curve. All particles are initially at  $x_0 = \text{wavelength}/2 - 0.001$  and depth  $z_0 = -0.1, -0.5$  and  $-0.9$ .

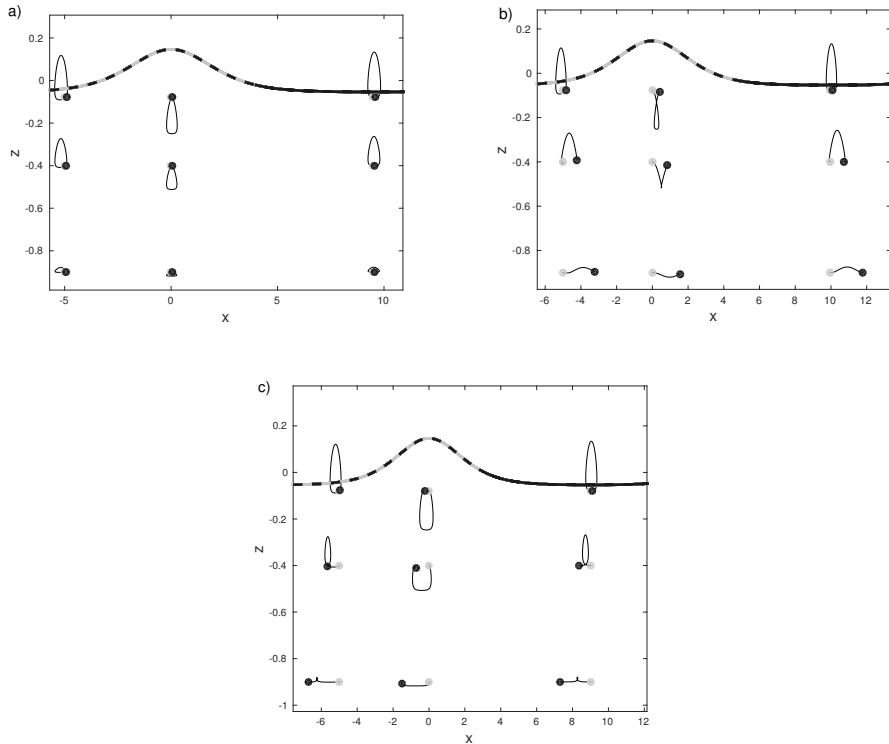


Figure 4.5: The left upper panel shows the periodic wave with amplitude 0.2, wavelength 18.9885, period 18.6397, phase speed 1.0187 and  $\Gamma = 0$  at  $t = 0$  (light-gray) and  $t = 18.6397$  (black). The right upper panel shows the periodic wave with amplitude 0.2, wavelength 19.9285, period 18.6248, phase speed 1.07 and  $\Gamma = -0.1$  at  $t = 0$  (light-gray) and  $t = 18.6248$  (black). The lower panel shows the periodic wave with amplitude 0.2, wavelength 18.0328, period 18.5905, phase speed 0.97 and  $\Gamma = 0.1$  at  $t = 0$  (light-gray) and  $t = 18.5905$  (black). The paths of fluid particles are located at  $x, z$  where initial  $x$ -coordinate are  $x = -5, 0$  and wavelength/2 - 0.001 and depth  $z = -0.9, -0.4$  and  $-0.078$ .

## 4.4 Breaking criterion

As explained in the introduction, if the horizontal velocity near the crest of a wave exceeds the speed of the wave, then the wave break occurs. Let us denote propagation speed by  $c$  and horizontal velocity by  $U$ . The horizontal velocity  $U$  can be obtained from (4.10) and wave breaking occurs if

$$c_+ \eta + \frac{-1}{2(2c_+ + \Gamma)} \eta^2 + \frac{1 + 3c_+^2}{6(2c_+ + \Gamma)} \eta_{xx} - c_+ \frac{1}{2} (1 + z)^2 \eta_{xx} + z\Gamma > c.$$

Using appropriate wave solutions ( $\eta(x, t)$ ) of the KdV equation (4.9), one can find the critical wave heights where the horizontal component of the particle velocity matches the phase velocity of the wave in the presence of uniform shear flow shown in Fig. 4.1.

In paper D, the critical waveheights for the solitary and cnoidal wave solutions of the KdV equation (4.9) are studied using kinematic breaking criterion (4.31).

## 4.5 Further work

In the paper C, the study focused on particles as passive tracers in the water flow. Another possible study would be the motion of point vortices placed underneath a free surface. As this study is devoted to one-dimensional cases, it should be possible to extend it to the two-dimensional case. It would also be interesting to look at higher-order models such as the fully nonlinear models.



# Bibliography

- [1] G. B. Airy, Tides and waves, *Encyclopedia Metropolitana*, 1845, **192**, 241–396.
- [2] A. Ali and H. Kalisch, Mechanical balance laws for Boussinesq models of surface water waves, *J. Nonlinear Sci.*, 2012, **22**, 371–398.
- [3] A. Ali and H. Kalisch, On the formation of mass, momentum and energy conservation in the KdV equation, *Acta Appl. Math.*, 2014, **133**, 113–131.
- [4] T. B. Benjamin, The solitary wave on a stream with an arbitrary distribution of vorticity, *J. Fluid Mech.*, 1962, **12** (1), 97–116.
- [5] T. B. Benjamin, J. B. Bona and J. J. Mahony, Model equations for long waves in nonlinear dispersive systems, *Philos. T. Roy. Soc. A*, 1972, **272**, 47–78.
- [6] M. Bjørkavåg and H. Kalisch, Wave breaking in Boussinesq models for undular bores, *Phys. Lett. A*, 2011, **375** (14), 1570–1578.
- [7] J. L. Bona, M. Chen and J. C. Saut, Boussinesq equations and other systems for small-amplitude long waves in nonlinear dispersive media. I: Derivation and linear theory, *J. Nonlinear sci.*, 2002, **12** (4), 283–318.
- [8] J. Boussinesq, Théorie de l'intumescence liquide appelée “onde solitaire” ou “de translation”, se propageant dans un canal rectangulaire, *C. R. Acad. Sci. Paris*, 1871, **72**, 755–759.
- [9] J. Boussinesq, Théorie des ondes et des remous qui se propagent le long d'un canal rectangulaire horizontal, en communiquant au liquide contenu dans ce canal des vitesses sensiblement pareilles de la surface au fond, *J. Math. Pures Appl.*, 1872, **17**, 55–108.
- [10] M. K. Brun and H. Kalisch, Convective wave breaking in the KdV equation, *arXiv:1603.09104 [physics.flu-dyn]*, 2016.

- [11] J. C. Burns, Long waves in running water, *Mathematical Proceedings of the Cambridge Philosophical Society*, 1953, **49**(4), 695–706.
- [12] F. E. Camfield and R. L. Street, Shoaling of solitary waves on small slopes, *J. Waterw. Harb. Coast. Eng.*, 1969, **95** (1), 1–22.
- [13] M. Chen, Exact solutions of various Boussinesq systems, *Appl. Math. Lett.*, 1998, **11** (5), 45–49.
- [14] M. Chen, Equations for bi-directional waves over an uneven bottom, *Math. Comput. Simulat.*, 2003, **62** (1-2), 3–9.
- [15] W. Choi, Strongly nonlinear long gravity waves in uniform shear flows, *Physical review E*, 2003, **68**.
- [16] C. R. Chou and K. Quyang, The deformation of solitary waves on steep slopes, *J. Chin. Inst. Eng.*, 1999, **22** (6), 805–812.
- [17] C. R. Chou and K. Quyang, Breaking of solitary waves on uniform slopes, *China Ocean Eng.*, 1999, **13** (4), 429–442.
- [18] C. R. Chou, R. S. Shih and J. Z. Yim, Numerical study on breaking criteria for solitary waves, *China Ocean Eng.*, 2003, **17** (4), 589–604.
- [19] A. Constantin and W. Strauss, Pressure beneath a Stokes wave, *Comm. Pure Appl. Math.*, **63** (4), 2010, 533–557.
- [20] P. G. Drazin and R. S. Johnson, Solitons: an introduction, *Cambridge University Press*, 1989.
- [21] J. H. Duncan, Spilling breakers, *Annu. Rev. Fluid Mech.*, 2001, **33**, 519–547.
- [22] N. C. Freeman and R. S. Johnson, Shallow water waves on shear flow, *J. Fluid Mech.*, 1970, **42** (2), 401–409.
- [23] D. Gottlieb and S. A. Orszag, Numerical Analysis of Spectral Methods: Theory and applications, *SIAM, Philadelphia*, 1977.
- [24] A. E. Green and P. M. Naghdi, A derivation of equations for wave propagation in water of variable depth, *J. Fluid Mech.*, 1976, **78** (2), 237–246.
- [25] S. T. Grilli, R. Subramanya, I. A. Svendsen and J. Veeramony, Shoaling of solitary waves on plane beaches, *J. Waterw. Port C-ASCE*, 1994, **120**, 609–628.

- [26] S. T. Grilli, I.A. Svendsen and R. Subramanya, Breaking criterion and characteristics for solitary waves on slopes, *J. Waterw. Port C-ASCE*, 1997, **123**, 102–112.
- [27] R. Grimshaw, The solitary wave in water of variable depth, *J. Fluid Mech.*, 1970, **42**, 639–656.
- [28] R. Grimshaw, The solitary wave in water of variable depth. Part 2, *J. Fluid Mech.*, 1971, **46**, 611–622.
- [29] M. Y. Hussaini, D. A. Kopriva and A. T. Patera, Spectral collocation Method, *Applied Numerical Mathematics* 5, 1989, 177-208.
- [30] A. T. Ippen and G. Kulin, The shoaling and breaking of the solitary wave, *Coast. Eng. Proc.*, 1954, No 5, 27–47.
- [31] R. S. Johnson, On the development of a solitary wave moving over uneven bottom, *Proc. Cambridge Philos. Soc.*, 1973, **73**, 183–203.
- [32] H. Kalisch and A. Senthilkumar, Derivation of Boussinesq's shoaling law using a coupled BBM system, *Nonlin. Processes Geophys.*, 2013, **20**, 213–219.
- [33] A. B. Kennedy, Q. Chen, J. T. Kirby, and R. A. Dalrymple, Boussinesq modeling of wave transformation, breaking, and runup. I: 1D, *J. Waterw. Port C-ASCE*, 2000, **126**, 39–47.
- [34] Z. Khorsand and H. Kalisch, On the shoaling of solitary waves in the KdV equation, *Coast. Eng. Proc.*, 2014, **34**, waves 44.
- [35] T. Kishi and H. Saeki, The shoaling, breaking and runup of the solitary wave on impermeable rough slope, *Coast. Eng. Proc.*, 2011, **10**, 322-347.
- [36] D. J. Korteweg and G. de Vries, On the change of form of long waves advancing in a rectangular channel, and on a new type of long stationary wave, *Phil. Mag.*, 1895, **39(5)**, 422–443.
- [37] D. F. Lawden, Elliptic functions and applications, *Springer, New York*, 1989.
- [38] M. S. Longuet-Higgins, On the mass, momentum, energy and circulation of a solitary wave, I, *Proc. Roy. Soc. A.*, 1974, **337**, 1–13.
- [39] M. S. Longuet-Higgins and J. D. Fenton, On the mass, momentum,energy and circulation of a solitary wave. II, *Proc. Roy. Soc. A.*, 1974, **340**, 471–493.

- [40] O. S. Madsen and C. C. Mei, The Transformation of a solitary wave over an uneven bottom, *J. Fluid Mech.*, 1969, **39**, 781–791.
- [41] P. A. Madsen, R. Murray and O. R. Sørensen, A new form of the Boussinesq equations with improved linear dispersion characteristics, *Coast. Eng.*, 1991, **15** (4), 371–388.
- [42] P. A. Madsen and H. A. Schäffer, Higher-order Boussinesq-type equations for surface gravity waves: derivation and analysis, *Philos. T. Roy. Soc. A.*, 1998, **356**, 3123–3184.
- [43] J. McCowan, On the highest wave of permanent type, *Philos. Mag.*, 1894, **38**, 351–357.
- [44] J. W. Miles, On the Korteweg–de Vries equation for a gradually varying channel, *J. Fluid Mech.*, 1979, **91**, 181–190.
- [45] D. E. Mitsotakis, Boussinesq systems in two space dimensions over a variable bottom for the generation and propagation of tsunami waves, *Math. Comput. Simulat.*, 2009, **80** (4), 860–873.
- [46] A. Nachbin, and R. Ribeiro-Junior, A boundary integral formulation for particle trajectories in Stokes waves, *Discrete and continuous dynamical systems*, 2014, **34** (8), 3135–3153.
- [47] H. M. Nepf, C. H. Wu and E. S. Chan, A comparison of two- and three-dimensional wave breaking, *J. Phys. Oceanogr.*, 1998, **28**, 1496–1510.
- [48] O. Nwogu, Alternative form of Boussinesq equations for nearshore wave propagation, *J. Waterw. Port C-ASCE*, 1993, **119**, 618–638.
- [49] L. A. Ostrovsky and E. N. Pelinovsky, Wave transformation on the surface of a fluid of variable depth, *Atmos. Oceanic Phys.*, 1970, **6**, 552–555.
- [50] E. N. Pelinovsky and T. G. Talipova, Height variations of large amplitude solitary waves in the near-shore zone, *Oceanology*, 1977, **17**, 1–3.
- [51] E. N. Pelinovsky and T. G. Talipova, Change of height of the solitary wave of large amplitude in the beach zone, *Mar. Geodesy*, 1979, **2** (4), 313–321.
- [52] D. H. Peregrine, Long waves on a beach, *J. Fluid Mech.*, 1967, **27**, 815–827.
- [53] Lord Rayleigh, On waves, *Phil. Mag.*, 1876, **1**, 257–279.

- [54] J. S. Russell, Report on waves, *Fourteenth meeting of the British Association for the Advancement of Science*, 1844.
- [55] A. Senthilkumar, BBM equation with non-constant coefficients, *Turk. J. Math.*, 2013, **37**, 652–664.
- [56] A. Senthilkumar, On the influence of wave reflection on shoaling and breaking solitary waves, *Proceedings of the Estonian Academy of Sciences*, 2016, **65** (4), 414–430.
- [57] J. J. Stoker, Water Waves. The Mathematical Theory with Applications, *New York: Interscience Publ. Inc.*, 1957.
- [58] G. Stokes, On the theory of oscillatory waves, *Transactions of the Cambridge Philosophical Society*, 1847, **8**, 441–455.
- [59] I. A. Svendsen, Introduction to nearshore hydrodynamics, *World Scientific, Singapore*, 2006.
- [60] C. E. Synolakis, The runup of solitary waves, *J. Fluid Mech.*, 1987, **185**, 523–545.
- [61] M. H. Teng and T. Y. Wu, Evolution of long water waves in variable channels, *J. Fluid Mech.*, 1994, **266**, 303–317.
- [62] R. Thomas, C. Kharif and M. Manna, A nonlinear Schroedinger equation for water waves on finite depth with constant vorticity, *Phys. Fluids*, 2012, **24** (12), doi: 10.1063/1.4768530.
- [63] L. N. Trefethen, Spectral methods in Matlab, *SIAM, Philadelphia*, 2000.
- [64] V. Vasan and K. Oliveras, Pressure beneath a traveling wave with constant vorticity, *Discrete Contin. Dyn. Syst.*, (2014) **34**, 3219–3239.
- [65] E. Wahlén, Hamiltonian long-wave approximations of water waves with constant vorticity, *Physics Letters A*, 2008, **372**(15), 2597–2602.
- [66] G. Wei, J. T. Kirby, S. T. Grilli and R. Subramanya, A fully nonlinear Boussinesq model for surface waves. Part 1. Highly nonlinear, unsteady waves, *J. Fluid Mech.*, 1995, **294**, 71–92.
- [67] G. Whitham, Linear and nonlinear waves, *Wiley-Interscience*, New York, 1974.
- [68] C. H. Wu and H. M. Nepf, Breaking criteria and energy losses for three-dimensional wave breaking, *J. Geophys. Res.*, 2002, **107**, 3177–3195

- [69] C. Yaosong, L. Guocan and J. Tao, Non-linear water waves on shearing flows, *Acta mechanics sinica*, 1994, **10** (2), 97–102.

## **Part II**

# **Included Papers**



## Paper A

# Derivation of Boussinesq's Shoaling Law Using a Coupled BBM System



# Derivation of Boussinesq's shoaling law using a coupled BBM system

H. Kalisch and A. Senthilkumar

Department of Mathematics, University of Bergen, Postbox 7800, 5020 Bergen, Norway

Correspondence to: H. Kalisch (henrik.kalisch@math.uib.no) and A. Senthilkumar (amutha.senthilkumar@math.uib.no)

Received: 30 November 2012 – Revised: 17 February 2013 – Accepted: 20 February 2013 – Published: 14 March 2013

**Abstract.** This paper is focused on finding rules for waveheight change in a solitary wave as it runs up a slowly increasing bottom. A coupled BBM system is used to describe the solitary waves. Expressions for energy density and energy flux associated with the BBM system are derived, and the principle of energy conservation is used to develop an equation relating the waveheight and undisturbed depth to the initial undisturbed depth and the incident waveheight. In the limit of zero waveheight, Boussinesq's shoaling law is recovered.

## 1 Introduction

The study of surface gravity waves is one of the classical problems in fluid mechanics and is of fundamental importance in coastal engineering. One particular case of interest, both theoretically and in practice, is the development of ocean waves as they propagate shorewards and experience a decrease in the water depth. A significant amount of work has been focused on this phenomenon, which is known as wave shoaling. The literature on the subject includes experimental studies in controlled environments in particular, such as wave flumes, and a large number of theoretical studies.

Among the first to study the problem was Boussinesq, who treated wave shoaling in the framework of his theory of weakly nonlinear long waves. Based on the assumption that the energy content of the wave is unchanged as it propagates, Boussinesq developed a simple rule for the waveheight change of a long wave as it runs up on a bottom slope. Suppose the initial undisturbed depth of the fluid is  $h_0$ , and the initial waveheight is denoted by  $H_0$ . If the local depth is denoted by  $h$ , and the associated waveheight is denoted by  $H$ , then Boussinesq's law can be written as

$H/H_0 = h_0/h$ . This law applies in the context of the so-called Boussinesq scaling, where the waveheight is small and the wavelength is long when compared to the initial undisturbed depth  $h_0$ . In the case where the effects on nonlinear steepening and of linear dispersion are approximately balanced, solitary waves can be found, and it appears that Boussinesq's law applies primarily to the shoaling of solitary waves. As explained in Miles (1980), Boussinesq's law has been rediscovered a number of times with varying degrees of rigor. Probably the most careful derivation was given in Grimshaw (1970, 1971), where Boussinesq's result actually follows from a more general analysis of the wave action principle. Indeed, Grimshaw (1971) studied the evolution of solitary waves in water of variable depth and he observed that for small values of initial waveheight, the shoaling rates are not exactly given by Boussinesq's law, but that they approach Boussinesq's law in the limit  $H_0 \rightarrow 0$ .

In the present paper, the Boussinesq law is derived using a different approach, which is based directly on Boussinesq's original assumption that energy is conserved as the wave shoals. Using this assumption, and a careful analysis of the energy density associated to a particular Boussinesq system featuring exact solitary-wave solutions, waveheight changes can be computed in a straightforward manner. The system used here is known as the coupled BBM system. The method used to find the associated energy density is an extension of the recent work Ali and Kalisch (2012) where approximations of energy density and flux in the context of the Boussinesq scaling were found. The computations actually show that for waves of finite waveheight, the shoaling rate is somewhat lower than Boussinesq's law suggests. However, in the limit of zero waveheight, Boussinesq's law is recovered. In this sense, the results are in line with the findings of Grimshaw (1971).

It should be noted that we do not incorporate an uneven bottom profile into the equations, but rather consider the transition of the wave on the slope as a gradual adjustment process of which only the initial and final states are considered. Since the effects of the bottom slope are only modeled indirectly, our analysis of wave shoaling using the conservation of energy depends strongly on the adiabatic approximation. In clear terms, it must be assumed that the wavelength  $l$  of the wave running up the slope is much smaller than the characteristic length  $h\Delta x/(h_0 - h)$  of the depth variation. If this is the case, then the wave undergoes an adiabatic change, and the relation between wavelength and wave amplitude stays approximately intact. If the bottom gradient is too large, then the wave will change character and violate the Boussinesq scaling as it runs up the slope. Moreover, larger slopes will lead to reflected waves and significant steepening and asymmetry of the main wave, and none of these figure into the present analysis.

Let us briefly introduce the model system to be used here. Assuming  $a$  is a typical amplitude and  $l$  is a typical wavelength of the waves to be described, the parameter  $\alpha = a/h_0$  represents the waveheight to depth ratio, and the parameter  $\beta = h_0^2/l^2$  represents a water depth to wavelength ratio. The Boussinesq scaling consists of the assumptions that nonlinearity is weak ( $\alpha \ll 1$ ), and dispersive effects are also weak ( $\beta \ll 1$ ), and the two parameters of the same order. In other words, the Stokes number  $S = \alpha/\beta$  should be  $\mathcal{O}(1)$ . In Bona et al. (2002), a general family of Boussinesq system was found, and one particular case is the coupled BBM system to be used in the present study. In the non-dimensional variables to be defined in Section 2, the system takes the form

$$\tilde{\eta}_t + \tilde{w}_{\tilde{x}} + \alpha(\tilde{\eta}\tilde{w})_{\tilde{x}} - \frac{1}{2}\left(\theta^2 - \frac{1}{3}\right)\beta\tilde{\eta}_{\tilde{x}\tilde{x}\tilde{t}} = \mathcal{O}(\alpha\beta, \beta^2), \quad (1)$$

$$\tilde{w}_t + \tilde{\eta}_{\tilde{x}} + \alpha\tilde{w}\tilde{w}_{\tilde{x}} - \frac{1}{2}(1-\theta^2)\beta\tilde{w}_{\tilde{x}\tilde{x}\tilde{t}} = \mathcal{O}(\alpha\beta, \beta^2). \quad (2)$$

Here  $\tilde{\eta}$  represents the non-dimensional excursion of the free surface, and  $\tilde{w}$  represents the non-dimensional horizontal velocity at a non-dimensional height  $0 \leq \theta \leq 1$  in the fluid column. Disregarding terms of order  $\mathcal{O}(\alpha^2, \alpha\beta, \beta^2)$  yields the evolution system governing the approximate dynamics of the flow. The point of view adopted in the present paper is that Eq. (1) represents an approximate mass conservation equation, and Eq. (2) represents approximate momentum conservation. Since energy conservation is not an independent principle in homogeneous fluids, it should be possible to express energy conservation in terms of the unknowns  $\tilde{\eta}$  and  $\tilde{w}$  of Eqs. (1) and (2). The approximate energy balance equation can be written in the form

$$\frac{\partial}{\partial \tilde{t}}\tilde{E}(\tilde{\eta}, \tilde{w}) + \frac{\partial}{\partial \tilde{x}}\tilde{q}_E(\tilde{\eta}, \tilde{w}) = \mathcal{O}(\alpha^2, \alpha\beta, \beta^2), \quad (3)$$

and the principal task is to find appropriate expressions for the energy density  $\tilde{E}(\tilde{\eta}, \tilde{w})$  and energy flux  $\tilde{q}_E(\tilde{\eta}, \tilde{w})$ . These quantities will be computed in Sect. 2. Section 3 is devoted

to the derivation of an approximate shoaling law, and Sect. 4 contains a brief discussion.

## 2 Energy balance

For an inviscid, incompressible fluid, the surface water-wave problem is given by the Euler equations with no-flow conditions at the bottom and kinematic and dynamic boundary conditions at the free surface. Let the spatial coordinates be  $(x, z)$  and the  $x$ -axis be oriented in the horizontal direction. Assume that the motion is uniform in the direction perpendicular to the  $xz$ -plane (long-crested waves). The gravitational acceleration  $g$  acts in the negative  $z$ -direction. Let  $\eta(x, t)$  denote the surface elevation, and let  $\phi(x, z, t)$  be the velocity potential.

From the incompressibility of the fluid, the potential  $\phi$  satisfies Laplace's equation in the domain  $\{(x, z) \in \mathbb{R}^2 | -h_0 < z < \eta(x, t)\}$ . The complete problem is written as follows.

$$\Delta\phi = 0 \quad \text{in } -h_0 < z < \eta(x, t), \quad (4)$$

$$\phi_z = 0 \quad \text{on } z = -h_0, \quad (5)$$

$$\left. \begin{aligned} \eta_t + \phi_x \eta_x - \phi_z &= 0, \\ \phi_t + \frac{1}{2}(\phi_x^2 + \phi_y^2) + g\eta &= 0, \end{aligned} \right\} \quad \text{on } z = \eta(x, t). \quad (6)$$

As the derivation of the coupled BBM-system is well known (see Bona et al., 2002 and Whitham, 1974), we only sketch the outline for the interested reader. Denote the limiting long-wave speed by  $c_0 = \sqrt{gh_0}$ , and define non-dimensional variables by

$$\tilde{x} = \frac{x}{l}, \quad \tilde{z} = \frac{z + h_0}{h_0}, \quad \tilde{\eta} = \frac{\eta}{a}, \quad \tilde{t} = \frac{c_0 t}{l}, \quad \tilde{\phi} = \frac{c_0 \phi}{gal}.$$

As explained by Whitham (1974), one may use the ansatz

$$\tilde{\phi} = \sum_{m=0}^{\infty} \tilde{f}_m(\tilde{x}, \tilde{t}) \tilde{z}^m \beta^m \quad (7)$$

to represent the non-dimensional velocity potential in terms of the unknown functions  $\tilde{f}_m(\tilde{x}, \tilde{t})$ . Now Laplace's equation and the bottom boundary condition Eq. (5) may be used to arrive at the expression

$$\tilde{\phi} = \tilde{f} - \frac{\tilde{z}^2}{2} \tilde{f}_{\tilde{x}\tilde{x}} \beta + \mathcal{O}(\beta^2), \quad (8)$$

where  $\tilde{f} = \tilde{f}_0$ . From Eq. (8) and the second boundary condition at the free surface, we have the relation

$$\tilde{\eta} + \tilde{f}_t - \frac{\beta}{2} \tilde{f}_{\tilde{x}\tilde{x}\tilde{t}} + \frac{\alpha}{2} \tilde{f}_{\tilde{x}}^2 = \mathcal{O}(\alpha\beta, \beta^2). \quad (9)$$

Differentiating Eq. (9) with respect to  $\tilde{x}$ , and inserting the expansion for  $\phi$  in the first boundary condition at the free

surface, Eq. (6) yields a system of equations in terms of the horizontal velocity at the bottom  $\tilde{v} = \tilde{v}_{\tilde{x}}$ . However, for the purposes of the present article, a different but equivalent system will have to be used. Denoting by  $\tilde{w}$  the non-dimensional horizontal velocity at a non-dimensional height  $0 \leq \theta \leq 1$  in the fluid column, elementary considerations (see Bona et al., 2002) show that  $\tilde{v}$  and  $\tilde{w}$  are related by

$$\tilde{v} = \tilde{w} + \frac{\beta}{2} \theta^2 \tilde{w}_{\tilde{x}\tilde{x}} + \mathcal{O}(\beta^3). \quad (10)$$

One may use Eq. (10) and the first-order relations  $\tilde{v}_{\tilde{t}} + \tilde{\eta}_{\tilde{x}} = \mathcal{O}(\alpha, \beta)$ ,  $\tilde{\eta}_{\tilde{t}} + \tilde{v}_{\tilde{x}} = \mathcal{O}(\alpha, \beta)$  to arrive at a general model system for small-amplitude long waves. The system is given in non-dimensional variables by

$$\begin{aligned} \tilde{\eta}_{\tilde{t}} + \tilde{w}_{\tilde{x}} + \alpha(\tilde{\eta}\tilde{w})_{\tilde{x}} + \frac{1}{2}\left(\theta^2 - \frac{1}{3}\right)\lambda\beta\tilde{w}_{\tilde{x}\tilde{x}\tilde{x}} \\ - \frac{1}{2}\left(\theta^2 - \frac{1}{3}\right)(1-\lambda)\beta\tilde{\eta}_{\tilde{x}\tilde{x}\tilde{t}} = \mathcal{O}(\alpha\beta, \beta^2), \end{aligned} \quad (11)$$

$$\begin{aligned} \tilde{w}_{\tilde{t}} + \tilde{\eta}_{\tilde{x}} + \alpha\tilde{w}\tilde{w}_{\tilde{x}} + \frac{1}{2}(1-\theta^2)\mu\beta\tilde{\eta}_{\tilde{x}\tilde{x}\tilde{x}} \\ - \frac{1}{2}(1-\theta^2)(1-\mu)\beta\tilde{w}_{\tilde{x}\tilde{x}\tilde{t}} = \mathcal{O}(\alpha\beta, \beta^2). \end{aligned} \quad (12)$$

Here  $\lambda$  and  $\mu$  are modeling parameters which have no physical meaning, but can be chosen arbitrarily in the range  $0 \leq \lambda, \mu \leq 1$ . Choosing in particular  $\lambda = 0$  and  $\mu = 0$  yields the coupled BBM system Eqs. (1) and (2).

In order to derive the associated energy balance equation, we need expressions for the velocity field and pressure. The velocity field is easily seen to be given by

$$\tilde{\phi}_{\tilde{x}} = \tilde{w} + \frac{\beta}{2}(\theta^2 - \tilde{z}^2)\tilde{w}_{\tilde{x}\tilde{x}} + \mathcal{O}(\beta^2), \quad (13)$$

$$\tilde{\phi}_{\tilde{z}} = -\tilde{z}\tilde{w}_{\tilde{x}}\beta + \mathcal{O}(\beta^2). \quad (14)$$

The dynamic pressure  $P'$ , which measures the deviation from hydrostatic pressure, is given quite generally by

$$P' = P - P_{\text{atm}} + \rho g z = -\rho\phi_t - \frac{\rho}{2}|\nabla\phi|^2.$$

We use the scaling  $\rho g a \tilde{P}' = P'$ . Then as shown by Ali and Kalisch (2012), the dynamic pressure can be found with the help of Eq. (9) to be

$$\tilde{P}' = \tilde{\eta} + \frac{1}{2}\beta(\tilde{z}^2 - 1)\tilde{w}_{\tilde{x}\tilde{t}} + \mathcal{O}(\alpha\beta, \beta^2). \quad (15)$$

Next, we examine energy balance of the BBM system. If we assume that the potential energy of a particle is zero at the undisturbed free surface, and the potential energy is zero when no wave motion is present, then the total energy inside a control volume of unit width, delimited by the interval  $[x_1, x_2]$  on the lateral sides, and by the bottom and the free surface can be written as

$$E = \frac{1}{2} \int_{x_1}^{x_2} \int_{-h_0}^{\eta} \rho |\nabla\phi|^2 dz dx + \int_{x_1}^{x_2} \int_0^{\eta} \rho g z dz dx,$$

where the first term represents the kinetic energy, and the second term represents potential energy. The conservation of total mechanical energy (see Stoker, 1957, chap.1.) is written as

$$\begin{aligned} \frac{d}{dt} \frac{1}{2} \int_{x_1}^{x_2} \int_{-h_0}^{\eta} \rho |\nabla\phi|^2 dz dx + \frac{d}{dt} \int_{x_1}^{x_2} \int_0^{\eta} \rho g z dz dx \\ = \left[ \int_{-h_0}^{\eta} \left\{ \frac{\rho}{2} |\nabla\phi|^2 + \rho g z + P \right\} \phi_x dz \right]_{x_1}^{x_2}. \end{aligned}$$

Expressing the above relation in non-dimensional variables gives

$$\begin{aligned} \frac{d}{d\tilde{t}} \int_{x_1/l}^{x_2/l} \int_0^{1+\alpha\tilde{\eta}} \left\{ \frac{\alpha^2}{2} \left( \tilde{\phi}_{\tilde{x}}^2 + \frac{1}{\beta} \tilde{\phi}_{\tilde{z}}^2 \right) \right\} d\tilde{z} d\tilde{x} \\ + \frac{d}{d\tilde{t}} \int_{x_1/l}^{x_2/l} \int_1^{1+\alpha\tilde{\eta}} (\tilde{z} - 1) d\tilde{z} d\tilde{x} = \left[ \int_0^{1+\alpha\tilde{\eta}} \left\{ \frac{\alpha^3}{2} \left( \tilde{\phi}_{\tilde{x}}^3 + \frac{1}{\beta} \tilde{\phi}_{\tilde{z}}^2 \tilde{\phi}_{\tilde{x}} \right) \right. \right. \\ \left. \left. + \alpha(\tilde{z} - 1)\tilde{\phi}_{\tilde{x}} + \alpha^2 \tilde{P}' \tilde{\phi}_{\tilde{x}} + \alpha(1 - \tilde{z})\tilde{\phi}_{\tilde{x}} \right\} d\tilde{z} \right]_{x_1/l}^{x_2/l}. \end{aligned} \quad (16)$$

If we substitute the expressions for  $\tilde{\phi}_{\tilde{x}}$ ,  $\tilde{\phi}_{\tilde{z}}$  and  $\tilde{P}'$  found in Eqs. (13) and (15) respectively, and integrate with respect to  $\tilde{z}$ , then we obtain

$$\begin{aligned} \frac{d}{d\tilde{t}} \int_{x_1/l}^{x_2/l} \left\{ \frac{\alpha^2(\tilde{w}^2 + \tilde{\eta}^2)}{2} + \frac{\alpha^2\beta}{2} \left( \theta^2 - \frac{1}{3} \right) \tilde{w}\tilde{w}_{\tilde{x}\tilde{x}} \right. \\ \left. + \frac{\alpha^2\beta}{6}(\tilde{w}_{\tilde{x}})^2 + \frac{\alpha^3\tilde{w}^2}{2}\tilde{\eta} \right\} d\tilde{x} = \left[ \frac{\alpha^3}{2}\tilde{w}^3 + \alpha^2\tilde{\eta}\tilde{w} + \alpha^3\tilde{\eta}^2\tilde{w} \right. \\ \left. + \frac{\alpha^2}{2}\beta \left( \theta^2 - \frac{1}{3} \right) \tilde{\eta}\tilde{w}_{\tilde{x}\tilde{x}} - \frac{\alpha^2}{3}\beta\tilde{w}\tilde{w}_{\tilde{x}\tilde{t}} \right]_{x_1/l}^{x_2/l} + \mathcal{O}(\alpha^2\beta^2, \alpha^3\beta, \alpha^4). \end{aligned}$$

Taking the limit as  $x_2 \rightarrow x_1$ , and omitting the common factor  $\alpha^2$ , we obtain the differential energy balance equation

$$\begin{aligned} \frac{d}{d\tilde{t}} \left[ \frac{(\tilde{w}^2 + \tilde{\eta}^2)}{2} + \frac{\beta}{2} \left( \theta^2 - \frac{1}{3} \right) \tilde{w}\tilde{w}_{\tilde{x}\tilde{x}} + \frac{\beta}{6}(\tilde{w}_{\tilde{x}})^2 + \frac{\alpha\tilde{w}^2}{2}\tilde{\eta} \right] + \\ \frac{d}{d\tilde{x}} \left[ \frac{\alpha}{2}\tilde{w}^3 + \tilde{\eta}\tilde{w} + \alpha\tilde{\eta}^2\tilde{w} + \frac{1}{2}\beta \left( \theta^2 - \frac{1}{3} \right) \tilde{\eta}\tilde{w}_{\tilde{x}\tilde{x}} - \frac{1}{3}\beta\tilde{w}\tilde{w}_{\tilde{x}\tilde{t}} \right] \\ = \mathcal{O}(\beta^2, \alpha\beta, \alpha^2). \end{aligned}$$

From Eq. (16), we get the non-dimensional energy density

$$\begin{aligned} \tilde{E} = \frac{\alpha^2(\tilde{w}^2 + \tilde{\eta}^2)}{2} + \frac{\alpha^2\beta}{2} \left( \theta^2 - \frac{1}{3} \right) \tilde{w}\tilde{w}_{\tilde{x}\tilde{x}} \\ + \frac{\alpha^2\beta}{6}(\tilde{w}_{\tilde{x}})^2 + \frac{\alpha^3\tilde{w}^2}{2}\tilde{\eta}, \end{aligned}$$

and the non-dimensional energy flux

$$\begin{aligned}\tilde{q}_{\tilde{E}} &= \frac{\alpha^3}{2}\tilde{w}^3 + \alpha^2\tilde{\eta}\tilde{w} + \alpha^3\tilde{\eta}^2\tilde{w} \\ &+ \frac{\alpha^2}{2}\beta\left(\theta^2 - \frac{1}{3}\right)\tilde{\eta}\tilde{w}_{\tilde{x}\tilde{x}} - \frac{\alpha^2}{3}\beta\tilde{w}\tilde{w}_{\tilde{x}\tilde{t}}.\end{aligned}$$

The dimensional versions of these quantities are given by

$$\begin{aligned}E &= \frac{\rho}{2}h_0w^2 + \frac{\rho}{2}g\eta^2 + \frac{\rho}{2}h_0^3\left(\theta^2 - \frac{1}{3}\right)ww_{xx} \\ &+ \frac{\rho}{6}h_0^3w_x^2 + \frac{\rho}{2}w^2\eta\end{aligned}\quad (17)$$

and

$$\begin{aligned}q_E &= \frac{\rho}{2}h_0w^3 + \rho c_0^2\eta w + \frac{1}{h_0}\rho c_0^2w\eta^2 \\ &+ \frac{\rho}{2}c_0^2h_0^2\left(\theta^2 - \frac{1}{3}\right)\eta w_{xx} - \frac{\rho}{3}h_0^3ww_{xt}.\end{aligned}$$

We would like to point out that it would be interesting to derive similar quantities for the system derived by Green and Naghdi (1976), which does not have the same limitations on the wave amplitude as the BBM system used in the present analysis. The Green–Naghdi system is also applicable for variable bottom topography, and has been used in the modeling of tsunamis by Zheleznyak and Pelinovsky (1985). In fact, a pressure formula similar to Eq. (15), but valid for the Green–Naghdi system has already been found by Pelinovsky and Choi (1993).

### 3 Solitary wave shoaling

One of the most readily investigated changes in a wave transmitting into shallower water is the variation in waveheight, and this is the main object of this section. We focus on the case of a solitary wave which runs up on a gentle slope with no variation in the transverse direction. Even in this two-dimensional case, there are a number of important physical effects which are neglected in the model at hand. In particular, we do not take account of viscosity and rotational effects; and as explained in the introduction, we also assume that wave reflection can be neglected to a first approximation, such as for instance in the case of a very gentle slope. Moreover, we consider long-crested waves shoaling on a plane beach, so that wave refraction does not play a role. As the solitary wave starts to propagate over a sloping bottom, it will become slightly skewed, and the waveheight will increase. Eventually, the wave will steepen and break. The different stages of this shoaling process have been minutely detailed by Synolakis and Skjelbreia (1993).

As shown by Chen (1998), the coupled BBM system Eqs. (1) and (2) features solitary-wave solutions in a closed form in the case that  $\theta^2 = \frac{7}{9}$ . Since the analysis of the energy balance in a shoaling wave given here relies on the exact formula for the solitary wave, the coupled BBM system with

$\theta^2 = \frac{7}{9}$  is used in the present work. In dimensional variables, this system takes the form

$$\eta_t + h_0w_x + (\eta w)_x - \frac{h_0^2}{2}\frac{4}{9}\eta_{xxt} = 0,\quad (18)$$

$$w_t + g\eta_x + ww_x - \frac{h_0^2}{2}\frac{2}{9}w_{xxt} = 0.\quad (19)$$

The solitary wave solutions of Eqs. (18) and (19) are given by

$$\eta_0(x, t) = H_0 \operatorname{sech}^2(\kappa_0(x - C_0t)),\quad (20)$$

$$w_0(x, t) = W_0 \operatorname{sech}^2(\kappa_0(x - C_0t)).\quad (21)$$

The constant  $H_0$  is the initial waveheight, and the constants  $W_0$ ,  $C_0$  and  $\kappa_0$  are given by

$$\begin{aligned}W_0 &= \sqrt{\frac{3g}{H_0 + 3h_0}}H_0, \\ C_0 &= \frac{3h_0 + 2H_0}{\sqrt{3h_0(H_0 + 3h_0)}}\sqrt{gh_0},\end{aligned}$$

and

$$\kappa_0 = \frac{3}{2h_0}\sqrt{\frac{H_0}{2H_0 + 3h_0}}.$$

Now let us consider a channel of depth  $h_0$  and suppose the depth of the water is slowly decreasing to a smaller value  $h$ . We suppose that the waveheight of the incident wave is  $H_0$ , and denote waveheight of the wave at the new depth by  $H$ . In an experimental setting, the waveheight is usually continuously varying, and the waveheight change is recorded over the extent of the slope (cf. Fig. 1). In order to invoke energy conservation in a theoretical sense, we assume that the wave travels up a gentle slope, and reorganizes into a solitary wave on the new even bottom with undisturbed depth  $h$ .

Using the expression for  $E$  obtained in the previous section, and evaluating the integral  $\mathcal{E} = \int E dx$  for the total energy at two different instants in time, one at which the wave is located over the initial depth  $h_0$ , and one at which the wave is located above a different depth  $h$  then yields an equation relating the waveheights  $H_0$  and  $H$  at the two different depths.

Since the solitary wave features exponential decay, energy conservation may be stated in the form

$$\int_{-\infty}^{\infty} E(\eta_0, w_0) dx = \int_{-\infty}^{\infty} E(\eta, w) dx,\quad (22)$$

where  $\eta$  and  $w$  are given by Eq. (20) with the constants  $W$ ,  $C$  and  $\kappa$  given in terms of  $h$  and  $H$  instead of  $h_0$  and  $H_0$ . After performing the integration with respect to  $x$ , we find the relation

$$\frac{h_0}{2}\frac{W_0^2}{\kappa_0} - \frac{2}{45}h_0^3\kappa_0W_0^2 + \frac{2}{5}W_0^2H_0\frac{1}{\kappa_0} + \frac{1}{2}gH_0^2\frac{1}{\kappa_0} = \quad (23)$$

$$\frac{h}{2}\frac{W^2}{\kappa} - \frac{2}{45}h^3\kappa W^2 + \frac{2}{5}W^2H\frac{1}{\kappa} + \frac{1}{2}gH^2\frac{1}{\kappa}.$$

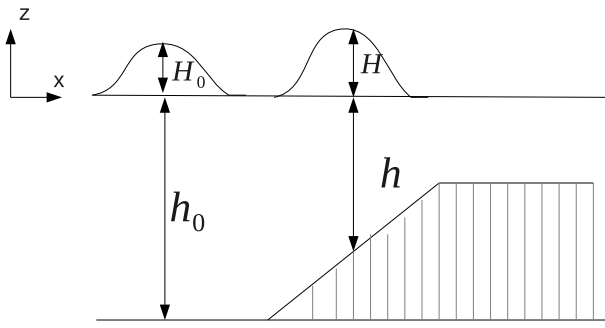


**Fig. 1.** The geometry of the problem. The waveheight  $H$  is measured on the slope.

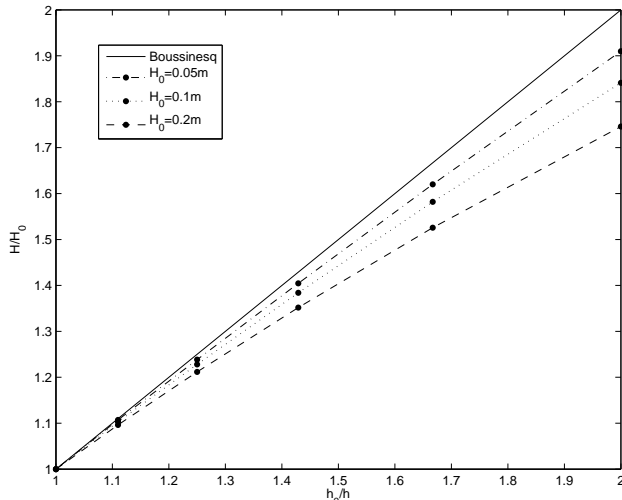


**Fig. 2.** Computations for the shoaling of solitary waves from relation Eq. (23). The solid line depicts the shoaling relation according to Boussinesq's law. Shoaling rates for waves of initial waveheight  $H_0 = 0.05$  m, 0.1 m and 0.2 m are computed. As the waveheight of the incident solitary waves decreases, the shoaling relation approaches Boussinesq's result.

From Eq. (23), it is plain that  $H$  may be expressed in terms of  $h_0$ ,  $h$  and  $H_0$ , though in general the values of  $H$  will have to be approximated numerically. We have computed wave shoaling for initial undisturbed depth  $h_0 = 1$  m and initial waveheights  $H_0$  equal to 0.05 m, 0.1 m and 0.2 m, and for a ratio of undisturbed to initial depth of up to 0.5. The relative wave height  $H/H_0$  computed for these waves is plotted in Fig. 2. Boussinesq's relation which gives shoaling rates  $\propto h^{-1}$ , is plotted as a solid line. It is apparent that the computed curves get close to the line  $h^{-1}$  for decreasing initial waveheight.

#### 4 Discussion and conclusions

Shoaling of solitary waves has been analyzed using conservation of energy in the Boussinesq scaling. It appears that for waves of very small waveheight, Boussinesq's shoaling law is approximately recovered. To explain the discrepancy observed for larger waveheights, we note that the Boussinesq shoaling law follows for small waveheights if only the last term in the expression Eq. (17) for the energy density is used to compute the energy of the solitary wave. This can also be done in the context of other Boussinesq-type systems found by Bona et al. (2002). In particular, in the case of the KdV equation, the total mechanical energy for a solitary wave is given by

$$\mathcal{E} = \rho g \frac{8}{3^{3/2}} H^{3/2} h^{3/2}, \quad (24)$$

which along with conservation of energy during an adiabatic shoaling process, yields Boussinesq's law  $H/H_0 = h_0/h$ . In the limit of small amplitude, solitary-wave solutions of all the Boussinesq-type systems are equivalent to solitary waves of the KdV equation, so that the formula Eq. (24) is valid asymptotically for  $H_0 \rightarrow 0$  also for solitary waves governed by Eqs. (18) and (19). As explained by Bona et al. (2002), these Boussinesq-type systems are valid for waves for which the Stokes number  $S = \alpha/\beta$  is of  $\mathcal{O}(1)$ . Shoaling rates for other waves can be quite different. In particular, for small amplitude waves, one often finds the so-called Green's law  $H/H_0 \sim 1/h^{1/4}$ , which can be derived from linear wave theory (see Lamb, 1932 and Synolakis, 1991).

For comparison, we have included some aspects of a shoaling study which was first presented by Pelinovsky and Talipova (1977, 1979). In these works, the waveheight–wave energy relation for numerical solutions of the full water-wave problem found by Longuet-Higgins (1974); Longuet-Higgins and Fenton (1974) is used. The results are displayed in Fig. 3, and indicate shoaling rates similar to Boussinesq's law for most cases, since the slopes of the curves are seen to be close to 1 for the most part. Only the very first part of the curve for  $H_0 = 0.05$  m has a smaller slope, and might suggest shoaling rates closer to Green's law for very small amplitude waves and small differences in depth. Since Green's laws can be derived in the case when there is no particular relationship between the wavelength and the amplitude, it is not surprising that for solitary waves, which generally respect the relation  $\alpha \sim \beta$ , the Boussinesq law is a more generic outcome.

Besides the works Pelinovsky and Talipova (1977, 1979) already mentioned, there have also been other analytic studies. For instance, in Pelinovsky et al. (1993), nonlinear ray theory is used to derive a rather general shoaling law, including wave diffraction and dissipation. The shoaling relation derived by Pelinovsky et al. (1993) reduces to Green's law in the case that nonlinearity and dispersion are neglected. In the case of a periodic sequence of solitary waves, the relation

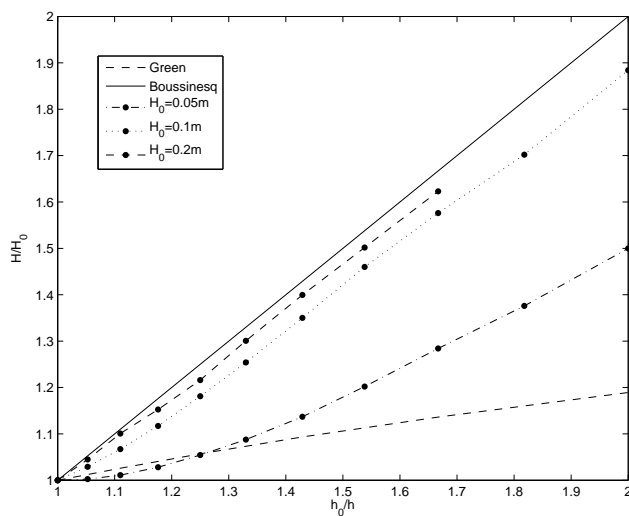


**Fig. 3.** Computations for the shoaling of solitary waves using the method of Pelinovsky and Talipova (1977, 1979), and using numerical data found by Longuet-Higgins (1974); Longuet-Higgins and Fenton (1974). The solid line depicts the shoaling relation according to Boussinesq's law. The lower dashed line depicts the shoaling relation according to Green's law. Shoaling rates for waves of initial waveheight  $H_0 = 0.05$  m, 0.1 m and 0.2 m are computed. The dashed curve terminates because the maximum wave energy is reached.

reduces to a “nonlinear” Green's law, such as found by Ostrovsky and Pelinovsky (1970). See also Ostrovsky and Pelinovsky (1975) for nonlinear wave refraction.

Comparisons with wave tank experiments indicate that reliable results can be obtained for variations of the Stokes number  $S$  over nearly two orders of magnitude (see Bona et al. (1981)). However, these comparisons also indicate that an appropriate damping mechanism should be included into the description. The effect of different models of bottom friction on the waveheight changes in surface waves were investigated by Caputo and Stepanyants (2003). It was found that of the three dissipation models considered, Chezy-type dissipation had the strongest damping effect in a channel of decreasing depth, while Reynolds dissipation had the weakest effect. These authors also considered the influence of a channel of changing width. In particular, a generalised Green's law is proposed which takes account of both changing depth and width.

There have also been several experimental and purely numerical studies directed towards understanding shoaling rates of long-crested waves in shallow water. Early experimental work of Ippen and Kulin (1954) and Camfield and Street (1969) suggested that wave shoaling may be approximated by Green's law (see Madsen and Mei (1969)), but some of these date feature high scatter, and some also suggest shoaling rates higher than Green's law. The systematic study of Synolakis and Skjelbreia (1993) found that solitary

wave shoaling can be described well if the evolution is classified in different phases. There are two pre-breaking phases, the first is relatively well approximated by Green's law the second which features more rapid shoaling can be approximated by Boussinesq's law.

Using a numerical approximation of a Boussinesq model similar to the system studied in this paper, Peregrine (1967) found that the shoaling rates can be qualitatively predicted by Green's laws, but that there is no systematic variation of the waveheight change with either slope or initial waveheight. Shuto (1973) suggested that growth rates of both Boussinesq's result and Green's law are correct, and the validity of either depends on the parameter range of any particular situation. In fact, Shuto displays graphs which suggest that both the experiments by Camfield and Street (1969) and Ippen and Kulin (1954) could be interpreted using Boussinesq's law or Green's law, in certain areas. In his review article on solitary waves, Miles (1980) noted that Boussinesq's shoaling law should be appropriate for sufficiently small values of the bottom slope, but that Green's law is a better approximation for larger slopes or sufficiently small waveheight of the incident wave.

*Acknowledgements.* This research was supported by the Research Council of Norway. The authors would like to thank Efim Pelinovsky and Yury Stepanyants for helpful comments on this work.

Edited by: R. Grimshaw

Reviewed by: E. Pelinovsky and Y. A. Stepanyants

## References

- Ali, A. and Kalisch, H.: Mechanical balance laws for Boussinesq models of surface water waves, *J. Nonlinear Sci.*, 22, 371–398, doi:10.1007/s00332-011-9121-2, 2012.
- Benjamin, T. B., Bona, J. B. and Mahony, J. J.: Model equations for long waves in nonlinear dispersive systems, *Philos. T. R. Soc. A*, 272, 47–78, 1972.
- Bjørkavåg, M. and Kalisch, H.: Wave breaking in Boussinesq models for undular bores, *Phys. Lett. A*, 375, 1570–1578, doi:10.1016/j.physleta.2011.02.060, 2011.
- Bona, J. L. and Chen, M.: A Boussinesq system for two-way propagation of nonlinear dispersive waves, *Physica D*, 116, 191–224, doi:10.1016/S0167-2789(97)00249-2, 1998.
- Bona, J. L., Chen, M., and Saut, J.-C.: Boussinesq equations and other systems for small-amplitude long waves in nonlinear dispersive media.I: Derivation and linear theory. *J. Nonlinear Sci.*, 12, 283–318, doi:10.1007/s00332-002-0466-4, 2002.
- Bona, J. L., Pritchard, W. G., and Scott, L. R.: An evaluation of a model equation for water waves, *Philos. T. R. Soc. A*, 302, 457–510, 1981.
- Camfield, F. E. and Street, R. L.: Shoaling of solitary waves on small slopes, *J. Waterway Harb. Div., Proc. ASCE* 95, 1–22, 1969.
- Caputo, J.-G. and Stepanyants, Y. A.: Bore formation, evolution and disintegration into solitons in shallow inhomogeneous channels,

- Nonlin. Processes Geophys., 10, 407–424, doi:10.5194/npg-10-407-2003, 2003.
- Chen, M.: Exact solutions of various Boussinesq systems, *Appl. Math. Lett.*, 11, 45–49, doi:10.1016/S0893-9659(98)00078-0, 1998.
- Choi, B. H., Pelinovsky, E., Kim, D. C., Didenkulova, I., and Woo, S.-B.: Two- and three-dimensional computation of solitary wave runup on non-plane beach, *Nonlin. Processes Geophys.*, 15, 489–502, doi:10.5194/npg-15-489-2008, 2008.
- Dean, R. G. and Dalrymple, R. A.: *Water Wave Mechanics for Engineers and Scientists*, World Scientific, Singapore, 1991.
- Green, A. E. and Naghdi, P. M.: A derivation of equations for wave propagation on water of variable depth, *J. Fluid Mech.*, 78, 237–246, doi:10.1017/S0022112076002425, 1976.
- Grimshaw, R.: The solitary wave in water of variable depth, *J. Fluid Mech.*, 42, 639–656, doi:10.1017/S0022112070001520, 1970.
- Grimshaw, R.: The solitary wave in water of variable depth. Part 2, *J. Fluid Mech.*, 46, 611–622, doi:10.1017/S0022112071000739, 1971.
- Ippen, A. T. and Kulin, G.: The shoaling and breaking of the solitary wave, *Proc. 5th Conf. on Coast. Eng.*, Grenoble, 27–47, 1954.
- Kishi, T. and Saeki, H.: The shoaling, breaking and runup of the solitary wave on impermeable rough slopes. *Proc. 10th Conf. Coastal Engineering*, Tokyo, 322–348, 1966.
- Lamb, H.: *Hydrodynamics*, Cambridge Univ. Press, California, 1932.
- Longuet-Higgins, M. S.: On the mass, momentum, energy and circulation of a solitary wave. I, *P. Roy. Soc. Lond. A Mat.*, 337, 1–13, doi:10.1098/rspa.1974.0035, 1974.
- Longuet-Higgins, M. S. and Fenton, J. D.: On the mass, momentum, energy and circulation of a solitary wave. II, *P. Roy. Soc. Lond. A Mat.*, 340, 471–493, doi:10.1098/rspa.1974.0166, 1974.
- Madsen, O. S. and Mei, C. C.: The transformation of a solitary wave over an uneven bottom, *J. Fluid Mech.*, 39, 781–791, doi:10.1017/S0022112069002461, 1969.
- Miles, J. W.: Solitary waves, *Annu. Rev. Fluid Mech.*, 12, 11–43, doi:10.1146/annurev.fl.12.010180.000303, 1980.
- Ostrovsky, L. A. and Pelinovsky, E. N.: Wave transformation on the surface of a fluid of variable depth, *Atmos. Oceanic Phys.*, 6, 552–555, 1970.
- Ostrovsky, L. A. and Pelinovsky, E. N.: Refraction of nonlinear ocean waves in a beach zone, *Atmos. Oceanic Phys.*, 11, 37–41, 1975.
- Peregrine, D. H.: Long waves on a beach, *J. Fluid Mech.*, 27, 815–827, doi:10.1017/S0022112067002605, 1967.
- Pelinovsky, E. N.: *Nonlinear Dynamics of Tsunami Waves* (Applied Physics Institute Press, Gorky, 1982).
- Pelinovsky, E. N. and Choi, H. S.: A Mathematical model for nonlinear waves due to moving disturbances in a basin of variable depth, *J. Korean Soc. Coastal Ocean Eng.*, 5, 191–197, 1993.
- Pelinovsky, E. N., Stepanyants, Y. A. and Talipova, T. G.: Nonlinear dispersion model of sea waves in the coastal zone, *J. Korean Soc. Coastal Ocean Eng.*, 5, 307–317, 1993.
- Pelinovsky, E. N. and Talipova, T. G.: Height variations of large-amplitude solitary waves in the near-shore zone, *Oceanology*, 17, 1–3, 1977.
- Pelinovsky, E. N. and Talipova, T. G.: Change of height of the solitary wave of large amplitude in the beach zone, *Mar. Geodesy*, 2, 313–321, 1979.
- Shuto, N.: Shoaling and deformation of non-linear waves, *Coast. Eng. Japan*, 14, 25–42, 1973.
- Stoker, J. J.: *Water waves: The mathematical theory with applications*, Pure and Applied Mathematics, IV, Interscience Publishers, New York, 1957.
- Synolakis, C. E.: Green's law and the evolution of solitary waves, *Phys. Fluids A*, 3, 490–491, 1991.
- Synolakis, C. E. and Skjelbreia, J. E.: Evolution of maximum amplitude of solitary waves on plane beaches, *J. Waterw. Port. C-Asce.*, 119, 323–342, 1993.
- Whitham, G. B.: *Linear and nonlinear waves*, Wiley, New York, 1974.
- Zheleznyak, M. I. and Pelinovsky, E. N.: Physical and mathematical models of the tsunami climbing a beach, *Tsunami Climbing a Beach*, 8–34, Applied Physics Instituts Press, Gorky, 1985.

## Paper B

# On the Influence of Wave Reflection on Shoaling and Breaking Solitary Waves



## On the influence of wave reflection on shoaling and breaking solitary waves

Amutha Senthilkumar

Department of Mathematics, University of Bergen, Postbox 7803, 5020 Bergen, Norway; amutha.senthilkumar@math.uib.no

Received 22 January 2016, revised 28 April 2016, accepted 4 May 2016, available online 24 November 2016

© 2016 Author. This is an Open Access article distributed under the terms and conditions of the Creative Commons Attribution-NonCommercial 4.0 International License (<http://creativecommons.org/licenses/by-nc/4.0/>).

**Abstract.** A coupled BBM system of equations is studied in the situation of water waves propagating over a decreasing fluid depth. A conservation equation for mass and also a wave breaking criterion, both valid in the Boussinesq approximation, are found. A Fourier collocation method coupled with a 4-stage Runge–Kutta time integration scheme is employed to approximate solutions of the BBM system. The mass conservation equation is used to quantify the role of reflection in the shoaling of solitary waves on a sloping bottom. Shoaling results based on an adiabatic approximation are analysed. Wave shoaling and the criterion of the breaking of solitary waves on a sloping bottom are studied. To validate the numerical model the simulation results are compared with reference results and a good agreement between them can be observed. Shoaling of solitary waves is calculated for two different types of mild slope model systems. Comparison with reference solutions shows that both of these models work well in their respective regimes of applicability.

**Key words:** coupled BBM system, shoaling rates, mass conservation law.

### 1. INTRODUCTION

Model equations for free surface water waves propagating in a horizontal channel of uniform depth have been widely studied for many years. Boussinesq models incorporate the lowest-order effects of nonlinearity and frequency dispersion as corrections to the linear long wave equation. These models are widely used for describing the propagation of non-linear shallow water waves near coastal regions. In Boussinesq theory, it is important to assume that water is incompressible and inviscid and the flow is irrotational. There are two important parameters: the nonlinearity, the ratio of amplitude to depth, represented by  $\alpha = a/h_0$ , and the dispersion, the ratio of depth to wavelength, represented by  $\beta = h_0^2/l^2$ . As explained in detail in [5], the Boussinesq approximation is valid only when both  $\alpha$  and  $\beta$  are small and have the same order of magnitude.

The more realistic situation of an uneven bottom profile is fundamental to studies of ocean wave dynamics in coastal regions. Several authors [15,19,21,28,30,40,43] have included the effect of smooth and slowly varying bottom topographies in both Boussinesq and shallow water theory. Wave shoaling is the effect by which surface waves propagating shorewards experience a decrease in the water depth. The study of shoaling waves is of importance in the nearshore areas and in the design of coastal structures. The

'classical' Boussinesq model was applied to shallow water of uneven bottom in two horizontal dimensions by Peregrine [36], who used depth-averaged velocity as a dependent variable and derived the system

$$\begin{aligned} \eta_t + \nabla \cdot [(h + \eta)\bar{\mathbf{u}}] &= 0 \\ \bar{\mathbf{u}}_t + \nabla \eta + (\bar{\mathbf{u}} \cdot \nabla) \bar{\mathbf{u}} - \frac{h}{2} \nabla(\nabla \cdot (h\bar{\mathbf{u}}_t)) + \frac{h^2}{6} \nabla(\nabla \cdot (\bar{\mathbf{u}}_t)) &= 0 \end{aligned} \quad (1)$$

where

$$\bar{\mathbf{u}} = \frac{1}{h + \eta} \int_{-h}^{\eta} \mathbf{u} dz, \quad (2)$$

$\nabla = (\partial_x, \partial_y)^T$ ,  $\eta = \eta(x, y, t)$  represents the deviation of the free surface from its rest position at time  $t$ ,  $\mathbf{u} = \mathbf{u}(x, y, z, t)$  denotes the horizontal velocity of the fluid at some height,  $\bar{\mathbf{u}}$  denotes the depth-averaged velocity, and the bottom is  $z = -h(x, y)$ .

Several improved Boussinesq-type models have been developed, starting with Madsen et al. [27], Nwogu [32], and Wei et al. [42], among others. Madsen et al. [27] achieved an improved linearized model by rearranging higher-order terms in the classical momentum equations, which are formally equivalent to zero within the accuracy of the model. Nwogu [32] demonstrated the flexibility obtained by using the velocity at an arbitrary depth as the velocity variable. Wei et al. [42] used Nwogu's approach to derive a fully nonlinear extension of Boussinesq equations, which further extended the range of validity of Boussinesq models without the weak nonlinearity restriction. It is worth mentioning that in [8,31] the Boussinesq model (1) is extended to the moving bottom topography, where the bottom topography depends on  $x$ ,  $y$ , and  $t$ . In [31], a Benjamin–Bora–Mahony (BBM–BBM) type system (see [3]) is derived and solved numerically using a finite element method. One aspect in which the BBM system differs from Peregrine's Boussinesq' system is that it is amenable to numerical integration. Indeed, it is much easier to define a stable numerical approximation to a system of BBM type than to other Boussinesq systems, such as the Peregrine system. On the other hand, the Peregrine system features exact mass conservation while mass conservation in the BBM–BBM type systems is only approximate. Nevertheless, in the current work, we use a system of BBM type for numerical convenience.

The main contribution of the present paper is an in-depth study of wave reflection in a shoaling analysis based on Boussinesq systems such as (1). As part of our analysis, we formulate an approximate mass balance law associated with the Boussinesq scaling developed for flat bottoms in [1]. We also extend the wave breaking criterion from [4] to the case of uneven beds. The mass balance equation is used in quantifying wave reflection due to the bottom slope, and the wave breaking criterion is used to determine an approximate termination point for the shoaling curves. A significant amount of literature has focused on the use of nonlinear shallow water equations to analyse long wave shoaling on a mildly sloping beach, and both experimental and numerical investigations have been carried out. However, reflection has not been quantified.

Many experimental studies, including the early studies [6,18], were aimed partly at comparison with classical shoaling laws such as the laws of Green and Boussinesq. However, most experimental work on wave shoaling has shown that actual shoaling curves vary considerably from the predictions of both Green's and Boussinesq's law. Grilli et al. [17] solved the full Euler equations by direct numerical integration, and this work compares their shoaling results with the numerical solution obtained in the present work.

Wave breaking is also important in studying nearshore area phenomena and tsunami propagation in coastal regions, because solitary waves are often used to model steep surface waves shoaling on beaches. An enormous literature also exists on breaking waves in a number of situations, including shoaling, wave breaking in open bodies of water, and breaking induced by a wave-maker (see [12,38], for instance). Chou and Quyang [9,10] and Chou et al. [11] discussed the criterion for the breaking of solitary waves on different slopes using the boundary element method to simulate the process of wave breaking. Using the fully nonlinear potential flow wave model, Grilli et al. [17] derived a criterion for wave breaking. In this paper, a different criterion of breaking solitary waves on a sloping bottom of a BBM–BBM type system is derived based on previous work in [4]. Characteristics such as the breaking index, the wave height, the water depth,

and the maximum particle velocity at the breaking point are studied and the breaking indices are compared with those obtained by Grilli et al. [17] and Chou et al. [11]. The relation between breaking and reflection is investigated.

The present paper is organized as follows. In Section 2, the outline for the derivation of the coupled BBM–BBM type system [31] is given, and also the mass balance equations and the wave breaking criterion are derived. In Section 3, the coupled BBM–BBM type system is solved numerically using a Fourier collocation method coupled with a 4-stage Runge–Kutta time integration scheme and the convergence of the numerical scheme is validated. In Section 4, we demonstrate the effectiveness of the numerical method applied to our model system in simulations of solitary wave shoaling on a sloping bottom. Shoaling and wave breaking are studied numerically. This paper compares two models: the coupled BBM–BBM type system derived by Chen [8] and the one in Mitsotakis [31] with respect to the evolution of solitary waves. This comparison is concerned with initial wave profiles and wave shoaling on slopes that correspond to unidirectional propagation. In Section 5, the mass balance expressions are tabulated and the reflection of a small amplitude wave propagating over a slope is examined. Finally, a short conclusion is given in Section 6.

## 2. DERIVATION OF THE SYSTEM

The main model system to be used here belongs to the family of models derived in Mitsotakis [31]. In order to obtain the Boussinesq system, the full water wave problem is used. A Cartesian coordinate system  $(x, z)$  is considered, with the  $x$ -axis along the still water level and the  $z$ -axis pointing vertically upwards. The fluid domain is bounded by the sea bed at  $z = -h(x)$  and the free surface  $z = \eta(x, t)$ . Then the system of Euler equations for potential flow theory in the presence of a free surface is used. The derivation of the Boussinesq system is only briefly sketched. For a full derivation, the interested reader may consult [8] and [31]. The variables are non-dimensionalized using the following scaling:

$$\tilde{x} = \frac{x}{l}, \quad \tilde{z} = \frac{z}{h_0}, \quad \tilde{t} = \frac{\sqrt{gh_0}t}{l}, \quad (3a)$$

$$\tilde{h} = \frac{h}{h_0}, \quad \tilde{\eta} = \frac{\eta}{a}, \quad \tilde{\phi} = \frac{h_0}{al\sqrt{gh_0}}\phi, \quad (3b)$$

where the tilde ( $\sim$ ) denotes non-dimensional variables, and  $h_0$ ,  $l$ , and  $a$  denote characteristic water depth, wave length, and wave amplitude, respectively.

Consider a standard asymptotic expansion of the velocity potential  $\phi$  and using the Laplace condition ( $\Delta\phi = 0$ ,  $-h < z < \eta$ ), write the velocity potential  $\tilde{\phi}$  in the simplest form

$$\tilde{\phi} = \tilde{\phi}^{(0)} + \frac{\tilde{z}}{1!}\tilde{\phi}^{(1)} + (-\beta)\left[\frac{\tilde{z}^2}{2!}\frac{\partial^2}{\partial\tilde{x}^2}\tilde{\phi}^{(0)} + \frac{\tilde{z}^3}{3!}\frac{\partial^2}{\partial\tilde{x}^2}\tilde{\phi}^{(1)}\right] + (\beta^2)\left[\frac{\tilde{z}^4}{4!}\frac{\partial^4}{\partial\tilde{x}^4}\tilde{\phi}^{(0)} + \frac{\tilde{z}^5}{5!}\frac{\partial^4}{\partial\tilde{x}^4}\tilde{\phi}^{(1)}\right] + \mathcal{O}(\beta^3), \quad (4)$$

which is a series solution with only two unknown functions  $\tilde{\phi}^{(0)}$  and  $\tilde{\phi}^{(1)}$ . Then the velocity field can be expressed as

$$\tilde{u}(\tilde{x}, \tilde{z}, \tilde{t}) = \tilde{\phi}_{\tilde{x}} = \hat{u} + \beta\left[\frac{\tilde{z}}{1!}\hat{w}_{\tilde{x}} - \frac{\tilde{z}^2}{2!}\hat{u}_{\tilde{x}\tilde{x}}\right] + \beta^2\left[-\frac{\tilde{z}^3}{3!}\hat{w}_{\tilde{x}\tilde{x}\tilde{x}} + \frac{\tilde{z}^4}{4!}\hat{u}_{\tilde{x}\tilde{x}\tilde{x}\tilde{x}}\right] + \mathcal{O}(\beta^3), \quad (5a)$$

$$\tilde{w}(\tilde{x}, \tilde{z}, \tilde{t}) = \tilde{\phi}_{\tilde{z}} = \beta[\hat{w} - \tilde{z}\hat{u}_{\tilde{x}}] + \beta^2\left[-\frac{\tilde{z}^2}{2!}\hat{w}_{\tilde{x}\tilde{x}} + \frac{\tilde{z}^3}{3!}\hat{u}_{\tilde{x}\tilde{x}\tilde{x}}\right] + \mathcal{O}(\beta^3), \quad (5b)$$

where  $\hat{u}$  and  $\hat{w}$  are the velocities at  $\tilde{z} = 0$  and given by  $\hat{u} = \tilde{\phi}_{\tilde{x}}^{(0)}$ ,  $\hat{w} = (1/\beta)\tilde{\phi}^{(1)}$ .

In order to establish the relation between  $\hat{u}$  and  $\hat{w}$ , use the bottom kinematic boundary condition ( $\phi_z + h_x \phi_x = 0$  at  $z = -h$ ), which has the following form after substituting the above asymptotic expressions:

$$\hat{w} = -(\tilde{h}\hat{u})_{\tilde{x}} + \beta \frac{\partial}{\partial \tilde{x}} \left( \frac{\tilde{h}^3}{3!} \hat{u}_{\tilde{x}\tilde{x}} - \frac{\tilde{h}^2}{2!} (\tilde{h}\hat{u})_{\tilde{x}\tilde{x}} \right) + \mathcal{O}(\beta^2). \quad (6)$$

Now inserting (4), (5), and (6) into free surface boundary conditions, one may derive the following Boussinesq system with variable bottom

$$\hat{u}_t + \tilde{\eta}_{\tilde{x}} + \alpha \hat{u} \hat{u}_{\tilde{x}} = \mathcal{O}(\alpha\beta, \beta^2), \quad (7a)$$

$$\tilde{\eta}_{\tilde{t}} + (\alpha \tilde{\eta} \hat{u} + \tilde{h}\hat{u})_{\tilde{x}} - \beta \frac{\partial}{\partial \tilde{x}} \left( \frac{\tilde{h}^3}{3!} \hat{u}_{\tilde{x}\tilde{x}} - \frac{\tilde{h}^2}{2!} (\tilde{h}\hat{u})_{\tilde{x}\tilde{x}} \right) = \mathcal{O}(\alpha\beta, \beta^2). \quad (7b)$$

It is emphasized that from the above system, and in terms of  $\hat{u}$ , one can extend the system in terms of other velocity variables, such as the velocity at an arbitrary  $z$  location. In this work we use a trick due to [32]. Namely, a new velocity variable  $\tilde{u}^\theta$  defined at an arbitrary water level  $\tilde{z} = -\tilde{h} + \theta(\alpha\tilde{\eta} + \tilde{h})$ , with  $0 \leq \theta \leq 1$ . Applying the standard techniques of inversion it is not difficult to derive the following expression as an asymptotic formula for  $\hat{u}$  in terms of  $\tilde{u}^\theta$ :

$$\hat{u} = \tilde{u}^\theta + \beta \left( \tilde{h}(\theta - 1)(\tilde{h}\tilde{u}^\theta)_{\tilde{x}\tilde{x}} + (\tilde{h})^2(\theta - 1)^2 \frac{1}{2!} (\tilde{u}^\theta)_{\tilde{x}\tilde{x}} \right) + \mathcal{O}(\alpha\beta, \beta^2). \quad (8)$$

Switching to the variable  $\tilde{u}^\theta$ , the following expressions are obtained:

$$\tilde{\eta}_{\tilde{t}} = -\left(\tilde{h}\tilde{u}^\theta\right)_{\tilde{x}} + \mathcal{O}(\alpha, \beta), \quad \tilde{u}_{\tilde{t}}^\theta = -\tilde{\eta}_{\tilde{x}} + \mathcal{O}(\alpha, \beta). \quad (9)$$

Following the methodology in [5], for arbitrary  $\mu, v \in \mathbb{R}$  and using (9), the following equations are derived

$$(\tilde{h}\tilde{u}^\theta)_{\tilde{x}\tilde{x}} = \mu(\tilde{h}\tilde{u}^\theta)_{\tilde{x}\tilde{x}} - (1 - \mu)\tilde{\eta}_{\tilde{x}\tilde{x}} + \mathcal{O}(\alpha, \beta), \quad (10a)$$

$$\tilde{u}_{\tilde{t}\tilde{x}\tilde{x}}^\theta = (1 - v)\tilde{u}_{\tilde{x}\tilde{x}\tilde{x}}^\theta - v\tilde{\eta}_{\tilde{x}\tilde{x}\tilde{x}} + \mathcal{O}(\alpha, \beta). \quad (10b)$$

Using equations (7)–(10) and appropriate expansions, the following system is derived:

$$\tilde{u}_{\tilde{t}}^\theta + \tilde{\eta}_{\tilde{x}} + \alpha \tilde{u}^\theta \tilde{u}_{\tilde{x}}^\theta + \beta \left\{ B\tilde{h} [(\tilde{h}_{\tilde{x}}\tilde{\eta}_{\tilde{x}})_{\tilde{x}} + \tilde{h}_{\tilde{x}}\tilde{\eta}_{\tilde{x}\tilde{x}}] + C\tilde{h}^2 \tilde{\eta}_{\tilde{x}\tilde{x}\tilde{x}} - D\tilde{h}^2 \tilde{u}_{\tilde{x}\tilde{x}\tilde{x}}^\theta \right\} = \mathcal{O}(\alpha\beta, \beta^2), \quad (11a)$$

$$\tilde{\eta}_{\tilde{t}} + (\alpha \tilde{\eta} \tilde{u}^\theta + \tilde{h}\tilde{u}^\theta)_{\tilde{x}} + \beta \frac{\partial}{\partial \tilde{x}} \left\{ A\tilde{h}^2 [(\tilde{h}_{\tilde{x}}\tilde{u}^\theta)_{\tilde{x}} + \tilde{h}_{\tilde{x}}\tilde{u}_{\tilde{x}}^\theta] + C\tilde{h}^2 (\tilde{h}\tilde{u}^\theta)_{\tilde{x}\tilde{x}} - B\tilde{h}^2 \tilde{\eta}_{\tilde{x}\tilde{x}} \right\} = \mathcal{O}(\alpha\beta, \beta^2). \quad (11b)$$

The parameters  $a, b, c$  and  $d$  are the same as in [5], where

$$\begin{aligned} A &= \frac{1}{2} \left[ \frac{1}{3} - (\theta - 1)^2 \right], & B &= 1 - \theta, \\ a &= \frac{1}{2} \left( \theta^2 - \frac{1}{3} \right) \mu, & b &= \frac{1}{2} \left( \theta^2 - \frac{1}{3} \right) (1 - \mu), \\ c &= \frac{1}{2} (1 - \theta^2) v, & d &= \frac{1}{2} (1 - \theta^2) (1 - v). \end{aligned} \quad (12)$$

The coupled BBM–BBM type system is derived from (11) by selecting  $\mu = 0$  and  $v = 0$ . Disregarding terms of order  $\mathcal{O}(\alpha\beta, \beta^2)$  and dropping the superscript  $\theta$ , the system takes the following form in dimensional variables

$$u_t + g\eta_x + uu_x + 2Bghh_x\eta_{xx} + Bghh_{xx}\eta_x - dh^2 u_{xxt} = 0, \quad (13a)$$

$$\eta_t + (\eta u + hu)_x + \frac{\partial}{\partial x} \left\{ 2Ah^2 h_x u_x + Ah^2 h_{xx} u - bh^2 \eta_{xt} \right\} = 0. \quad (13b)$$

Assuming the depth  $h$  is constant, the above system reduces to the original coupled BBM system in [5].

## 2.1. Mass balance

As mentioned in the introduction, the use of the BBM system necessitates the derivation of an approximate mass balance law. The following mass balance derivation is based on the work in [1], where mass balance theory is presented for the Boussinesq models with an even bottom profile. Since we are interested in varying bottom topography, we provide the following derivation. The integral form of the equation of mass conservation is

$$\frac{d}{dt} \int_{x_1}^{x_2} \int_{-h(x)}^{\eta} \rho dz dx = \left[ \int_{-h(x)}^{\eta} \rho \phi_x dz \right]_{x_2}^{x_1}, \quad (14)$$

because there is no mass flux through the bottom or through the free surface. In non-dimensional variables the above relation becomes

$$\frac{d}{d\tilde{t}} \int_{\tilde{x}_1}^{\tilde{x}_2} \int_{-\tilde{h}}^{\alpha\tilde{\eta}} d\tilde{z} d\tilde{x} = \left[ \int_{-\tilde{h}}^{\alpha\tilde{\eta}} \alpha\tilde{\phi}_{\tilde{x}} d\tilde{z} \right]_{\tilde{x}_2}^{\tilde{x}_1}. \quad (15)$$

After integration with respect to  $\tilde{z}$  and use of asymptotic expansion of  $\tilde{\phi}$ , we obtain

$$\int_{\tilde{x}_1}^{\tilde{x}_2} (\alpha\tilde{\eta} + \tilde{h})_{\tilde{t}} d\tilde{x} = \alpha \left[ \hat{u}(\tilde{h} + \alpha\tilde{\eta}) + \frac{\tilde{h}^2}{2!} \beta(\hat{u}\tilde{h})_{\tilde{x}\tilde{x}} - \frac{\tilde{h}^3}{3!} \beta(\hat{u})_{\tilde{x}\tilde{x}\tilde{x}} \right]_{\tilde{x}_2}^{\tilde{x}_1} + \mathcal{O}(\alpha\beta, \beta^2). \quad (16)$$

Note that if we take the limit  $\tilde{x}_2 \rightarrow \tilde{x}_1$ , where  $\tilde{x}_2 = x_2/l$  and  $\tilde{x}_1 = x_1/l$ , then we obtain the balance equation (17), i.e,

$$\frac{\partial}{\partial \tilde{t}} \tilde{M} + \frac{\partial}{\partial \tilde{x}} \tilde{q}_M = \mathcal{O}(\alpha\beta, \beta^2), \quad (17)$$

where

$$\tilde{M} = \alpha\tilde{\eta} + \tilde{h}, \quad \tilde{q}_M = \alpha \left[ \left( \alpha\tilde{\eta}\tilde{u}^\theta + \tilde{h}\tilde{u}^\theta \right) + \beta \left( \theta - \frac{1}{2} \right) \tilde{h}^2 (\tilde{h}\tilde{u}^\theta)_{\tilde{x}\tilde{x}} + \beta \tilde{h}^3 \left( \frac{1}{2}(\theta - 1)^2 - \frac{1}{6} \right) (\tilde{u}^\theta)_{\tilde{x}\tilde{x}} \right].$$

The derivation could also be based on the differential form of the mass conservation, such as in [2]. If we use the scalings  $M = \rho h_0 \tilde{M}$  and  $q_M = \rho h_0 \sqrt{(gh_0)} \tilde{q}_M$ , then the dimensional forms of these quantities are

$$M = \rho(\eta + h(x)), \quad q_M = \rho \left[ u(h + \eta) + h^2 \left( \theta - \frac{1}{2} \right) (hu)_{xx} + \frac{1}{2} h^3 ((\theta - 1)^2 - \frac{1}{3}) u_{xx} \right]. \quad (18)$$

Equation (17) is an approximate mass balance equation. The net mass transfer to or from a control volume during a time interval  $\Delta t$  is equal to the net change (increase or decrease) in the total mass in the control volume during  $\Delta t$ . In [1], they proved that the maximum error in the conservation of mass is smaller than  $\mathcal{O}(\alpha\beta, \beta^2)$  in the case of an even bottom profile when a coupled BBM system is used. In Section (5) the amount of mass reflection will be computed for different cases.

## 2.2. Wave breaking in the BBM model system

As waves approach the shoreline the wave length and phase velocity decrease and the wave amplitude grows larger. The wave then crashes onto the shore because it becomes too steep for the bottom of the wave to carry it. The breaking of waves mostly depends on wave steepness and beach slope. As explained in [4], if the horizontal velocity near the crest of a wave exceeds the celerity of the wave, then the wave will break. Let us denote the propagation speed by  $U$  and the horizontal velocity by  $u$ . The horizontal velocity  $u$  can be obtained from (5a) and (8):

$$\tilde{u} = \tilde{u}^\theta + \beta \left( (\tilde{h}(\theta - 1) - \tilde{z})(\tilde{h}\tilde{u}^\theta)_{\tilde{x}\tilde{x}} + ((\tilde{h})^2(\theta - 1)^2 - \tilde{z}^2) \frac{1}{2!} (\tilde{u}^\theta)_{\tilde{x}\tilde{x}} \right) + \mathcal{O}(\alpha\beta, \beta^2). \quad (19)$$

It is evident that once  $u^\theta(x, t)$  is known, (19) can be used to approximate the horizontal velocity at any depth. After neglecting the second-order term, the dimensional form of the equation is given by

$$u = u^\theta + (h(\theta - 1) - z)(hu^\theta)_{xx} + (h^2(\theta - 1)^2 - z^2)\frac{1}{2!}(u^\theta)_{\tilde{x}\tilde{x}}. \quad (20)$$

Wave breaking occurs if

$$u^\theta + (h(\theta - 1) - \eta)(hu^\theta)_{xx} + (h^2(\theta - 1)^2 - \eta^2)\frac{1}{2!}(u^\theta)_{xx} > U. \quad (21)$$

Since the fluid domain depends on the surface profile, the value  $z = \eta$  is used to approximate velocities near the surface. It is clear that the solutions  $\eta(x, t)$  and  $u^\theta(x, t)$  of system (13) and propagation speed  $U$  are needed to find the breaking criterion.

### 3. NUMERICAL METHODS

System (13) has been solved numerically using a Fourier collocation method coupled with a 4-stage Runge–Kutta time integration scheme. For numerical computations, periodic boundary conditions on the domain  $[0, L]$  are used. The problem is translated to the interval  $[0, 2\pi]$  using the scaling  $u(\lambda x, t) = v(x, t)$ ,  $\eta(\lambda x, t) = \xi(x, t)$  and  $h(\lambda x) = h_1(x)$ , where  $\lambda = \frac{L}{2\pi}$ . Then the BBM–BBM system (13) becomes

$$\begin{aligned} \lambda^3 v_t + \lambda^2 g \xi_x + \lambda^2 v v_x + 2Bgh_1 h_{1x} \xi_{xx} + Bgh_1 h_{1xx} \xi_x - \lambda d h_1^2 v_{xxt} &= 0, \quad x \in [0, 2\pi], \\ \lambda^3 \xi_t + \lambda^2 (\xi v + h_1 v)_x + \frac{\partial}{\partial x} \{ 2Ah_1^2 h_{1x} v_x + Ah_1^2 h_{1xx} v - \lambda b h_1^2 \xi_{xt} \} &= 0, \quad x \in [0, 2\pi], \\ v(x, 0) = u(\lambda x, 0), \quad \xi(x, 0) = \eta(\lambda x, 0), \\ v(0, t) = v(2\pi, t), \quad \xi(0, t) = \xi(2\pi, t), \text{ for } t \geq 0. \end{aligned} \quad (22)$$

Consider the set of  $N$  evenly spaced grid points  $x_j = \frac{2\pi j}{N}$ ,  $j = 1, \dots, N$  in the interval  $[0, 2\pi]$  referred to as collocation nodes. The spectral-collocation method is implemented in the physical space by seeking approximate solutions through a global periodic interpolation polynomial of the form

$$v_N(x) = \sum_{j=1}^N v_N(x_j) g_j(x), \quad \xi_N(x) = \sum_{j=1}^N \xi_N(x_j) g_j(x),$$

where  $g_j(x) = \frac{1}{N} \sin\left(\frac{N(x-x_j)}{2}\right) \cot\left(\frac{1}{2}(x-x_j)\right)$  and  $v_N(x)$ ,  $\xi_N(x)$  are interpolations of the function  $v(x)$  and  $\xi(x)$ , respectively, i.e.,  $v_N(x_j) = v(x_j)$ ,  $\xi_N(x_j) = \xi(x_j)$  (see [14,41]). Moreover, the corresponding Fourier collocation differentiation matrices  $D_x$  and  $D_{xx}$  are given by

$$D_{ij}^{(1)} = \frac{dg_j}{dx}(x_i) = \begin{cases} \frac{1}{2}(-1)^j \cot\left(\frac{x_i-x_j}{2}\right) & i \neq j, \\ 0 & i = j, \end{cases} \quad (23a)$$

$$D_{ij}^{(2)} = \frac{d^2 g_j}{dx^2}(x_i) = \begin{cases} -\frac{(-1)^j}{2\sin^2((x_i-x_j)/2)} & i \neq j, \\ -\frac{\pi^2}{3h^2} - \frac{1}{6} & i = j. \end{cases} \quad (23b)$$

Then at the collocation points  $x = x_j$ , the system becomes

$$\begin{aligned} [\lambda^3 I_N - \lambda b D_N \text{diag}(h_1^2) D_N] \xi_{Nt} &= -\lambda^2 D_N(\text{diag}(h_1)v_N) - \lambda^2 D_N(\xi_N v_N) \\ &\quad - D_N(2Ah_1^2 h_{1x} D_N(v_N) + Ah_{1xx} h_1^2 v_N), \end{aligned} \quad (24a)$$

$$\begin{aligned} [\lambda^3 I_N - \lambda d \text{diag}(h_1^2) D_N^{(2)}] v_{Nt} &= -\lambda^2 g D_N(\xi_N) - \lambda^2 (0.5) D_N(v_N^2) \\ &\quad - 2Bgh_1 h_{1x} D_N^{(2)}(\xi_N) - Bgh_1 h_{1xx} D_N(\xi_N), \end{aligned} \quad (24b)$$

where  $I_N$  is the unit  $N \times N$  matrix and  $D_N, D_N^{(2)}$  are square matrices with the dimensions  $N \times N$  following from (23a) and (23b), respectively, and  $\text{diag}(h_1)$ ,  $\text{diag}(h_1^2)$  are the diagonal matrices of  $h_1$  and  $h_1^2$ , respectively. This is a system of  $N$  ordinary differential equations for  $\xi_N$  and also  $v_N$ . The system is solved by using a fourth-order explicit Runge–Kutta scheme with time step  $\Delta t$ .

### 3.1. Convergence study

It is important to verify the convergence of the numerical scheme. This is done following [37]. A numerical method is convergent if the numerically computed solution approaches the exact solution as the step size approaches 0. To test the convergence of these numerical methods, the following discrete  $L^2$ -norm is used

$$\|\xi\|_{N,2}^2 = \frac{1}{N} \sum_{j=1}^N |\xi(x_j)|^2,$$

and the corresponding relative  $L^2$ -error is then defined to be

$$\frac{\|\xi - \xi_N\|_{N,2}}{\|\xi\|_{N,2}},$$

where  $\xi_N(x_j)$  is the approximated numerical solution and  $\xi(x_j)$  is the exact solution at a time  $T$ , for  $j = 1, 2, \dots, N$ .

Supposing the case of an even bottom, the coupled BBM system features solitary-wave solutions in a closed form if  $\theta^2 = \frac{7}{9}$  (see [7]). Since the analysis of the solitary wave shoaling and breaking given here depend on the exact formula for the solitary wave,  $\theta^2 = \frac{7}{9}$  is used in the present work. Then the exact solitary wave solutions of system of equations (13) take the forms

$$\eta(x,t) = H_0 \operatorname{sech}^2(\kappa_0(x - C_0 t)), \quad (25)$$

$$u(x,t) = W_0 \operatorname{sech}^2(\kappa_0(x - C_0 t)), \quad (26)$$

and the constants  $W_0$ ,  $C_0$ , and  $\kappa_0$  are given by

$$W_0 = \sqrt{\frac{3g}{H_0 + 3h_0}} H_0, \quad C_0 = \frac{3h_0 + 2H_0}{\sqrt{3h_0(H_0 + 3h_0)}} \sqrt{gh_0} \quad \text{and} \quad \kappa_0 = \frac{3}{2h_0} \sqrt{\frac{H_0}{2H_0 + 3h_0}},$$

where  $h_0$  is the undisturbed depth,  $H_0$  is wave amplitude.

To check the convergence of these methods, we determine the  $L^2$ -error each time for  $n$  steps and set the step size as  $\Delta t = (t_{\max} - t_{\min})/n$  for different  $n$  values  $n = 20, 40, 80, \dots$  (Table 1) and different number of grid points  $N = 256, 512, 1024, \dots$  (Table 2) in the case of an even bottom topography. A representative result for a wave of amplitude 0.5 m is given in Tables 1 and 2. The numerical scheme was implemented in MATLAB. In this calculation, the solution was approximated from  $T = 0$  s to  $T = 5$  s and the size of the domain was  $L = 100$  m. In the computations shown in Table 1,  $N = 1024$  Fourier modes were used. Table 1 shows fourth-order convergence of the Runge–Kutta method in terms of the time step  $\Delta t$ . The fourth-order convergence of the scheme is apparent up to  $\Delta t = 0.0039$  s, when the error became dominated by the spatial discretization and the artificial periodicity. Table 2 shows the results of some computations aimed at validating the spatial convergence of the code. As expected, spectral convergence in terms of the number of spatial grid points  $N$  was achieved in these computations. Computations were also performed for other solitary waves with heights between 0.1 m and 0.6 m, and similar results were obtained for these cases.

**Table 1.**  $L^2$ -error and convergence rate for Runge–Kutta method for different fixed step sizes in case of even bottom profile BBM–BBM type system. Here the convergence rate is the ratio of consecutive  $L^2$ -errors

No. of time steps ( $n$ )	Step size ( $\Delta t$ )	$L^2$ -error	Convergence rate
20	0.2500	5.33e-02	—
40	0.1250	3.93e-03	13.58
80	0.0625	2.39e-04	16.44
160	0.0312	1.44e-05	16.49
320	0.0156	8.89e-07	16.29
640	0.0078	5.50e-08	16.15
1280	0.0039	3.60e-09	15.35
2560	0.0020	1.07e-09	03.36

**Table 2.**  $L^2$ -error and convergence rate due to spatial discretization in case of even bottom profile BBM–BBM type system. Here the convergence rate is the ratio of consecutive  $L^2$ -errors

No. of spatial grid points ( $N$ )	Step size ( $\Delta t$ )	$L^2$ -error	Convergence rate
256	0.0001	2.3e-04	—
512	0.0001	2.77e-09	84 364.95
1024	0.0001	3.09e-012	896.81
2048	0.0001	5.371e-011	0.05

To indicate the significance of the improvement, Tables 3 and 4 show the results of computing approximate solutions of the inhomogeneous BBM–BBM type system

$$u_t + g\eta_x + uu_x + 2Bghh_x\eta_{xx} + Bghh_{xx}\eta_x - dh^2u_{xxt} = f(x, t), \quad (27a)$$

$$\eta_t + (\eta u + hu)_x + \frac{\partial}{\partial x} \{ 2Ah^2h_xu_x + Ah^2h_{xx}u - bh^2\eta_{xt} \} = g(x, t), \quad (27b)$$

where the functions  $\eta(x, t) = 0.3 \cos(x - t)$  and  $u(x, t) = 0.3 \sin(x - t)$  are used as the exact solutions and the bottom  $h(x) = 0.5 - (0.1) \cos(x)$  is assumed. Then the relative  $L^2$ -error for various pairs of combinations between the time steps  $\Delta t = 0.1/2n$  for  $n = 1, 2, 3, \dots$ ; and  $N = m \times 64$  for  $m = 1, 2, 3, \dots$  is calculated. The results are shown in Table 3 and Table 4, where the solutions were approximated from  $T = 0$  s to  $T = 5$  s. These tables show that the numerical implementation of a BBM–BBM type system with the periodic bottom function  $h(x)$  is correct. Similar results can be obtained for other  $2\pi$ -periodic functions  $u$ ,  $\eta$ , and  $h(x)$ .

**Table 3.** Inhomogeneous BBM–BBM type system (27);  $L^2$ -error and convergence rate due to temporal discretization. Here the convergence rate is the ratio of consecutive  $L^2$ -errors

No. of time steps ( $n$ )	Step size ( $\Delta t$ )	$L^2$ -error	Convergence rate
50	0.1000	1.3046e-05	—
100	0.0500	8.2126e-07	15.89
200	0.0250	5.1277e-08	16.02
400	0.0125	3.2023e-09	16.01
800	0.0063	2.0007e-10	16.01
1600	0.0031	1.2500e-11	16.01
3200	0.0016	9.3000e-13	13.41
6400	0.0008	6.2000e-13	01.51

**Table 4.** Inhomogeneous BBM–BBM type system (27);  $L^2$ -error and convergence rate due to spatial discretization. Here the convergence rate is the ratio of consecutive  $L^2$ -errors

No. of spatial grid points ( $N$ )	Step size ( $\Delta t$ )	$L^2$ -error	Convergence rate
64	0.0001	9.6e-01	—
128	0.0001	5.4e-06	176234.99
256	0.0001	2.1e-13	26437130.31
512	0.0001	6.6e-13	0.31
1024	0.0001	6.5e-13	1.007

#### 4. EVOLUTION OF SOLITARY WAVES ON A SLOPING BOTTOM

Shoaling of solitary waves with different wave heights for the initial undisturbed depth  $h_0 = 1$  m to a smaller new depth up to  $h = 0.1$  m is considered. The maximum wave heights were computed at different locations over the slope  $S = 1 : 35$ . Figure 1 shows results for a solitary wave of 0.6 m height. It shows that wave crests become steeper while shoaling on the slope. We generally see the reflection of a small amplitude wave when a solitary wave goes through a slope. After carefully measuring wave heights over the different slopes the relative maximum local wave height  $H/H_0$  versus the relative local depth  $h_0/h$  are plotted in Fig. 2, where  $h$ ,  $h_0$ ,  $H$ , and  $H_0$  represent the local water depth, the constant reference water depth, local solitary wave height, and initial solitary wave height, respectively. For later reference, we define the shoaling rate to be the exponent  $\alpha$  if the relation  $\frac{H}{H_0} = \left(\frac{h_0}{h}\right)^\alpha$  holds.

The effect of a varying bottom on water waves of this class is of obvious engineering importance and numerical solutions were obtained by Peregrine [36] and Madsen and Mei [26] using a finite difference scheme to compute the deformation of a solitary wave climbing a beach. Experimental results for wave shoaling and breaking of solitary waves were obtained by Ippen and Kulin [18], Kishi and Saeki [23], Camfield and Street [6], and Synolakis [39]. Note also that Pelinovsky and Talipova [34,35] studied the shoaling curves obtained by the wave height–wave energy relation for numerical solutions of the full water wave problem found by Longuet-Higgins [24] and Longuet-Higgins and Fenton [25]. In the case of a periodic sequence of solitary waves, Ostrovsky and Pelinovsky [33] found that the shoaling relation reduces to a ‘nonlinear’ Green’s law. The experimental results of Grilli et al. in [16] and numerical studies based on the potential flow theory for the Euler equations presented by Grilli et al. in [17] concentrate on shoaling studies. It is noteworthy that the studies of Grilli et al. [16,17] give a nice picture of different shoaling regimes and predict a variety of scaling relations for the local wave amplitude ahead and beyond the breaking point.

For comparison, we have considered numerical results of Grilli et al. [17]. Figure 2 shows plots of data taken from [17]. Figure 2 shows that the shoaling curves of the current work are in good agreement with the numerical results of Grilli et al. [17]. It can be seen that the shoaling rate increases initially more slowly than predicted by Green’s law, but then increases as the water depth keeps decreasing. Although there is no breaking point in our numerical calculation, it can be noticed that the breaking points appeared in the results obtained by Grilli et al. [17]. For instance, (21) is used to check the breaking criterion as discussed above.

It can be seen from Fig. 2 that for waves on a mild slope ( $1 : 100$ ) the water depth at breaking,  $h_b/h_0$ , will be larger than that on a steep slope ( $1 : 35$ ). Furthermore, under the same wave conditions, the amplitude at breaking points  $H_b/h_0$  is larger for a mild slope than for a steep slope. In particular, the agreement of the breaking criterion (21) with the results of Grilli et al. [17] is much better on a mild slope.

Figure 3 shows plots of shoaling rates for a wave of initial amplitude 0.1 m with slopes  $1 : 100$ ,  $1 : 400$ , and  $1 : 800$ . It is apparent that for the slope  $1 : 100$ , the shoaling rate is lower than predicted by Green’s law for small  $h_0/h$  and higher for large  $h_0/h$ . However, for the smaller slopes  $1 : 400$  and  $1 : 800$ , the shoaling

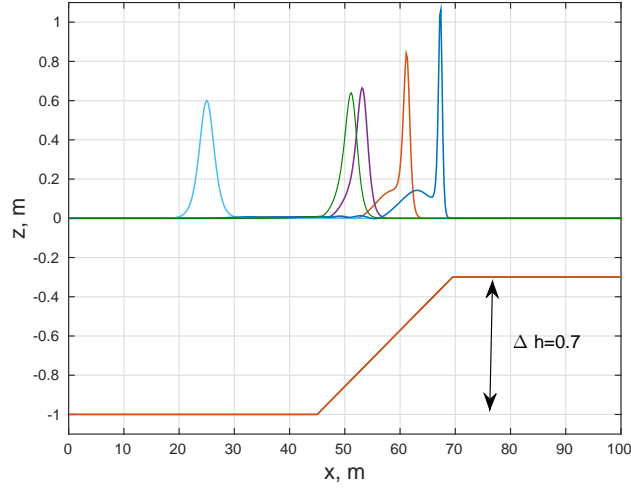


**Fig. 1.** Transformation of a solitary wave of initial amplitude 0.6 m on the slope  $S = 1 : 35$ . Here  $\Delta h$  is the height of the topography. Note that the bottom topography is smoothed near the corners.

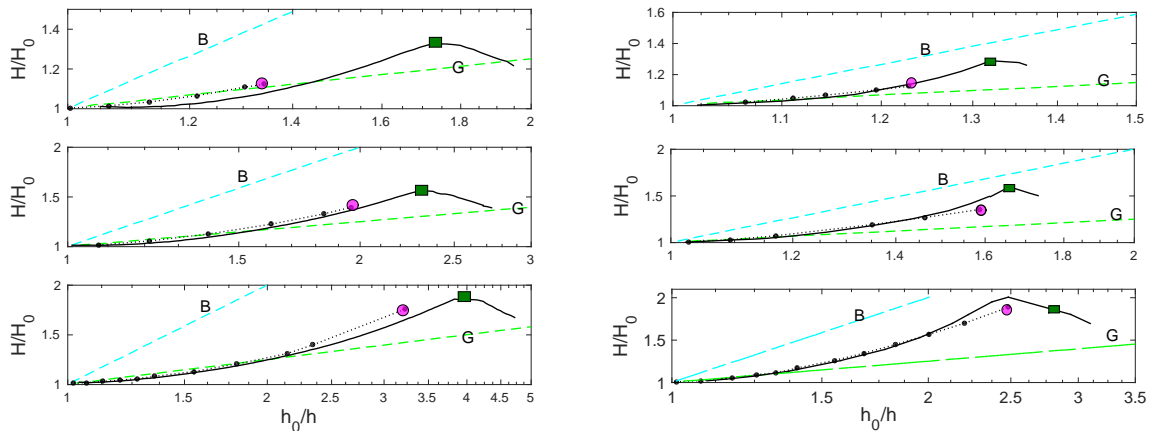


**Fig. 2.** Computations for the shoaling curves with initial amplitudes 0.6 m (upper panel), 0.4 m (middle panel), 0.2 m (lower panel) on slopes 1 : 35 (left panel) and 1 : 100 (right panel). The relative maximum local wave height  $H/H_0$  versus the relative local depth  $h_0/h$  are plotted. Here G denotes Green's law, B denotes Boussinesq's law, the dotted curves are our numerical results, and the solid curves are numerical results from Grilli et al. [17]. Rectangular and circular symbols denote the breaking points of Grilli et al. [17] and the present work, respectively.

rate is closer to the line  $h^{-1}$  for large  $h_0/h$ . Apparently, the computed curves get close to those predicted by Boussinesq's law for smaller slopes.

Now the breaking criterion (21) is applied to the solitary wave solutions. In order to find wave breaking in these solitary wave solutions, the  $x$ -location of the maximum wave height at each time step is found. The propagation speed  $U$  is then estimated using these  $x$ -locations at each time step. Finally, if the computed horizontal velocity  $u$  exceeds the mean propagation speed  $U$ , we can conclude that around this time step the wave is starting to break.

The water depth at breaking measured under the wave crest is denoted as  $h_b$  and the corresponding solitary wave height at breaking is denoted as  $H_b$ . In Table 5 the relative breaking wave height  $H_b/h_b$  at the corresponding breaking points is compared with those of Grilli et al. [17] and Chou et al. [11]. For a

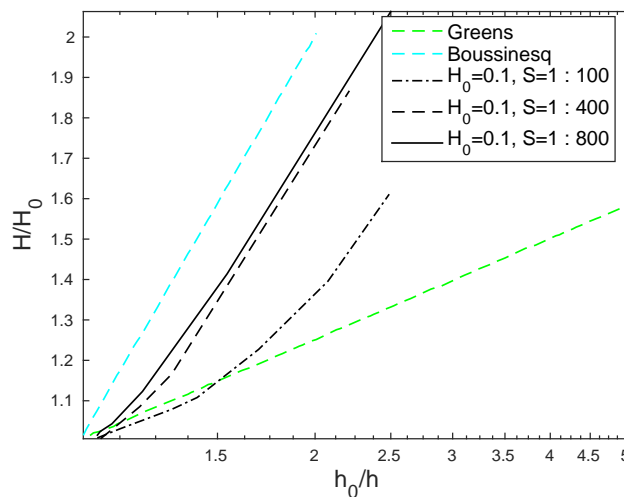


**Fig. 3.** Computations for the shoaling curves with the initial amplitude  $H_0 = 0.1$  m on different slopes. The relative maximum local wave height  $H/H_0$  versus the relative local depth  $h_0/h$  is plotted.

large wave amplitude the wave height will exceed the breaking criterion very soon after it propagates on the slope and so wave breaking occurs almost instantly without too much change in height. The ratio of relative breaking wave height is larger for small amplitude waves than for large amplitude waves. Wave breaking occurs sooner for larger initial waves.

McCowan [29] theoretically defined the breaker depth index as  $H_b/h_b = 0.78$  for a solitary wave travelling over a horizontal bottom using the assumption that instability is reached when the particle velocity at the crest equals the wave celerity and that the crest angle is then  $120^\circ$ . To estimate the initial breaking wave height on a mild-slope beach, this value ( $H_b/h_b = 0.78$ ) is most commonly used in engineering practice as a first estimate. Ippen and Kulin [18] showed that the upper limit of the breaking criterion should be 0.78 for a solitary wave over a very mild slope. In this article the slope 1 : 35 is used and it was found that the relative breaking wave heights  $H_b/h_b$  are smaller for higher amplitude waves (Table 5). It can be seen that the relative breaking wave heights  $H_b/h_b$  at breaking points are well above the McCowan limit 0.78. Since the relative breaking wave heights  $H_b/h_b$  at breaking points are smaller than those obtained by Grilli et al. [17] and Chou et al. [11], we might consider a higher order Boussinesq model for further study.

**Table 5.** Comparison of the relative breaking wave height  $H_b/h_b$  and the wave height at breaking points  $H_b/h_0$  for waves with initial amplitudes 0.2 m, 0.25 m, 0.3 m, and 0.4 m on slope 1 : 35 from Chou et al. [11], Grilli et al. [17], and the present work

$H_0$	$H_b/h_b$			$H_b/h_0$		
	Chou	Grilli	Present	Chou	Grilli	Present
0.2	1.330	1.402	1.180	0.402	0.364	0.3530
0.25	1.314	1.385	1.065	0.465	0.422	0.4018
0.3	1.283	1.380	1.049	0.514	0.476	0.4543
0.4	1.26	1.378	0.984	0.614	0.592	0.5359

#### 4.1. Comparison to mild slope model systems

For comparison, the work of Chen [8] is considered. Chen presented equations for bi-directional waves over an uneven bottom, which may be written in non-dimensional, unscaled variables and disregarding terms of order  $\mathcal{O}(\alpha\beta, \beta^2)$  as

$$u_t + g\eta_x + uu_x - \frac{1}{2}(1 - \theta^2)h_0^2 u_{xxt} = 0, \quad (28a)$$

$$\eta_t + (\eta u + hu)_x - \frac{1}{2}\left(\theta^2 - \frac{1}{3}\right)h_0^2 \eta_{xxt} = 0. \quad (28b)$$

The models of Chen [8] and Mitsotakis [31] represent the same type of coupled BBM–BBM type system, derived in the context of the Boussinesq scaling. One can derive a number of special cases of the general Boussinesq system. Since we are interested in coupled BBM–BBM type system, the model of Chen was chosen for comparisons. The above system (28) is solved using the same numerical technique as above. The main difference between the two systems (13) and (28) is approximation of bottom motion. In (13), the bottom motion is non-dimensionalized by  $\tilde{h} = \frac{h-h_0}{h_0}$ , and in (28), it is non-dimensionalized by  $\tilde{h} = \frac{h-h_0}{a_0}$ , which is similar to the approximation of wave amplitude  $\eta$ . Figure 4 shows computations for the shoaling curves with the initial amplitude 0.4 m. It can be noticed that the shoaling curve corresponding to system (28) lies below that predicted by Green's law because of the lower order approximation.

In [8], the bottom function  $h(x)$  is assumed to be  $\mathcal{O}(\alpha)$  and in [31], the bottom function  $h(x)$  is assumed to be  $\mathcal{O}(1)$ . The results are in line with the assumptions used in their respective derivations.

In Fig. 5, the shoaling curves close to a breaking point of a solitary wave with an initial wave height 0.2 m are shown. A comparison between the present shoaling result using system (13) derived by Mitsotakis [31] and the numerical results of the Nwogu system [32] presented in [13] and also the numerical results of system (28) derived by Chen [8] is shown in the left panel of Fig. 5. It can be seen that the Nwogu system, which is derived in terms of amplitude–velocity, quickly over-shoals.

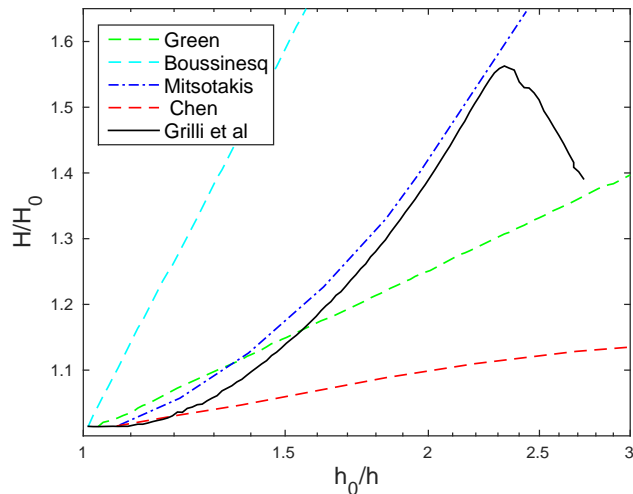


**Fig. 4.** Computations for the relative maximum local wave height  $H/H_0$  versus the relative local depth  $h_0/h$  plotted with initial amplitude 0.4 m on a slope 1 : 35. The dashed-dotted curve represents numerical results for system (13) derived by Mitsotakis [31], the solid curve shows the numerical results from Grilli et al. [17], and the dashed curve represents numerical results for system (28). Indeed, system (28) works for small-amplitude bottom variations as expected, since the bottom function  $h(x)$  is assumed to be of order  $\mathcal{O}(\alpha)$ .

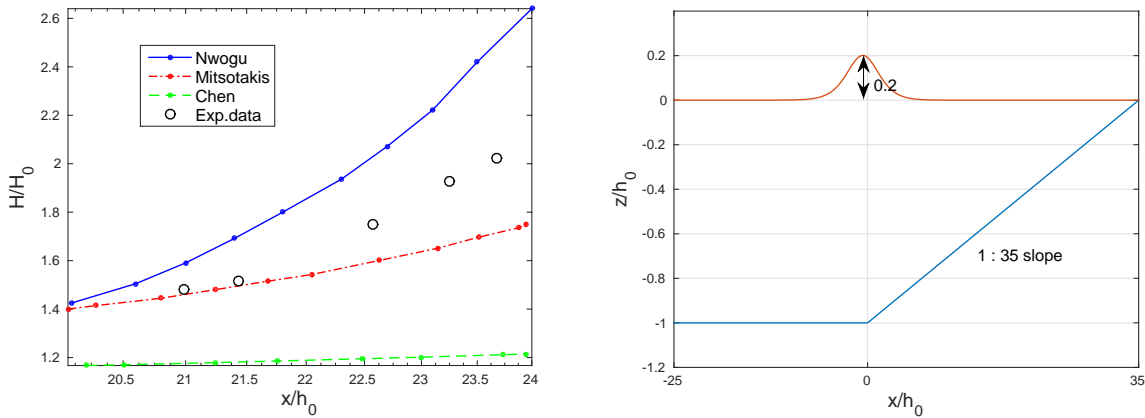


**Fig. 5.** Computations for the shoaling curves with the initial amplitude 0.2 m on a slope 1 : 35 close to the breaking point. Right panel: computational setup. Left panel: close-up of shoaling curves near breaking points. In the left panel, the dashed-dotted curve represents numerical results for system (13) derived by Mitsotakis [31], the solid curve shows the numerical results from the Nwogu system [32], the circular symbols denote the data of the laboratory experiments of [16], and the dashed curve represents numerical results for system (28) derived by Chen [8]. Here  $x$  is the horizontal coordinate,  $z$  is the vertical coordinate,  $h_0$  is the constant reference water depth, and  $H/H_0$  is the relative maximum local wave height.

## 5. MASS CONSERVATION ON A SLOPING BOTTOM

The effect of depth variations on solitary waves of shallow water wave theory is examined. The BBM–BBM type system (13) is simulated. In all the numerical results of this section we use  $N = 1024$ ,  $\theta^2 = \frac{7}{9}$ . Mass conservation is used to quantify the role of reflection in the shoaling of solitary waves. Note that the piecewise smooth linear bottom topography is used. To avoid the generation of small spurious oscillations due to the discontinuity in the derivative of the bottom function, it is smoothed near the singular points.

Consider a control volume delimited by the interval [50 m, 150 m] on the  $x$ -axis. The mass per unit width contained in this interval is defined by  $\int_{50}^{150} M(x, t) dx$  and the mass flux through the boundaries of the control volume is defined by  $q_M(50, t)$  and  $q_M(150, t)$ , where  $M$  and  $q_M$  are given in (18). The quantities  $M$  and  $q_M$  during the passage of a solitary wave are computed. It is observed that the mass outflux is approximately equal to the addition of mass influx and the reflection of the mass. As can be seen in Fig. 6, the mass reflection has negative values.

In Table 6, the results for various amplitudes of the solitary wave are displayed for  $\Delta h = 0.3$  m on a slope 1 : 35. For the height of the topography  $\Delta h = 0.3$  m, the mass influx through the initial boundary of the control volume is defined by ‘Mass outflux =  $\int_0^{15} q_m(50, t) dt$ ’, the mass outflux through the final boundary of the control volume is defined by ‘Mass outflux =  $\int_{15}^{60} q_m(150, t) dt$ ’, and the mass reflection through the initial boundary of the control volume is defined by ‘Mass reflection =  $\int_{15}^{60} q_m(50, t) dt$ ’. Note that the time limit may vary for other  $\Delta h$ ’s. The error is defined by ‘error = mass outflux–mass reflection–mass influx’. Table 6 suggests that mass conservation has a negligible error and that the error tends to 0 as  $\alpha = a/h_0$  approaches 0.

In Table 7, the results for various  $\Delta h$  of water level are displayed with initial amplitude  $a = 0.3$  m on a slope 1 : 35. It is clear from Table 6 and Table 7, that the mass conservation holds approximately for the coupled BBM system and the ratio between mass reflection and mass influx is called ‘mass ratio’, which is smaller for larger amplitude waves and smaller  $\Delta h$ .

The reflection of a small amplitude wave when a solitary wave goes through a slope is defined as ‘reflection’. To find the ratio between reflection and initial solitary wave, we use the following  $L^2$ -norm:

$$\|\eta\|_{L^2(\mathbb{R})}^2 = \int_{\mathbb{R}} |\eta(x)|^2 dx.$$

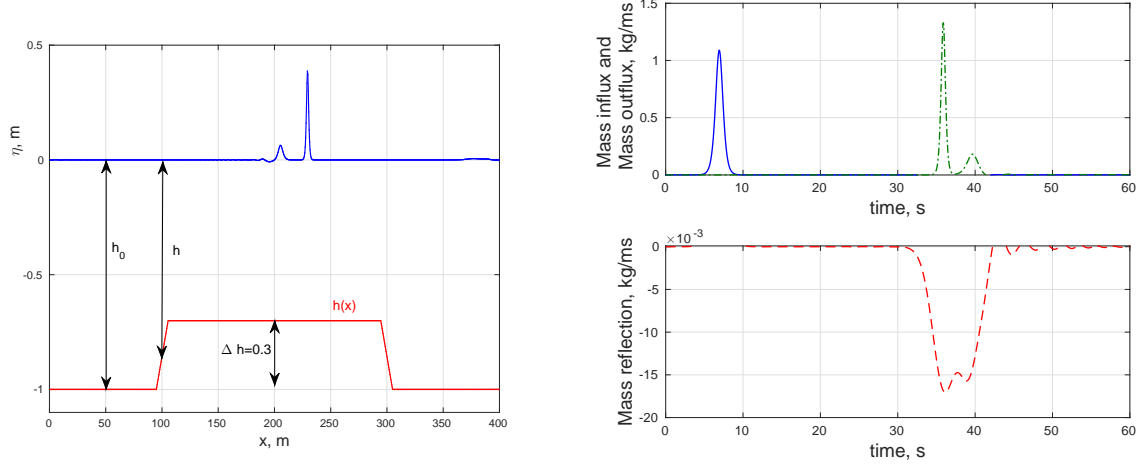


**Fig. 6.** The left panel shows a solitary wave solution for system (13) with the initial amplitude 0.3 m at time  $t = 60$  s. The right panel shows plots of time series of the mass influx at  $x = 50$  m (solid curve), the mass reflection at  $x = 50$  m (dashed curve), and mass outflux at  $x = 150$  m (dash-dotted curve), per unit span. The results are shown in the numerical domain.

**Table 6.** Error in mass conservation for different wave heights on a slope 1 : 35 and  $\Delta h = 0.3$  m (the height of the topography). The ‘error = mass outflux–mass reflection–mass influx’ quantifies the error in the mass balance law

Amplitude	Mass influx	Mass outflux	Mass reflection	Error	Reflection/ Influx
0.2	1.0995	1.0117	-0.0879	0.0001	0.0799
0.3	1.3856	1.2799	-0.1059	0.0002	0.0764
0.4	1.6438	1.5236	-0.1204	0.0002	0.0732
0.5	1.8856	1.7529	-0.1329	0.0002	0.0705
0.6	2.1166	1.9732	-0.1438	0.0003	0.0679

**Table 7.** The ratio between mass reflection and mass influx of a solitary wave with initial amplitude  $a = 0.3$  m on a slope 1 : 35 for different heights of the topography  $\Delta h$

$\Delta h$	Mass influx	Mass outflux	Mass reflection	Error	Reflection/ Influx
0.1	1.3856	1.3537	-0.0320	0.0001	0.0232
0.2	1.3856	1.3188	-0.0669	0.0001	0.0483
0.3	1.3856	1.2799	-0.1059	0.0002	0.0764
0.4	1.3856	1.2358	-0.1500	0.0002	0.1083
0.6	1.3856	1.1855	-0.2003	0.0002	0.1446

To calculate the  $L^2$ -norm of initial solitary waves, the value of  $\eta$  is integrated with respect to  $x$  on the fluid domain  $[0, L]$  at initial time  $t = 0$ . To determine the  $L^2$ -norm of a reflected wave, we run the solitary wave on the slope for long enough time to separate the reflection of the small wave from that of the solitary wave. The end point of the reflected waves on the  $x$ -axis is denoted by  $x_r$  (see Fig. 7). Then the reflected wave is integrated on the interval  $[0, x_r]$ . The corresponding ‘reflection coefficient’ is then defined to be

$$\frac{\|\eta_{\text{reflection}}\|_{L^2([0, x_r])}}{\|\eta_{\text{initial at } t=0}\|_{L^2([0, L])}}.$$

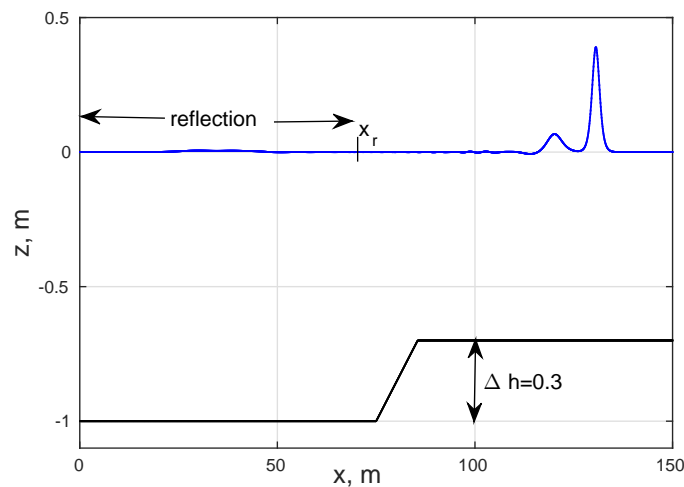


**Fig. 7.** Reflection of the transformation of solitary waves of initial amplitude 0.2 m on a slope  $S = 1 : 35$  and the height of the topography  $\Delta h = 0.3$  m in the physical domain.

**Table 8.** Calculation of the amount of ‘reflected’ waves for different slopes and amplitudes. It shows that the ‘reflection coefficient’ approaches zero as the slope becomes more and more gentle. Here  $\Delta h$  is the height of the topography and  $H_0$  is the initial wave amplitude

Slope	$\Delta h = 0.3, H_0 = 0.3$		$\Delta h = 0.2, H_0 = 0.2$		$\Delta h = 0.1, H_0 = 0.1$	
	$\ \eta_{\text{reflection}}\ _{L^2}$	Reflect. coeff.	$\ \eta_{\text{reflection}}\ _{L^2}$	Reflect. coeff.	$\ \eta_{\text{reflection}}\ _{L^2}$	Reflect. coeff.
1 : 35	4.70e-04	1.70e-03	1.76e-04	1.20e-03	2.61e-05	5.19e-04
1 : 100	1.77e-04	6.40e-04	7.11e-05	4.85e-04	1.45e-05	2.88e-04
1 : 400	2.82e-05	1.02e-04	1.42e-05	9.69e-05	4.24e-06	8.43e-05
1 : 800	8.73e-05	3.15e-05	3.04e-06	2.08e-05	3.56e-07	7.08e-06

The ‘reflection coefficient’ approaches zero as the slope becomes more and more gentle (Table 8). Moreover, the reflection coefficient for the steep slope (1 : 35) is approximately twice the value of that of the mild slope (1 : 100). For steeper slopes the reflection coefficient is large because the wave height at breaking points is smaller for a steep slope than for a mild slope.

## 6. CONCLUSION

In this article, a coupled BBM system of equations is studied in the situation of water waves propagating over a decreasing fluid depth. A conservation equation for mass and also a wave breaking criterion, both valid in the Boussinesq approximation, were found. A Fourier collocation method coupled with a 4-stage Runge–Kutta time integration scheme was employed in this work to approximate the solution of the BBM system. It is shown that the approximate mass conservation relation is reasonably accurate. Moreover, the results from the evaluation of the approximate mass conservation law show that the ratio of mass reflection to mass influx approaches zero as the difference in flow depths ( $\Delta h$ ) becomes small.

In our previous paper [20] we showed that for waves of very small amplitude, the shoaling relation approaches Boussinesq’s law for Boussinesq-type systems that are valid for waves with the Stokes number  $S = \alpha/\beta$  of order 1, and in this case we measured the transition of the wave only at the initial and final stage

assuming the wave undergoes an adiabatic adjustment. It is confirmed (Table 8) that the  $L^2$ -ratio between reflection and initial solitary wave approaches zero as the slope becomes more and more gentle. This lends additional credibility to shoaling results based on adiabatic approximation. In addition, the results displayed in Fig. 3 indicate that shoaling rates for small amplitude waves are closer to those predicted by Boussinesq's law for very gentle slopes.

Considering the shoaling of finite amplitude waves, we compared shoaling curves obtained with the current method to numerical results of Grilli et al. [17] for the Euler equations based on potential flow theory. The experimental results of Grilli et al. [16], and the corresponding shoaling curve of the current work were in good agreement with the numerical results of Grilli et al. [16,17]. It was found that the variation in wave height of a shoaling solitary wave initially increased at a lower rate than predicted by Green's law, but then increased similar to Boussinesq's law. Indeed, the shoaling curves achieved in this paper match the shoaling curves of Grilli et al. [17] better than the similar approximation established by Khorsand and Kalisch [22].

The comparison of shoaling curves of two model systems, (13) ([31]) and (28) ([8]), with the numerical results of Grilli et al. [17] showed that each of these models works well in their respective regimes of applicability. The agreement of the breaking criterion (21) with the results of Grilli et al. [17] is much better on a mild slope.

## ACKNOWLEDGEMENTS

I would like to thank my supervisor, Professor Henrik Kalisch for his helpful guidance, comments, and detailed correction on this work. This research was supported by the Research Council of Norway. I am grateful to the anonymous reviewers for their valuable comments and suggestions to improve the quality of the paper. The publication costs of this article were covered by the Estonian Academy of Sciences.

## REFERENCES

- Ali, A. and Kalisch, H. Mechanical balance laws for Boussinesq models of surface water waves. *J. Nonlinear Sci.*, 2012, **22**, 371–398.
- Ali, A. and Kalisch, H. On the formation of mass, momentum and energy conservation in the KdV equation. *Acta Appl. Math.*, 2014, **133**, 113–131.
- Benjamin, T. B., Bona, J. L., and Mahony, J. J. Model equations for long waves in nonlinear dispersive systems. *Philos. T. Roy. Soc. A*, 1972, **272**, 47–78.
- Bjørkavåg, M. and Kalisch, H. Wave breaking in Boussinesq models for undular bores. *Phys. Lett. A*, 2011, **375**(14), 1570–1578.
- Bona, J. L., Chen, M., and Saut, J. C. Boussinesq equations and other systems for small-amplitude long waves in nonlinear dispersive media. I: Derivation and linear theory. *J. Nonlinear Sci.*, 2002, **12**(4), 283–318.
- Camfield, F. E. and Street, R. L. Shoaling of solitary waves on small slopes. *J. Waterw. Harb. Coast. Eng.*, 1969, **95**(1), 1–22.
- Chen, M. Exact solutions of various Boussinesq systems. *Appl. Math. Lett.*, 1998, **11**(5), 45–49.
- Chen, M. Equations for bi-directional waves over an uneven bottom. *Math. Comput. Simulat.*, 2003, **62**(1-2), 3–9.
- Chou, C. R. and Quyang, K. The deformation of solitary waves on steep slopes. *J. Chin. Inst. Eng.*, 1999, **22**(6), 805–812.
- Chou, C. R. and Quyang, K. Breaking of solitary waves on uniform slopes. *China Ocean Eng.*, 1999, **13**(4), 429–442.
- Chou, C. R., Shih, R. S., and Yim, J. Z. Numerical study on breaking criteria for solitary waves. *China Ocean Eng.*, 2003, **17**(4), 589–604.
- Duncan, J. H. Spilling breakers. *Annu. Rev. Fluid Mech.*, 2001, **33**, 519–547.
- Filippini, A. G., Bellec, S., Colin, M., and Ricchiuto, M. On the nonlinear behaviour of Boussinesq type models: Amplitude-velocity vs amplitude-flux forms. *Coast. Eng.*, 2015, **99**, 109–123.
- Gottlieb, D. and Orszag, S. A. *Numerical Analysis of Spectral Methods: Theory and Applications*. SIAM, Philadelphia, 1977.
- Green, A. E. and Naghdi, P. M. A derivation of equations for wave propagation in water of variable depth. *J. Fluid Mech.*, 1976, **78**(2), 237–246.
- Grilli, S. T., Subramanya, R., Svendsen, I. A., and Veeramony, J. Shoaling of solitary waves on plane beaches. *J. Waterw. Port C-ASCE*, 1994, **120**, 609–628.
- Grilli, S. T., Svendsen, I. A., and Subramanya, R. Breaking criterion and characteristics for solitary waves on slopes. *J. Waterw. Port C-ASCE*, 1997, **123**, 102–112.
- Ippen, A. and Kulin, G. The shoaling and breaking of the solitary wave. *Coast. Eng. Proc.*, 1954, No 5, Chapter 4, 27–47.

19. Johnson, R. S. On the development of a solitary wave moving over uneven bottom. *Proc. Cambridge Philos. Soc.*, 1973, **73**, 183–203.
20. Kalisch, H. and Senthilkumar, A. Derivation of Boussinesq's shoaling law using a coupled BBM system. *Nonlin. Processes Geophys.*, 2013, **20**, 213–219.
21. Kennedy, A. B., Chen, Q., Kirby, J. T., and Dalrymple, R. A. Boussinesq modeling of wave transformation, breaking, and runup. I: 1D. *J. Waterw. Port C-ASCE.*, 2000, **126**, 39–47.
22. Khorsand, Z. and Kalisch, H. On the shoaling of solitary waves in the KdV equation. *Coast. Eng. Proc.*, 2014, **34**, waves 44.
23. Kishi, T. and Saeki, H. The shoaling, breaking and runup of the solitary wave on impermeable rough slopes. *Coast. Eng. Proc.*, 2011, **10**, 322–347.
24. Longuet-Higgins, M. S. On the mass, momentum, energy and circulation of a solitary wave. *Proc. Roy. Soc. A.*, 1974, **337**, 1–13.
25. Longuet-Higgins, M. S. and Fenton, J. D. On the mass, momentum, energy and circulation of a solitary wave II. *Proc. Roy. Soc. A.*, 1974, **340**, 471–493.
26. Madsen, O. S. and Mei, C. C. The transformation of a solitary wave over an uneven bottom. *J. Fluid Mech.*, 1969, **39**, 781–791.
27. Madsen, P. A., Murray, R., and Sørensen, O. R. A new form of the Boussinesq equations with improved linear dispersion characteristics. *Coast. Eng.*, 1991, **15**(4), 371–388.
28. Madsen, P. A. and Schäffer, H. A. Higher-order Boussinesq-type equations for surface gravity waves: derivation and analysis. *Philos. T. Roy. Soc. A.*, 1998, **356**, 3123–3184.
29. McCowan, J. On the highest wave of permanent type. *Philos. Mag.*, 1894, **38**, 351–357.
30. Miles, J. W. On the Korteweg–de Vries equation for a gradually varying channel. *J. Fluid Mech.*, 1979, **91**, 181–190.
31. Mitsotakis, D. E. Boussinesq systems in two space dimensions over a variable bottom for the generation and propagation of tsunami waves. *Math. Comput. Simulat.*, 2009, **80**(4), 860–873.
32. Nwogu, O. Alternative form of Boussinesq equations for nearshore wave propagation. *J. Waterw. Port C-ASCE.*, 1993, **119**, 618–638.
33. Ostrovsky, L. A. and Pelinovsky, E. N. Wave transformation on the surface of a fluid of variable depth. *Atmos. Oceanic Phys.*, 1970, **6**, 552–555.
34. Pelinovsky, E. N. and Talipova, T. G. Height variations of large amplitude solitary waves in the near-shore zone. *Oceanology*, 1977, **17**(1), 1–3.
35. Pelinovsky, E. N. and Talipova, T. G. Change of height of the solitary wave of large amplitude in the beach zone. *Mar. Geodesy*, 1979, **2**(4), 313–321.
36. Peregrine, D. H. Long waves on a beach. *J. Fluid Mech.*, 1967, **27**(4), 815–827.
37. Senthilkumar, A. BBM equation with non-constant coefficients. *Turk. J. Math.*, 2013, **37**, 652–664.
38. Svendsen, I. A. *Introduction to Nearshore Hydrodynamics*. World Scientific, Singapore, 2006, **24**.
39. Synolakis, C. E. The runup of solitary waves. *J. Fluid Mech.*, 1987, **185**, 523–545.
40. Teng, M. H. and Wu, T. Y. Evolution of long water waves in variable channels. *J. Fluid Mech.*, 1994, **266**, 303–317.
41. Trefethen, L. N. *Spectral Methods in Matlab*. SIAM, Philadelphia, 2000.
42. Wei, G., Kirby, J. T., Grilli, S. T., and Subramanya, R. A fully nonlinear Boussinesq model for surface waves. Part 1. Highly nonlinear unsteady waves. *J. Fluid Mech.*, 1995, **294**, 71–92.
43. Whitham, G. *Linear and Nonlinear Waves*. Wiley, New York, 1974.

## Peegeldumise mõjust üksiklaine teravdumisele ja murdumisele

Amutha Senthilkumar

Seostatud Benjamini-Bona-Mahony (BBM) võrrandisüsteemi on uuritud olukorras, kus pinnalained levivad kahaneva sügavusega vees. On leitud massijäävusvörrand ja laine murdumise tingimus, mis kehitivad Boussinesqi aproksimatsioonil. Lähendlahendi leidmiseks BBM võrrandisüsteemile on kasutatud Fourier' kollokatsioonimeetodit koos 4-astmelise Runge-Kutta ajas integreerimise numbrilise skeemiga. Peegeldumise mõju kvantitatiivseks hindamiseks üksiklaine teravdumisele ja murdumisele kaldega põhjaprofililt on kasutatud massijäävusvörrandit. On analüüsitud teravdumise tulemusi, mis tuginevad adiabaatilisele aproksimatsioonile. On uuritud üksiklaine teravdumist ja murdumist kaldega põhjaprofile korral. Numbrilise mudeli valideerimiseks on tulemusi kõrvutatud kirjandusest saadavaga, millega kokkulangevus on hea. Üksiklaine teravdumist on arvutatud kaht eri tüüpi väikese kaldega mudelusteedidele ja võrdlus kirjandusest saadavate lahenditega näitab, et kumbki mudel on oma rakenduspiirkonnas adekvaatne.

## Paper C

# Particle Trajectories in Nonlinear Waves on a Uniform Shear Flow

# Particle Trajectories in Nonlinear Waves on a Uniform Shear Flow

Henrik Kalisch and Amutha Senthilkumar  
Department of Mathematics, University of Bergen  
Postbox 7800, 5020 Bergen, Norway

January 18, 2017

## Abstract

This article is devoted to the numerical study of particle paths associated to the propagation of nonlinear water waves on linear shear flows over a flat bottom. Boussinesq-type equations for two-dimensional water waves with constant vorticity are derived under the assumption that nonlinear and dispersive terms are small and have the same order of magnitude. For the unidirectional case, Korteweg-de Vries (KdV) equations are found with coefficients which depend on the vorticity. The approximate velocity field associated with exact solutions of the KdV equation over a shear flow is found, and this velocity field is used to find approximate particle paths for flows corresponding to solitary waves and periodic traveling waves.

## 1 Introduction

Boussinesq-type models have been used for calculation of the transformation of nonlinear and dispersive waves in coastal areas where horizontal vorticity is assumed zero. In nature, mostly water flows include shear flows, it is no longer relevant to use the assumption of irrotational flows when gravity waves propagate on the surface of shear flows. Shallow-water theory is modified by the inclusion of the effects of the vorticity and this was first assumed by Burns [4], who studied the range of wave celerity for general velocity profiles. Recently, several authors [1, 2, 5, 6, 7, 8, 9, 11, 21, 22] have added the influence of horizontal vorticity on the waves in their works. To avoid mathematical complexity and to confine the consequence of background vorticity, a simple case of constant vorticity has been assumed.

In this current work the KdV equation is developed from the Boussinesq equations for all surface gravity waves for the particular case of flow with constant vorticity. This is solved to give first-order equations for solitary and cnoidal waves in terms of surface elevation and also careful examination of the derivation of the equation as a surface water-wave model in the presence of the shear flow shows that it is possible to reconstruct an approximate fluid velocity field underneath the free surface. In particular, it is potential to derive formulas showing the horizontal and vertical velocity components in terms of the principal unknown variable  $\eta$  which describes the shape of the free surface and known variable  $\Gamma$  which characterize the vorticity.

The study of particle trajectories beneath a surface wave is a problem of great interest that dates from the late nineteenth century [17]. Within the linear water wave theory, there

is a classical first order approximation showing that all particle trajectories are closed cf. [10, 14, 15, 18]. Stokes [19] showed that the particle paths are not closed for the periodic waves in deep water, due to the passage of a periodic surface wave, the particle trajectories lead to a net mass-transport in the direction of wave propagation for irrotational wave, and this result is known as the Stokes drift. Notable work was later done by Ursell [20] who indicated that Stokes's argument would be true for waves in channels of finite depth. Constantin [6] showed mathematically and geometrically that there are no closed particle paths and fluid particles experience a horizontal forward motion for a free boundary problem in an irrotational and inviscid flow over a flat bed in an Eulerian coordinate frame. In [3], they showed that the particle paths are nearly closed for cnoidal waves by considering exact solutions of the KdV equation.

However, Gerstner [12] was the first who applied Lagrangian coordinates to study the periodic surface gravity waves with finite vorticity, and arrived at the conclusion that the surface curve was trochoidal in form, that is all particles move on circles. In [13], there is a simple approach showing that Gerstner's flow is dynamically possible: each particle moves on a circle, but the particles never collide and fill out the entire region below the surface wave. Several years later, Constantin and Strauss [8] proved that there is the possibility of a closed particle trajectory in the presence of a current. Moreover in 2014, a diversity of orbit patterns were described numerically, including the case of a closed orbit, when a stokes wave propagates in the presence of an adverse current by Nachbin and Ribeiro-Junior [17].

The aim of this paper is to provide a clear qualitative picture of the particle trajectories throughout the fluid domain for nonlinear water waves on the shear flows. This paper is organized as follows: In Section 2, we briefly review the derivation of the family of Boussinesq system in the presence of the shear flow. Then the derivation of the KdV equation is outlined and the approximate velocity field in terms of the shape of the free surface  $\eta$  and constant vorticity  $\Gamma$ . In Section 3, we use the velocity field formulas in connection with exact solutions to consider numerical particle trajectories for different vorticity values associated to surface solitary wave. Section 4 is devoted to numerical study of particle trajectories associated with propagation of a periodic wave. Finally, Section 5 has the conclusions.

## 2 Formulation of the mathematical problem

For an inviscid and incompressible fluid, the surface water-wave problem is given by the Euler equations with no-flow conditions at the bottom and kinematic and dynamic boundary conditions at the free surface. Let the spatial coordinates be  $(x, z)$  and the  $x$ -axis be oriented in the horizontal direction. Assume that the motion is uniform in the direction perpendicular to the  $xz$ -plane (long-crested waves). The gravitational acceleration  $g$  is in the negative  $z$ -direction. Let  $\eta(x, t)$  denote the surface elevation. Assume that there is a uniform shear flow with free surface, as shown in Fig. 1 and for the case of constant vorticity  $\Gamma$ , the background velocity distribution is  $(-(z + h_0)\Gamma, 0)$ , where  $h_0$  is water depth. For  $\Gamma > 0$  we have a shear flow in the opposite wave-propagation direction, while for  $\Gamma \leq 0$  it is in a favorable direction.

Let us briefly introduce the model system for nonlinear waves on the uniform shear flow to be used here. Assuming  $a$  is a typical amplitude and  $l$  is a typical wavelength of the waves to be described, the parameter  $\alpha = a/h_0$  represents the waveheight to depth ratio and the parameter  $\beta = h_0^2/l^2$  represents a water depth to wavelength ratio.

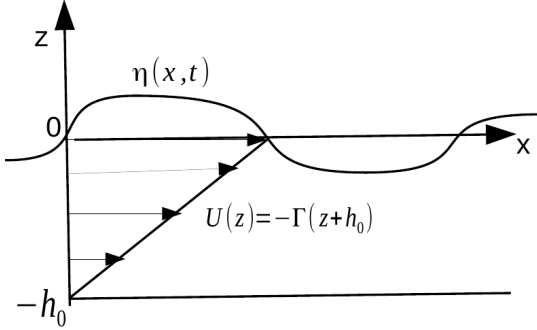


Figure 1: Wave propagation over a uniform shear flow. In this figure, the  $\Gamma$  is negative.

For uniform shear flow,  $\phi(x, z, t)$  is the velocity potential of the disturbances satisfying

$$\left. \begin{aligned} U &= u - (z + h_0)\Gamma = \frac{\partial \phi}{\partial x} - (z + h_0)\Gamma, \\ W &= w = \frac{\partial \phi}{\partial z}. \end{aligned} \right\} \quad (1)$$

In case of incompressible, inviscid fluid with conservative body force, the vorticity equation is

$$\frac{\partial \omega}{\partial t} + (\mathbf{u} \cdot \nabla) \omega = \omega \cdot \nabla \mathbf{u}. \quad (2)$$

Since  $\omega = \nabla \times \mathbf{u} = \Gamma e_y = \text{constant}$ , Eq. (2) is automatically satisfied for plane flow. And from the incompressibility condition  $\nabla \cdot \mathbf{u} = 0$ , we have

$$\frac{\partial}{\partial x} \left( \frac{\partial \phi}{\partial x} - (z + h_0)\Gamma \right) + \frac{\partial}{\partial z} \left( \frac{\partial \phi}{\partial z} \right) = 0.$$

The complete problem is written as follows.

$$\Delta \phi = 0 \quad \text{in } -h_0 < z < \eta(x, t), \quad (3)$$

$$\phi_z = 0 \quad \text{on } z = -h_0, \quad (4)$$

$$\left. \begin{aligned} \eta_t + U \eta_x - W &= 0, \\ \mathbf{u}_t + \frac{1}{2} \nabla |\mathbf{u}|^2 - \mathbf{u} \times \omega + g e_z &= 0, \end{aligned} \right\} \quad \text{on } z = \eta(x, t). \quad (5)$$

The next goal will be to derive a Boussinesq systems approximating the wave motion described by (3)-(5). To this end, we follow the development explained in [22]. For starters, the variables are non-dimensionalized using the following scaling:

$$\tilde{x} = \frac{x}{l}, \quad \tilde{z} = \frac{z}{h_0}, \quad \tilde{t} = \frac{\sqrt{gh_0}t}{l}, \quad (6a)$$

$$\text{and } \tilde{\Gamma} = \frac{\Gamma h_0}{\sqrt{gh_0}}, \quad \tilde{\eta} = \frac{\eta}{a}, \quad \tilde{\phi} = \frac{h_0}{al\sqrt{gh_0}}\phi. \quad (6b)$$

Then we get the equation

$$\beta \tilde{\phi}_{\tilde{x}\tilde{x}} + \tilde{\phi}_{\tilde{z}\tilde{z}} = 0 \quad -1 < \tilde{z} < \alpha \tilde{\eta}, \quad (7)$$

and the following boundary conditions: at the bottom  $\tilde{z} = -1$ , we have

$$\tilde{\phi}_{\tilde{z}} = 0, \quad (8)$$

and at the free surface  $\tilde{z} = \alpha\tilde{\eta}$ , the non-dimensional kinematic condition is

$$\beta \left\{ \frac{\partial \tilde{\eta}}{\partial \tilde{t}} + \left[ -(1 + \alpha\tilde{\eta})\tilde{\Gamma} + \alpha \frac{\partial \tilde{\phi}}{\partial \tilde{x}} \right] \frac{\partial \tilde{\eta}}{\partial \tilde{x}} \right\} = \tilde{\phi}_{\tilde{z}}, \quad (9)$$

while for the non-dimensional dynamic condition, we reformulate the dynamic Eq. (5) as

$$\nabla \left( \phi_t + \frac{|\mathbf{u}|^2}{2} + G + g\eta \right) = 0, \quad (10)$$

where

$$\nabla G = -\mathbf{u} \times \omega = (-\Gamma w, 0, \Gamma u - \Gamma^2(h_0 + z)), \quad (11)$$

$$\text{and } G = \Gamma \int_{-h_0}^z \frac{\partial \phi}{\partial x} dz - \frac{\Gamma^2}{2}(h_0 + z)^2. \quad (12)$$

So the non-dimensional dynamic condition may be expressed as

$$\beta(\tilde{\phi}_{\tilde{t}} + \tilde{\eta}) + \frac{\alpha\beta}{2} \left[ \tilde{\phi}_{\tilde{x}} - \frac{\tilde{\Gamma}}{\alpha}(1 + \alpha\tilde{\eta}) \right]^2 + \frac{\alpha}{2} \left[ \frac{\partial \tilde{\phi}}{\partial \tilde{z}} \right]^2 + \frac{\beta}{ag} G = 0. \quad (13)$$

The non-dimensional potential  $\tilde{\phi}$  is expressed in powers of  $(1 + \tilde{z})$  as

$$\tilde{\phi} = \sum_{n=0}^{\infty} (1 + \tilde{z})^n \phi_n. \quad (14)$$

From Eq. (7), Eq. (14) and Eq. (8), we have

$$\tilde{\phi} = \phi_0 - \frac{\beta}{2}(1 + \tilde{z})^2 \frac{\partial^2 \phi_0}{\partial \tilde{x}^2} + \frac{\beta^2}{24}(1 + \tilde{z})^4 \frac{\partial^4 \phi_0}{\partial \tilde{x}^4} + \mathcal{O}(\beta^3). \quad (15)$$

To find a closed system of two evolution equations, we substitute the asymptotic expression for  $\tilde{\phi}$  in the boundary conditions Eq. (9) and Eq. (13), and collect all terms of zeroth and first order in  $\alpha$  and  $\beta$ . Then we differentiate dynamic bottom boundary with respect to  $\tilde{x}$  and expressed the boundary conditions in terms of the non-dimensional horizontal velocity at the bottom  $\frac{\partial \phi_0}{\partial \tilde{x}} = \tilde{v}$ . This procedure yields the system of equations

$$\begin{aligned} \tilde{\eta}_{\tilde{t}} + \tilde{v}_{\tilde{x}} - \tilde{\Gamma}\tilde{\eta}_{\tilde{x}} - \alpha\tilde{\Gamma}\tilde{\eta}\tilde{\eta}_{\tilde{x}} + \alpha(\tilde{\eta}\tilde{v})_{\tilde{x}} - \frac{\beta}{6} \frac{\partial^3 \tilde{v}}{\partial \tilde{x}^3} &= \mathcal{O}(\alpha\beta, \beta^2), \\ \tilde{v}_{\tilde{t}} + \tilde{\eta}_{\tilde{x}} + \alpha\tilde{v}\tilde{\eta}_{\tilde{x}} - \frac{\beta}{2} \frac{\partial^3 \tilde{v}}{\partial \tilde{x}^2 \partial \tilde{t}} + \frac{\beta}{3} \tilde{\Gamma} \frac{\partial^3 \tilde{v}}{\partial \tilde{x}^3} &= \mathcal{O}(\alpha\beta, \beta^2). \end{aligned} \quad (16)$$

Next, a family of Boussinesq systems is derived using the standard technique of describing the horizontal velocity component at different heights in the fluid column. If we let  $\tilde{u}^\theta$  be the non-dimensional velocity at a non-dimensional height  $\tilde{z}_\theta = -1 + \theta(\alpha\tilde{\eta} + 1)$ , with  $0 \leq \theta \leq 1$ , then Taylor's formula shows that

$$\tilde{u}^\theta = \tilde{v} - \frac{\beta}{2}(1 + \tilde{z}_\theta)^2 \frac{\partial^2 \tilde{v}}{\partial \tilde{x}^2} + \mathcal{O}(\beta^2) = \tilde{v} - \frac{\beta}{2}\theta^2 \frac{\partial^2 \tilde{v}}{\partial \tilde{x}^2} + \mathcal{O}(\alpha\beta, \beta^2). \quad (17)$$

Applying the standard techniques of inversion it is not difficult to derive the following expression as an asymptotic formula for  $\tilde{v}$  in terms of  $\tilde{u}^\theta$ :

$$\tilde{v} = \tilde{u}^\theta + \frac{\beta}{2} \theta^2 \frac{\partial^2 \tilde{u}^\theta}{\partial \tilde{x}^2} + \mathcal{O}(\alpha\beta, \beta^2). \quad (18)$$

Substituting this representation into the system Eq. (16) yields

$$\begin{aligned} \tilde{\eta}_t + \tilde{u}_{\tilde{x}}^\theta - \tilde{\Gamma} \tilde{\eta}_{\tilde{x}} - \alpha \tilde{\Gamma} \tilde{\eta} \tilde{\eta}_{\tilde{x}} + \alpha (\tilde{\eta} \tilde{u}^\theta)_{\tilde{x}} + \frac{\beta}{2} (\theta^2 - \frac{1}{3}) \frac{\partial^3 \tilde{u}^\theta}{\partial \tilde{x}^3} &= \mathcal{O}(\alpha\beta, \beta^2), \\ \tilde{u}_t^\theta + \tilde{\eta}_{\tilde{x}} + \alpha \tilde{u}^\theta \tilde{u}_{\tilde{x}}^\theta + \frac{\beta}{2} (\theta^2 - 1) \frac{\partial^3 \tilde{u}^\theta}{\partial \tilde{x}^2 \partial t} + \frac{\beta}{3} \tilde{\Gamma} \frac{\partial^3 \tilde{u}^\theta}{\partial \tilde{x}^3} &= \mathcal{O}(\alpha\beta, \beta^2). \end{aligned} \quad (19)$$

Now for any real  $\lambda$  and  $\mu$ , the above system is a special case of the more general system

$$\begin{aligned} \tilde{\eta}_t + \tilde{u}_{\tilde{x}}^\theta - (1 + \alpha \tilde{\eta}) \tilde{\Gamma} \tilde{\eta}_{\tilde{x}} + \alpha (\tilde{\eta} \tilde{u}^\theta)_{\tilde{x}} + \frac{\beta}{2} (\theta^2 - \frac{1}{3}) \lambda \tilde{u}_{\tilde{x}\tilde{x}\tilde{x}}^\theta - \frac{\beta}{2} (\theta^2 - \frac{1}{3}) (1 - \lambda) \tilde{\eta}_{\tilde{x}\tilde{x}\tilde{x}} &= \mathcal{O}(\alpha\beta, \beta^2), \\ \tilde{u}_t^\theta + \tilde{\eta}_{\tilde{x}} + \alpha \tilde{u}^\theta \tilde{u}_{\tilde{x}}^\theta + \frac{\beta}{2} (1 - \theta^2) \mu \tilde{\eta}_{\tilde{x}\tilde{x}\tilde{x}} - \frac{\beta}{2} (1 - \theta^2) (1 - \mu) \tilde{u}_{\tilde{x}\tilde{x}\tilde{x}}^\theta + \frac{\beta}{3} \tilde{\Gamma} \tilde{u}_{\tilde{x}\tilde{x}\tilde{x}}^\theta &= \mathcal{O}(\alpha\beta, \beta^2). \end{aligned} \quad (20)$$

We now concentrate on unidirectional waves. In the lowest order the Boussinesq equation is the linear system

$$\tilde{\eta}_t + \tilde{u}_{\tilde{x}}^\theta - \tilde{\Gamma} \tilde{\eta}_{\tilde{x}} = 0, \quad \tilde{u}_t^\theta + \tilde{\eta}_{\tilde{x}} = 0. \quad (21)$$

The system can be diagonalized by introducing characteristic coordinates. Introduce new variables  $r$  and  $s$  defined by  $(r, s) = P^{-1}(\tilde{\eta}, \tilde{u}^\theta)$  where

$$P^{-1} = \frac{1}{1 + (\tilde{c}_+)^2} \begin{pmatrix} \tilde{c}_+ & 1 \\ -1 & \tilde{c}_+ \end{pmatrix}, \quad (22)$$

with  $\tilde{c}_+ = \frac{-\tilde{\Gamma}}{2} + \sqrt{\frac{\tilde{\Gamma}^2}{4} + 1}$ . A simple calculation shows that

$$\begin{pmatrix} r_t \\ s_t \end{pmatrix} + \begin{pmatrix} \tilde{c}_+ & 0 \\ 0 & \tilde{c}_- \end{pmatrix} \begin{pmatrix} r_x \\ s_x \end{pmatrix} = 0 \quad (23)$$

where  $\tilde{c}_- = \frac{-\tilde{\Gamma}}{2} - \sqrt{\frac{\tilde{\Gamma}^2}{4} + 1}$  is the conjugate of  $\tilde{c}_+$ . The solutions of system (23) are

$$r = r_0(x - \tilde{c}_+ t) \text{ and } s = s_0(x - \tilde{c}_- t). \quad (24)$$

The solution to Eq.(21) is, therefore,

$$\begin{aligned} \tilde{u}^\theta(x, t) &= \frac{1}{1 + \tilde{c}_+^2} \left[ \tilde{c}_+ \tilde{\eta}_0(x - \tilde{c}_+ t) + \tilde{u}_0^\theta(x - \tilde{c}_+ t) - \tilde{c}_+ \tilde{\eta}_0(x - \tilde{c}_- t) + \tilde{c}_+^2 \tilde{u}_0^\theta(x - \tilde{c}_- t) \right], \\ \tilde{\eta}(x, t) &= \frac{1}{1 + \tilde{c}_+^2} \left[ \tilde{c}_+^2 \tilde{\eta}_0(x - \tilde{c}_+ t) + \tilde{c}_+ \tilde{u}_0^\theta(x - \tilde{c}_+ t) + \tilde{\eta}_0(x - \tilde{c}_- t) - \tilde{c}_+ \tilde{u}_0^\theta(x - \tilde{c}_- t) \right]. \end{aligned} \quad (25)$$

The unidirectional KdV equation is derived from the system (19) by specializing to a wave moving to the right with speed  $\tilde{c}_+$ .

$$\tilde{u}^\theta = -\tilde{c}_- \tilde{\eta} + \alpha A + \beta B + \mathcal{O}(\alpha\beta, \beta^2), \quad (26)$$

where  $A$  and  $B$  are functions of  $\tilde{\eta}$  and its  $\tilde{x}$  derivatives. Then the system (19) becomes

$$\begin{aligned}\tilde{\eta}_{\tilde{t}} + \tilde{c}_+ \tilde{\eta}_{\tilde{x}} + \alpha(-2\tilde{c}_- \tilde{\eta} \tilde{\eta}_{\tilde{x}} - \tilde{\Gamma} \tilde{\eta} \tilde{\eta}_{\tilde{x}} + A_{\tilde{x}}) + \beta(B_{\tilde{x}} - \frac{1}{2}\tilde{c}_-(\theta^2 - \frac{1}{3})\tilde{\eta}_{\tilde{x}\tilde{x}\tilde{x}}) &= \mathcal{O}(\alpha\beta, \beta^2), \\ \tilde{\eta}_{\tilde{t}} + \tilde{c}_+ \tilde{\eta}_{\tilde{x}} + \alpha(\tilde{c}_+ A_{\tilde{t}} - \tilde{c}_- \tilde{\eta} \tilde{\eta}_{\tilde{x}}) + \beta(\tilde{c}_+ B_{\tilde{t}} + \frac{1}{2}(\theta^2 - 1)\tilde{\eta}_{\tilde{x}\tilde{x}\tilde{t}} + \frac{\tilde{\Gamma}}{3}\tilde{\eta}_{\tilde{x}\tilde{x}\tilde{x}}) &= \mathcal{O}(\alpha\beta, \beta^2).\end{aligned}\quad (27)$$

Since  $\tilde{\eta}_{\tilde{t}} = -\tilde{c}_+ \tilde{\eta}_{\tilde{x}}$ , all derivatives in the first order terms may be replaced by  $-\tilde{c}_+$  times the  $x$  derivatives. Then the two equations are consistent if

$$A = \frac{\tilde{c}_- + \tilde{\Gamma}}{2(1 + \tilde{c}_+^2)} \tilde{\eta}^2 \quad \text{and} \quad B = \left( \frac{\tilde{c}_+ + \tilde{\Gamma}}{3(1 + \tilde{c}_+^2)} - \frac{\tilde{c}_-}{6} + \frac{\tilde{c}_-}{2}\theta^2 \right) \tilde{\eta}_{\tilde{x}\tilde{x}}. \quad (28)$$

Hence we have

$$\tilde{u}^\theta = -\tilde{c}_- \tilde{\eta} + \alpha \frac{\tilde{c}_- + \tilde{\Gamma}}{2(1 + \tilde{c}_+^2)} \tilde{\eta}^2 + \beta \left( \frac{\tilde{c}_+ + \tilde{\Gamma}}{3(1 + \tilde{c}_+^2)} - \frac{\tilde{c}_-}{6} + \frac{\tilde{c}_-}{2}\theta^2 \right) \tilde{\eta}_{\tilde{x}\tilde{x}} + \mathcal{O}(\alpha\beta, \beta^2), \quad (29)$$

$$\tilde{\eta}_{\tilde{t}} + \tilde{c}_+ \tilde{\eta}_{\tilde{x}} + \alpha \frac{\tilde{c}_+(3 + \tilde{\Gamma}^2)}{(1 + \tilde{c}_+^2)} \tilde{\eta} \tilde{\eta}_{\tilde{x}} + \beta \frac{\tilde{c}_+ + \tilde{\Gamma}}{3(1 + \tilde{c}_+^2)} \tilde{\eta}_{\tilde{x}\tilde{x}\tilde{x}} = \mathcal{O}(\alpha\beta, \beta^2). \quad (30)$$

From Eq. (18), the non-dimensional horizontal velocity at the bottom is

$$\tilde{v} = -\tilde{c}_- \tilde{\eta} + \alpha \frac{\tilde{c}_- + \tilde{\Gamma}}{2(1 + \tilde{c}_+^2)} \tilde{\eta}^2 + \beta \frac{\tilde{c}_+ + \tilde{\Gamma}}{3(1 + \tilde{c}_+^2)} \tilde{\eta}_{\tilde{x}\tilde{x}} - \tilde{c}_- \frac{\beta}{6} \frac{\partial^2 \tilde{\eta}}{\partial \tilde{x}^2} + \mathcal{O}(\alpha\beta, \beta^2). \quad (31)$$

From Eq. (15), the non-dimensional horizontal velocity and the non-dimensional vertical velocity at the bottom become

$$\begin{aligned}\tilde{u} &= \tilde{v} - \frac{\beta}{2}(1 + \tilde{z})^2 \frac{\partial^2 \tilde{v}}{\partial \tilde{x}^2} + \mathcal{O}(\beta^2), \\ \tilde{w} &= -\beta(1 + \tilde{z}) \frac{\partial \tilde{v}}{\partial \tilde{x}} + \mathcal{O}(\beta^2).\end{aligned}\quad (32)$$

From Eq. (18) and Eq. (32), the non-dimensional horizontal velocity and the non-dimensional vertical velocity at a non-dimensional height  $\tilde{z}_\theta = -1 + \theta(\alpha\tilde{\eta} + 1)$  become

$$\begin{aligned}\tilde{u} &= \tilde{u}^\theta + \frac{\beta}{2} (\theta^2 - (1 + \tilde{z}_\theta)^2) \frac{\partial^2 \tilde{u}^\theta}{\partial \tilde{x}^2} + \mathcal{O}(\beta^2), \\ \tilde{w} &= -\beta(1 + \tilde{z}_\theta) \frac{\partial \tilde{u}^\theta}{\partial \tilde{x}} + \mathcal{O}(\beta^2).\end{aligned}\quad (33)$$

From Eq. (31) and Eq. (32), we have

$$\begin{aligned}\tilde{u} &= -\tilde{c}_- \tilde{\eta} + \alpha \frac{\tilde{c}_- + \tilde{\Gamma}}{2(1 + \tilde{c}_+^2)} \tilde{\eta}^2 + \beta \frac{\tilde{c}_+ + \tilde{\Gamma}}{3(1 + \tilde{c}_+^2)} \tilde{\eta}_{\tilde{x}\tilde{x}} - \tilde{c}_- \frac{\beta}{6} \frac{\partial^2 \tilde{\eta}}{\partial \tilde{x}^2} + \tilde{c}_- \frac{\beta}{2}(1 + \tilde{z})^2 \frac{\partial^2 \tilde{\eta}}{\partial \tilde{x}^2} + \mathcal{O}(\alpha\beta, \beta^2), \\ \tilde{w} &= \beta \tilde{c}_- \tilde{\eta}_{\tilde{x}}(1 + \tilde{z}) + \mathcal{O}(\alpha\beta, \beta^2).\end{aligned}\quad (34)$$

After neglecting the second-order term, the dimensional form of the velocities are given by

$$\begin{aligned}u &= \frac{\sqrt{gh_0}}{h_0} \left\{ -\tilde{c}_- \eta + \frac{\tilde{c}_- + \tilde{\Gamma}}{2(1 + \tilde{c}_+^2)} \frac{\eta^2}{h_0} + \frac{\tilde{c}_+ + \tilde{\Gamma}}{3(1 + \tilde{c}_+^2)} h_0^2 \eta_{xx} - \frac{\tilde{c}_-}{6} h_0^2 \eta_{xx} + \frac{\tilde{c}_-}{2} h_0^2 (1 + \frac{z}{h_0})^2 \eta_{xx} \right\}, \\ w &= \sqrt{gh_0} \tilde{c}_- \eta_x \left\{ 1 + \frac{z}{h_0} \right\}.\end{aligned}\quad (35)$$

In the following, it will be convenient to define non-dimensional variables adapted to the problem at hand. In particular, the new variables are defined by

$$x = h_0 x, \quad z = h_0 z, \quad \eta = h_0 \eta, \quad t = \frac{h_0}{\sqrt{gh_0}} t, \quad u = \sqrt{gh_0} u, \quad w = \sqrt{gh_0} w \quad \text{and} \quad \Gamma = \frac{\Gamma \sqrt{gh_0}}{h_0}. \quad (36a)$$

Then Eq. (35) can be rewritten in terms of new variables as

$$\begin{aligned} u &= \left\{ -c_- \eta + \frac{c_- + \Gamma}{2(1 + c_+^2)} \eta^2 + \frac{c_+ + \Gamma}{3(1 + c_+^2)} \eta_{xx} - \frac{c_-}{6} \eta_{xx} + \frac{c_-}{2} (1 + z)^2 \eta_{xx} \right\}, \\ w &= c_- \eta_x (1 + z). \end{aligned} \quad (37)$$

Here  $c_+ = \frac{-\Gamma}{2} + \sqrt{\frac{\Gamma^2}{4} + 1}$  and  $c_- = \frac{-\Gamma}{2} - \sqrt{\frac{\Gamma^2}{4} + 1}$ .

The Eq. (30) can be rewritten in terms of new variables as

$$\eta_t + c_+ \eta_x + \frac{c_+ (3 + \Gamma^2)}{(1 + c_+^2)} \eta \eta_x + \frac{c_+ + \Gamma}{3(1 + c_+^2)} \eta_{xxx} = 0. \quad (38)$$

The expressions for the horizontal and vertical velocities of a fluid particle at a height  $z = -1 + \theta(\eta + 1)$  are given in new variables as

$$\begin{aligned} u(x, z, t) &= u^\theta(x, t) + (\theta^2 - (1 + z)^2) \frac{\partial^2 u^\theta}{\partial x^2}, \\ w(x, z, t) &= -(1 + z) \frac{\partial u^\theta}{\partial x}, \end{aligned} \quad (39)$$

where

$$u^\theta = \left\{ -c_- \eta + \frac{c_- + \Gamma}{2(1 + c_+^2)} \eta^2 + \frac{c_+ + \Gamma}{3(1 + c_+^2)} \eta_{xx} - \frac{c_-}{6} \eta_{xx} + \frac{c_-}{2} \theta^2 \eta_{xx} \right\}. \quad (40)$$

Taking the functions  $\xi(t)$  and  $\zeta(t)$  to describe the  $x$ -coordinate and  $z$ -coordinate, respectively, of a particle originally located at the point  $(x, z) = (\xi_0, \zeta_0)$ , the dynamical system is then recast in the form

$$\begin{aligned} \frac{\partial \xi}{\partial t} &= u(\xi(t), \zeta(t), t) - (1 + \zeta) \Gamma, \\ \frac{\partial \zeta}{\partial t} &= w(\xi(t), \zeta(t), t), \\ (\xi(0), \zeta(0)) &= (\xi_0, \zeta_0), \end{aligned} \quad (41)$$

where now the effect of an underlying shear-flow has been added. Finally, the particle trajectories are found by numerically integrating the dynamical system (41) using the fourth-order Runge-Kutta method.

As explained in [3], as long as the waves are within the validity of the Boussinesq scaling, the results will be qualitatively the same for all values of  $\theta$ . In order to get more accurate results and nicer figures, we have used Eq. (39) for the numerical computations. The numerical results which are presented in the following sections have been simulated with several values of  $\theta$ , and variation of the results has been minor in comparison to their main qualitative features.

### 3 Particle trajectories in solitary-wave solutions

In this section, our aim is to describe the particle trajectories in the fluid due to the passage of a solitary wave at the surface. The solitary-wave solution of the KdV equation (38) is given by

$$\eta = \eta_0 \operatorname{sech}^2 \left( \sqrt{\frac{c_+(3+\Gamma^2)\eta_0}{4(c_++\Gamma)}}(x-x_0-ct) \right), \quad (42)$$

where  $\eta_0$  is the initial amplitude,  $x_0$  is the initial location of the wave crest and  $c = c_+ + \frac{c_+(3+\Gamma^2)\eta_0}{3(1+c_+^2)}$  is the phase velocity. Letting the argument  $\mathcal{A}(x, t) = \sqrt{\frac{c_+(3+\Gamma^2)\eta_0}{4(c_++\Gamma)}}(x-x_0-ct)$ , the relation (35) gives the horizontal and vertical velocities at an arbitrary point  $(x, z)$  in the fluid, at a time  $t$

$$\begin{aligned} u &= \eta_0 \operatorname{sech}^2 \mathcal{A} \left\{ -c_- + \frac{c_- + \Gamma}{2(1+c_+^2)} \eta_0 \operatorname{sech}^2 \mathcal{A} \right. \\ &\quad \left. + \frac{c_+(3+\Gamma^2)\eta_0}{4(c_++\Gamma)} \left( \frac{c_+ + \Gamma}{3(1+c_+^2)} - \frac{c_-}{6} + \frac{c_-}{2}(1+z)^2 \right) (4 - 6 \operatorname{sech}^2 \mathcal{A}) \right\}, \\ w &= -c_- (\eta_0)^{3/2} \sqrt{\frac{c_+(3+\Gamma^2)}{(c_++\Gamma)}} (1+z) \operatorname{sech}^2 \mathcal{A} \tanh \mathcal{A}. \end{aligned} \quad (43)$$

From the relations (39) and (40) the horizontal and vertical velocities of the fluid  $u$  and  $w$  at  $(x, z = -1 + \theta(\eta + 1))$  in the fluid, at a time  $t$  are given by

$$\begin{aligned} u &= \eta_0 \operatorname{sech}^2(\mathcal{A}) \left\{ -c_- + \left( \frac{c_+ + \Gamma}{3(1+c_+^2)} - \frac{c_-}{6} \right) \frac{c_+(3+\Gamma^2)}{(c_++\Gamma)} \eta_0 - \frac{(3+\Gamma^2)}{(c_++\Gamma)} \frac{\eta_0}{2} (z+1)^2 \right. \\ &\quad \left. + \eta_0 \operatorname{sech}^2(\mathcal{A}) \left[ \frac{c_- + \Gamma}{2(1+c_+^2)} - \left( \frac{c_+ + \Gamma}{3(1+c_+^2)} - \frac{c_-}{6} \right) \frac{3c_+(3+\Gamma^2)}{2(c_++\Gamma)} + \frac{3}{4} (z+1)^2 \frac{(3+\Gamma^2)}{(c_++\Gamma)} \right] \right. \\ &\quad \left. + \frac{1}{2} (\theta^2 - (1+z)^2) \frac{c_- + \Gamma}{2(1+c_+^2)} \frac{c_+(3+\Gamma^2)}{(c_++\Gamma)} \eta_0^2 \operatorname{sech}^2(\mathcal{A}) (4 - 5 \operatorname{sech}^2(\mathcal{A})) \right. \\ &\quad \left. - \frac{1}{16} (\theta^2 - (1+z)^2) \frac{c_+^2(3+\Gamma^2)^2 \eta_0^2}{(c_++\Gamma)^2} \right. \\ &\quad \left. (-8 + 60 \operatorname{sech}^2 \mathcal{A} - 60 \operatorname{sech}^4 \mathcal{A}) \left( \frac{c_+ + \Gamma}{3(1+c_+^2)} - \frac{c_-}{6} + \frac{c_-}{2} \theta^2 \right) \right\}, \\ w &= -(1+z)(\eta_0)^{3/2} \sqrt{\frac{c_+(3+\Gamma^2)}{4(c_++\Gamma)}} \operatorname{sech}^2 \mathcal{A} \tanh \mathcal{A} \left[ 2c_- - \frac{2(c_- + \Gamma)}{(1+c_+^2)} \eta_0 \operatorname{sech}^2(\mathcal{A}) \right. \\ &\quad \left. + \frac{2c_+(3+\Gamma^2)}{(c_++\Gamma)} \eta_0 \left( \frac{c_+ + \Gamma}{3(1+c_+^2)} - \frac{c_-}{6} + \frac{c_-}{2} \theta^2 \right) (-1 + 3 \operatorname{sech}^2(\mathcal{A})) \right]. \end{aligned} \quad (44)$$

The particle trajectories are shown during the propagation of a surface solitary wave with amplitude 0.2 in Figs. 2 - 4. The numerical particle trajectories beneath the solitary waves were obtained with the dynamical system (41) where the vector field is given implicitly in Eq. (44). In Figs. 2-4, the fluid particle location at the three instances where the wave profile is shown are color coded: the initial position is indicated by the light-gray dot, the

dark-gray dot shows its middle position while the black dot shows its final position. Fig. 2 shows the time evolution of a fluid particle located to the right of the crest in the surface for three different vorticity values (a)  $\Gamma = 0$  ; (b)  $\Gamma = -0.3$  ; (c)  $\Gamma = 0.3$ . The particle trajectory given by Eq. (41) is represented by the dashed curve. For the case of a favorable vorticity ( $\Gamma \leq 0$ ), it can be seen that fluid particle move to the right and upwards if they are located to the right of the crest, while the fluid particle moves to the left and upwards for the case of vorticity  $\Gamma > 0$ . This is in agreement with the results of [3, 7] in the absence of shear flow.

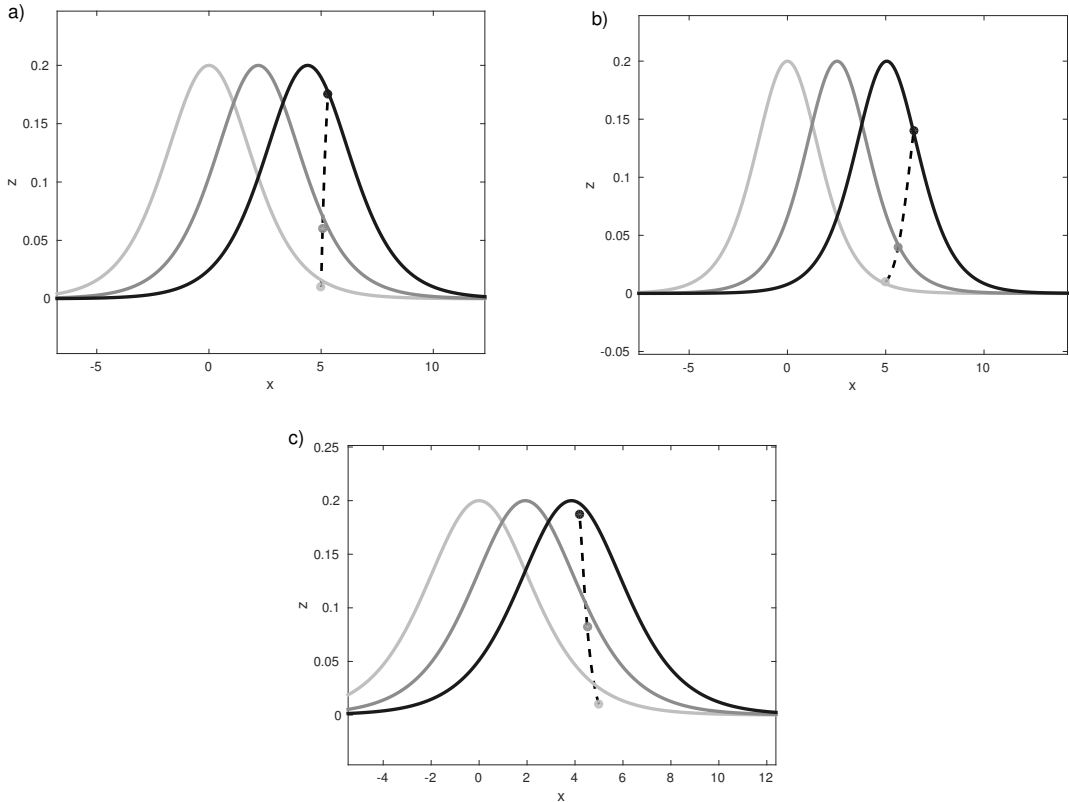


Figure 2: The waves are shown at time  $t = 0$  (light-gray),  $t = 2$  (dark-gray),  $t = 4$  (black). The wave crest is initially located at  $x = 0$ . The path of the fluid particles  $(\xi(t), \zeta(t))$  of (41) ( $u$  and  $w$  corresponds to the Eq. (44)) initially located at  $(5, -0.01)$  for different cases of vorticity (a)  $\Gamma = 0$  ; (b)  $\Gamma = -0.3$  ; (c)  $\Gamma = 0.3$  are shown. The particle locations at three instances where the wave profile is shown are color coded. The light-gray curve indicates the particle positions at time  $t = 0$ . The dark-gray curve indicates the particle positions at time  $t = 2$ . The black curve indicates the particle positions at time  $t = 4$ .

Fig. 3 illustrates the particle paths during one complete solitary wave cycle. It can be seen that the fluid particles closer to the bottom have smaller amplitude and at the bottom, the particle trajectories become straight line because the vertical movement of the particle is zero. Because of the lower vertical movement of the fluid particle at the bottom, the particle paths move in opposite direction than the original flow for the case of vorticity  $\Gamma > 0$ , and only a horizontal displacement exists. It is apparent that from Fig. 3 lower panel, the particle paths move to the right and upwards when the particles are closer to the bottom. We also

note in Fig. 3 that the horizontal displacement depends on the initial depth of the fluid particles.

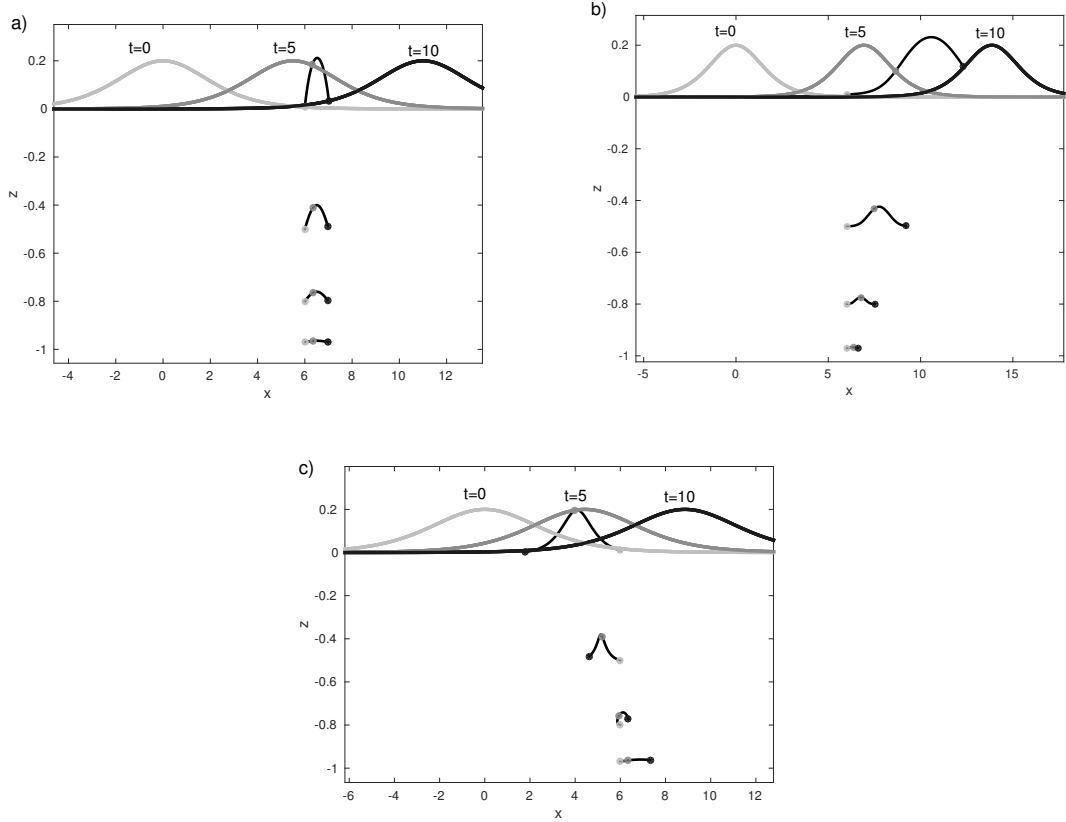


Figure 3: The waves are shown at time  $t = 0$  (light-gray),  $t = 5$  (dark-gray),  $t = 10$  (black). The wave crest is initially located at  $x = 0$ . The path of the fluid particles  $(\xi(t), \zeta(t))$  in (41) ( $u$  and  $w$  corresponds to the Eq. (44)) initially located at  $(6, -0.97)$ ,  $(6, -0.8)$ ,  $(6, -0.5)$  and  $(6, -0.01)$  are shown different cases (a) $\Gamma = 0$ ; (b)  $\Gamma = -0.5$ ; (c)  $\Gamma = 0.5$ . The particle locations at three instances, where the wave profile is shown, are color coded. The light-gray dot indicates the particle positions at time  $t = 0$ . The dark-gray dot indicates the particle positions at time  $t = 5$ . The black dot indicates the particle positions at time  $t = 10$ .

In the upper panels of Fig. 4, for  $\Gamma \leq 0$ , fluid particles move to the right and upwards if they are located to the right of the crest and particles located on the left of the crest move to the right and downwards. In the lower panel of Fig. 4, for  $\Gamma > 0$ , fluid particles move to the left and upwards if they are located to the right of the crest and particles located on the left of the crest move to the left and downwards. But as can be seen in Fig. 4 lower panel that particles closer to the bottom move to the right and upwards if they are located to the right of the crest and particles located on the left of the crest move to the right and downwards for the case  $\Gamma > 0$ . It is clear that for particles deeper into the fluid channel, the wave effect diminishes and therefore the effect due the vorticity can become dominant. Through the numerical simulations it is apparent that the closer the particle is to the free surface, the stronger it feels the wave effect.

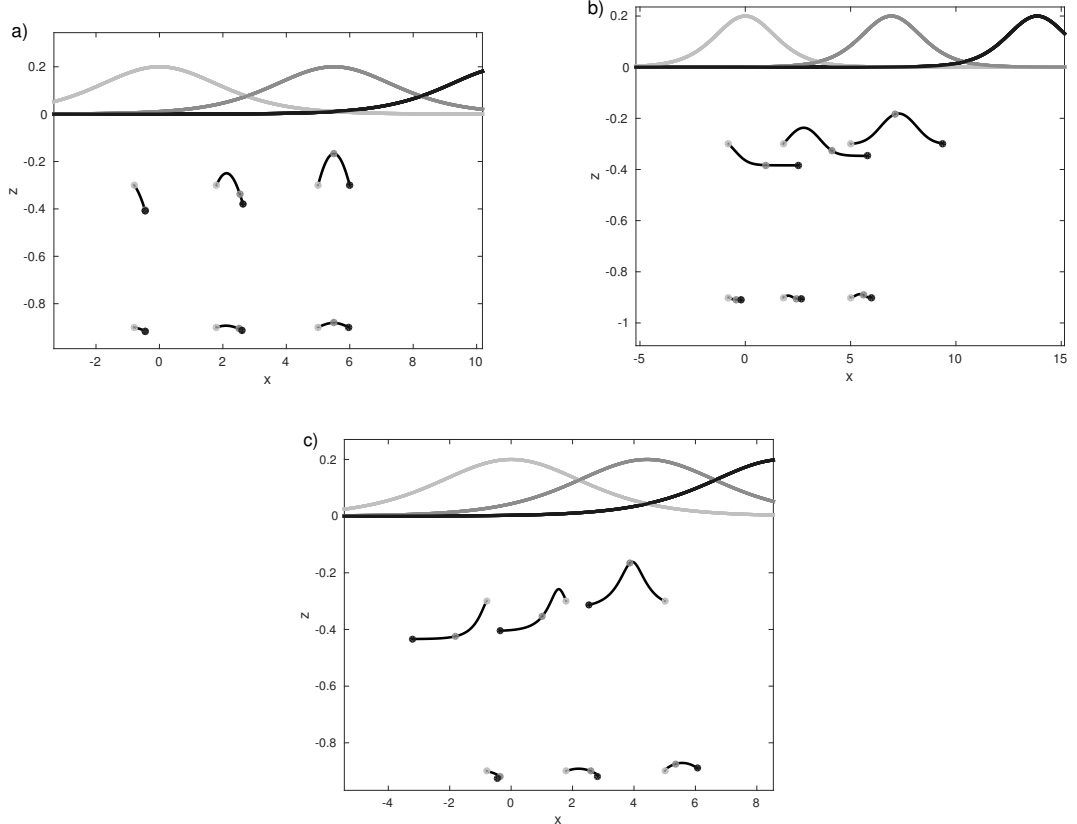


Figure 4: The waves are shown at time  $t = 0$  (light-gray),  $t = 5$  (dark-gray),  $t = 10$  (black). The wave crest is initially located at  $x = 0$ . The path of the fluid particles  $(\xi(t), \zeta(t))$  in (41) ( $u$  and  $w$  corresponds to the Eq. (44)) initially located at  $(-0.8, -0.3)$ ,  $(1.8, -0.3)$  and  $(5, -0.3)$ , and also  $(-0.8, -0.9)$ ,  $(1.8, -0.99)$  and  $(5, -0.9)$  are shown for different cases (a) $\Gamma = 0$  ; (b)  $\Gamma = -0.5$  ; (c)  $\Gamma = 0.5$ . The particle locations at three instances, where the wave profile is shown, are color coded. The light-gray curve indicates the particle positions at time  $t = 0$ . The dark-gray curve indicates the particle positions at time  $t = 5$ . The black curve indicates the particle positions at time  $t = 10$ .

## 4 Particle trajectories in periodic-wave solutions

Attention will now be turned to particle paths in the fluid flow due to the propagation of periodic travelling waves at the surface. Indeed, the KdV equation (38) admits the following solution in terms of cnoidal functions:

$$\eta = f_2 + (f_1 - f_2) \operatorname{cn}^2(\mathcal{B}), \quad (45)$$

where the solution is defined by the three constants  $f_1$ ,  $f_2$  and  $f_3$  which are arranged in the order  $f_3 < f_2 < f_1$ . The argument  $\mathcal{B} = \sqrt{\frac{c_+(3+\Gamma^2)}{4(c_++\Gamma)}}(f_1 - f_3)^{1/2}(x - x_0 - ct)$ ,  $\operatorname{cn}$  is one of the Jacobian elliptic functions defined by the incomplete elliptic integral of the first kind [16] and the modulus of  $\operatorname{cn}$  is given by  $m = (f_1 - f_2)/(f_1 - f_3)$ . The phase speed of the wave is  $c = c_+ + \frac{c_+(3+\Gamma^2)}{3(1+c_+^2)}(f_1 + f_2 + f_3)$  and the wavelength is given by  $\lambda = 4\sqrt{\frac{c_++\Gamma}{c_+(3+\Gamma^2)}}K(m)\frac{1}{\sqrt{f_1-f_3}}$ ,

where  $K(m)$  is the complete elliptic integral of the first kind. Using the relation (37), the horizontal and vertical velocities may be written in terms of the Jacobian elliptic functions cn, sn and dn as

$$\begin{aligned} u &= -c_-(f_2 + (f_1 - f_2)\text{cn}^2(\mathcal{B})) + \frac{c_- + \Gamma}{2(1 + c_+^2)}(f_2 + (f_1 - f_2)\text{cn}^2(\mathcal{B}))^2 \\ &\quad + \frac{c_+(3 + \Gamma^2)}{2(c_+ + \Gamma)}(f_1 - f_3)(f_1 - f_2) \left( \frac{c_+ + \Gamma}{3(1 + c_+^2)} - \frac{c_-}{6} + \frac{c_-}{2}(1 + z)^2 \right) \\ &\quad (\text{sn}^2(\mathcal{B})\text{dn}^2(\mathcal{B}) - \text{cn}^2(\mathcal{B})\text{dn}^2(\mathcal{B}) + m\text{sn}^2(\mathcal{B})\text{cn}^2(\mathcal{B})) , \\ w &= -c_-(1 + z)\sqrt{\frac{c_+(3 + \Gamma^2)}{(c_+ + \Gamma)}}(f_1 - f_2)(f_1 - f_3)^{1/2}\text{cn}(\mathcal{B})\text{sn}(\mathcal{B})\text{dn}(\mathcal{B}). \end{aligned} \quad (46)$$

And also using the relations (39) and (40), the horizontal and vertical velocity may be written in terms of the Jacobian elliptic functions cn, sn and dn as

$$\begin{aligned} u &= -c_-(f_2 + (f_1 - f_2)\text{cn}^2(\mathcal{B})) + \frac{c_- + \Gamma}{2(1 + c_+^2)}(f_2 + (f_1 - f_2)\text{cn}^2(\mathcal{B}))^2 + \frac{c_+(3 + \Gamma^2)}{2(c_+ + \Gamma)} \\ &\quad (f_1 - f_3)(f_1 - f_2) (\text{sn}^2(\mathcal{B})\text{dn}^2(\mathcal{B}) - \text{cn}^2(\mathcal{B})\text{dn}^2(\mathcal{B}) + m\text{sn}^2(\mathcal{B})\text{cn}^2(\mathcal{B})) \\ &\quad \left( \frac{c_+ + \Gamma}{3(1 + c_+^2)} - \frac{c_-}{6} + \frac{c_-}{2}(\theta)^2 \right) + (\theta^2 - (1 + z)^2) \frac{c_+(3 + \Gamma^2)}{8(c_+ + \Gamma)}(f_1 - f_3) \\ &\quad \left\{ 2c_-(f_1 - f_2) + 2\frac{c_- + \Gamma}{(1 + c_+^2)} (\text{sn}^2(\mathcal{B})\text{dn}^2(\mathcal{B}) - \text{cn}^2(\mathcal{B})\text{dn}^2(\mathcal{B}) + m\text{sn}^2(\mathcal{B})\text{cn}^2(\mathcal{B})) \right. \\ &\quad f_2(f_1 - f_2) - 2(f_1 - f_2)^2 (-m\text{sn}^2(\mathcal{B})\text{cn}^4(\mathcal{B}) + \text{cn}^4(\mathcal{B})\text{dn}^2(\mathcal{B}) - 3\text{sn}^2(\mathcal{B})\text{cn}^2(\mathcal{B})\text{dn}^2(\mathcal{B})) \\ &\quad + (-9m\text{cn}^2(\mathcal{B})\text{sn}^2(\mathcal{B})\text{dn}^2(\mathcal{B}) - m^2\text{cn}^4(\mathcal{B})\text{sn}^2(\mathcal{B}) + m\text{cn}^4(\mathcal{B})\text{dn}^2(\mathcal{B}) \\ &\quad + m^2\text{sn}^4(\mathcal{B})\text{cn}^2(\mathcal{B}) + m\text{sn}^4(\mathcal{B})\text{dn}^2(\mathcal{B}) + \text{dn}^4(\mathcal{B})\text{cn}^2(\mathcal{B}) - \text{dn}^4(\mathcal{B})\text{sn}^2(\mathcal{B})) \\ &\quad \left. \frac{c_- + \Gamma}{(1 + c_+^2)} \left( \frac{c_+ + \Gamma}{3(1 + c_+^2)} - \frac{c_-}{6} + \frac{c_-}{2}(\theta)^2 \right) (f_1 - f_2)(f_1 - f_3) \frac{2c_+(3 + \Gamma^2)}{(c_+ + \Gamma)} \right\} , \\ w &= -(1 + z)\sqrt{\frac{c_+(3 + \Gamma^2)}{4(c_+ + \Gamma)}}(f_1 - f_3)^{1/2} \left[ 2c_-(f_1 - f_2) - 2\frac{c_- + \Gamma}{(1 + c_+^2)}(f_1 - f_2)f_2 \right. \\ &\quad - 2\frac{c_- + \Gamma}{(1 + c_+^2)}(f_1 - f_2)^2\text{cn}^2(\mathcal{B}) + \left( \frac{c_+ + \Gamma}{3(1 + c_+^2)} - \frac{c_-}{6} + \frac{c_-}{2}(\theta)^2 \right) (f_1 - f_2)(f_1 - f_3) \\ &\quad \left. \frac{2c_+(3 + \Gamma^2)}{(c_+ + \Gamma)} (-m\text{sn}^2(\mathcal{B}) + m\text{cn}^2(\mathcal{B}) + \text{dn}^2(\mathcal{B})) \right] \text{cn}(\mathcal{B})\text{sn}(\mathcal{B})\text{dn}(\mathcal{B}). \end{aligned} \quad (47)$$

The particle path shown in Figs. 5 - 8 are numerical approximations of solutions of Eq. (41) where the vector field is given in Eq. (47). The cnoidal wave of the KdV equations can be specified by fixing the values of the parameters  $f_1, f_2$  and  $f_3$ . Of particular interest is the case of an adverse current and researchers [8, 17] predicted the existence of a closed orbit. Fig. 5 illustrates the particle path during one complete periodic cnoidal wave cycle with  $m = 0.99$  and  $H = f_1 - f_2 = 0.3$  for different vorticity values  $\Gamma = 0, -0.1$  and  $0.1$ . The crest of the wave is centered at  $x = 0$ , and depths  $z = -0.9, -0.4$  and  $-0.078$ . The particle

paths are nearly elliptic but not closed in the presence of the vorticity  $\Gamma \leq 0$ . For the case of positive vorticity  $\Gamma > 0$ , the particle paths are orbit loops.

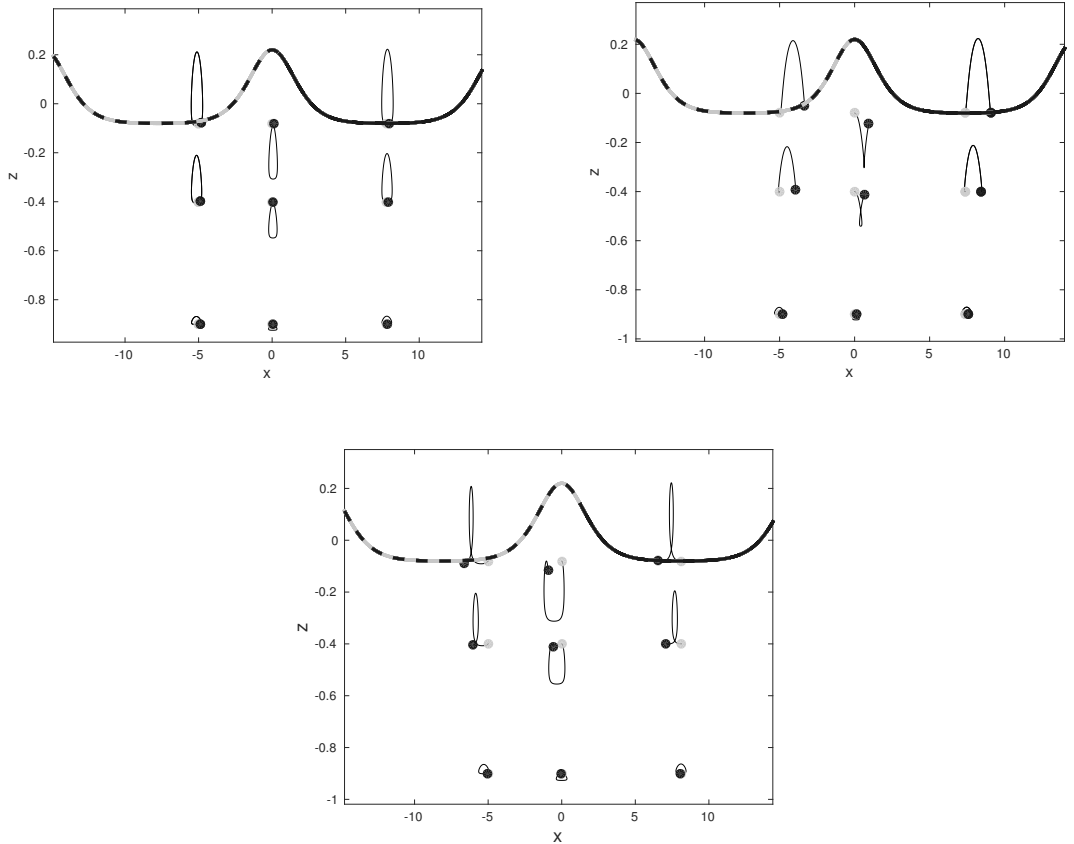


Figure 5: The left upper panel shows the periodic wave with amplitude 0.3, wavelength 15.5041, period 15.0808, phase speed 1.0281 and  $\Gamma = 0$  at  $t = 0$  (light-gray) and  $t = 15.08$  (black). The right upper panel shows the periodic wave with amplitude 0.3, wavelength 14.7237, period 13.6410, phase speed 1.0794 and  $\Gamma = -0.1$  at  $t = 0$  (light-gray) and  $t = 13.64$  (black). The lower panel shows the periodic wave with amplitude 0.3, wavelength 16.2715, period 16.6142, phase speed 0.9794 and  $\Gamma = 0.1$  at  $t = 0$  (light-gray) and  $t = 16.61$  (black). The paths of fluid particles are located at  $x, z$  where initial  $x$ -coordinate are  $x = -5, 0$  and wavelength/2 – 0.001, and depth  $z = -0.9, -0.4$  and  $-0.078$ .

Next we present a train of cnoidal wave for different vorticity values  $\Gamma = 0, -0.4$  and  $0.6$ . A close-up of particle paths initially located at the surface is shown in Fig. 6. The particle path during the propagation of the cnoidal wave over 4 periods at the three cases are shown and the initial particle locations are shown in light-gray dots. In the upper panels of Fig. 6, for  $\Gamma \leq 0$ , fluid particles move to the right and upwards. As can be seen in lower panel of Fig. 6 that particles move to the left and upwards for the case  $\Gamma > 0$ .

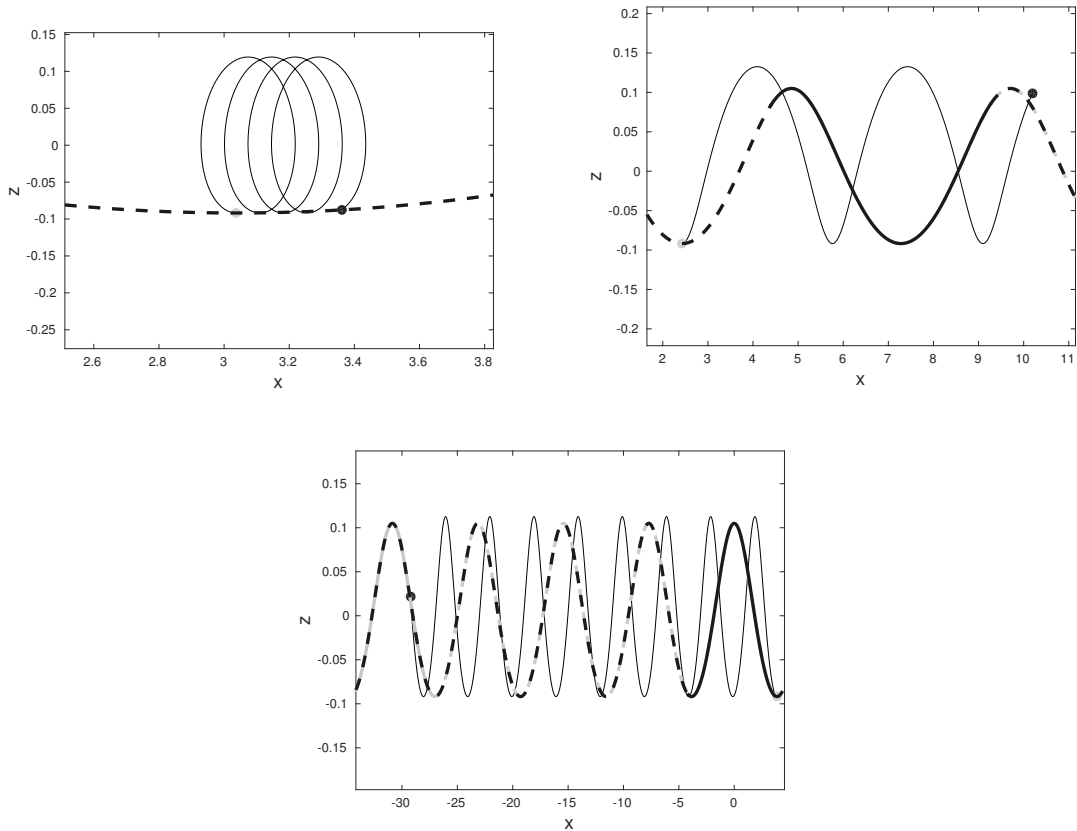


Figure 6: The left upper panel shows the periodic wave with amplitude 0.1968, wavelength 6.0755, period 7.3499, phase speed 0.826 and  $\Gamma = 0$  at  $t = 0$  (light-gray) and  $t = 4$  periods (black). The right upper panel shows the periodic wave with amplitude 0.1968, wavelength 4.8, period 4.6631, phase speed 1.0407 and  $\Gamma = -0.4$ . The lower panel shows the periodic wave with amplitude 0.1968, wavelength 7.7158, period 13.8271, phase speed 0.5586 and  $\Gamma = 0.6$ . The initial particle locations at the three cases are shown in light-gray curve. All particles are initially at  $x_0 = \text{wavelength}/2 - 0.001$  and depth  $z_0 = -0.1$ .

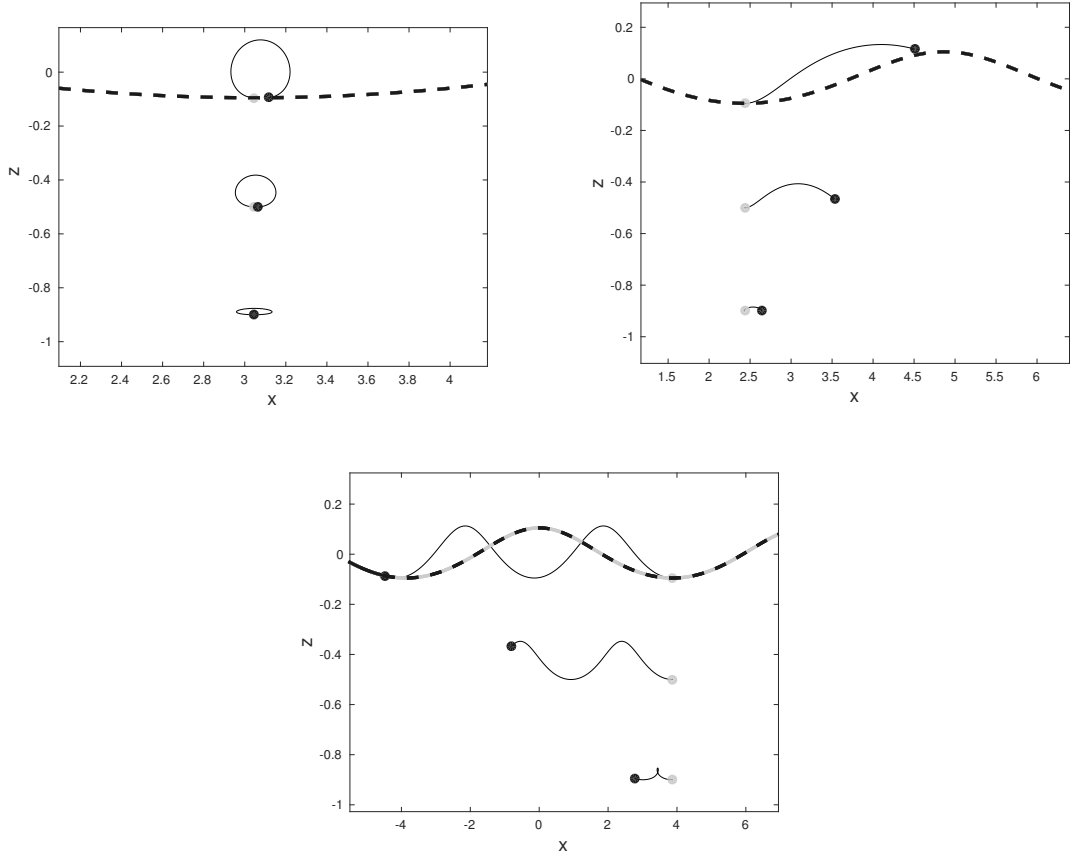


Figure 7: The left upper panel shows the periodic wave with amplitude 0.2, wavelength 6.0926, period 7.3499, phase speed 0.825 and  $\Gamma = 0$ . The right upper panel shows the periodic wave with amplitude 0.2, wavelength 4.8667, period 4.6838, phase speed 1.0391 and  $\Gamma = -0.4$ . The lower panel shows the periodic wave with amplitude 0.2, wavelength 7.7376, period 13.9090, phase speed 0.5563 and  $\Gamma = 0.6$ . The initial particle locations at the three cases are shown in light-gray curve. All particles are initially at  $x_0 = \text{wavelength}/2 - 0.001$ , and depth  $z_0 = -0.1, -0.5$  and  $-0.9$ .

In Figs. 7 and 8 the particle paths with different vorticity values are shown for different depths. As we observe that from upper panel in Fig. 8 that for particles closer to the bottom the wave effect diminishes and therefore the effect due to the vorticity can become dominant.

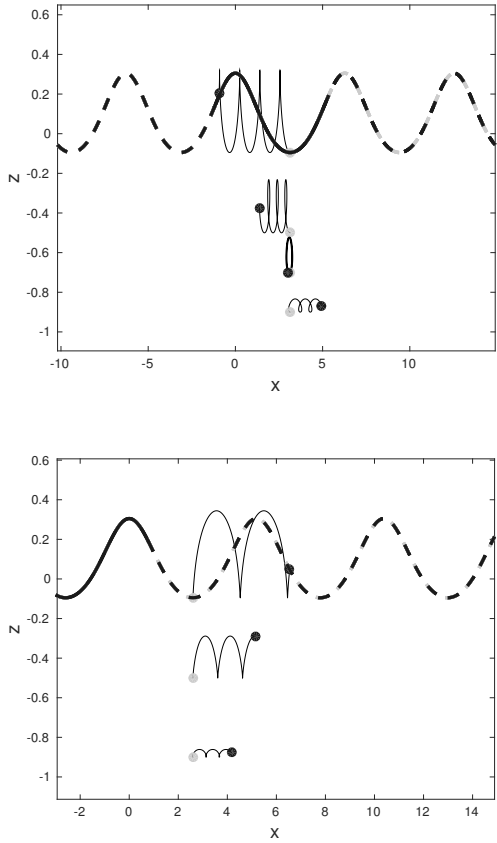


Figure 8: The upper panel ( $u$  and  $w$  corresponds to Eq. (47)) shows the periodic wave with amplitude 0.4, wavelength 6.2718, period 7.9036, phase speed 0.7935 and  $\Gamma = 0.28$  at  $t = 0$  (light-gray) and  $t = 23.7108$  (black). The lower ( $u$  and  $w$  corresponds to Eq. (47)) shows the periodic wave with amplitude 0.4, wavelength 5.1917, period 5.2623, phase speed 0.9866 and  $\Gamma = -0.12$  at  $t = 0$  (light-gray) and  $t = 15.7870$  (black). The initial particle locations are shown in light-gray curve.

## 5 Conclusion

In this study, the KdV equation in the presence of the shear flow has been used to describe the motion of particles in the fluid column below surface waves. The expressions for the velocity field of the fluid including vorticity below the surface have been deduced from the derivation of the KdV equation. The particle trajectories are described by two coupled ordinary differential equations which are defined in terms of the velocity field associated to a surface wave and vorticity constant. These coupled ordinary differential equations have been solved numerically by using a fourth-order Runge-Kutta method. The evaluation of particles in the fluid in the presence of a shear flow was investigated due to the passage of a solitary wave and a cnoidal wave at the surface. In the presence of a shear flow for solitary waves, approximate particle paths are found in closed form. A diversity of orbit patterns were described when a cnoidal wave propagates in the presence of a shear flow.

## References

- [1] Ali, A. and Kalisch, H. Reconstruction of the pressure in long-wave models with constant vorticity. *Eur. J. Mech. B Fluids*, 2013, **37**, 187–194.
- [2] Benjamin, T. B. The solitary wave on a stream with an arbitrary distribution of vorticity. *J. Fluid Mech.*, 1962, **12** (1), 97–116.
- [3] Borluk, H. and Kalisch, H. Particle dynamics in the KdV approximation. *Wave motion*, 2012, **49**, 691–709.
- [4] Burns, J. C. Long waves in running water. *Mathematical Proceedings of the Cambridge Philosophical Society*. 1953, **49** (4), 695–706.
- [5] Choi, W. Strongly nonlinear long gravity waves in uniform shear flows. *Physical review E*, 2003, **68**.
- [6] Constantin, A. The trajectories of particles in Stokes waves. *Invent. Math.*, 2006, **166** (3), 523–535.
- [7] Constantin, A. and Escher, J. Particle trajectories in solitary water waves. *Bull. Amer. math. soc.*, 2007, **44**, 423–431.
- [8] Constantin, A. and Strauss, W. Pressure beneath a Stokes wave, *Comm. Pure Appl. Math.*, **63** (4), 2010, 533–557
- [9] Constantin, A. and Villari, G. J. Particle trajectories in linear water waves. *J. Math. Fluid Mech.*, 2008, **10**, 1–18.
- [10] Debnath, L. Nonlinear Water Waves. *Academic Press Inc.*, 1994.
- [11] Freeman, N.C. and Johnson, R.S. Shallow water waves on shear flow. *J. Fluid Mech.*, 1970, **42** (2), 401–409.
- [12] Gerstner, F. J. Theory of waves. Abhandlungen der Königl., Böhmischen Gesellschaft der Wissenschaften zu Prag, 1802.
- [13] Henry, R. On Gerstner’s water wave. *Journal of Nonlinear Mathematical Physics*, 2008, **15** (2), 87–95.
- [14] Johnson, R. S. A Modern Introduction to the Mathematical Theory of Water Waves. *Cambridge University Press*, 1997.
- [15] Lamb, H. Hydrodynamics. *Dover Publications, New York*, 1945.
- [16] Lawden, D. F. Elliptic functions and applications. *Springer, New York*, 1989.
- [17] Nachbin, A. and Ribeiro-Junior, R. A boundary integral formulation for particle trajectories in Stokes waves. *Discrete and continuous dynamical systems*, 2014, **34** (8), 3135–3153.
- [18] Stoker, J. J. Water Waves. The Mathematical Theory with Applications. *New York: Interscience Publ. Inc.*, 1957.
- [19] Stokes, G. G. On the theory of oscillatory waves. *Trans. Camb. Phil. Soc.*, 441–455, 1847. Reprinted in: Stokes, G. G. *Mathematical and Physical Papers, Volume I*. *Cambridge University Press*, 197–229, 1880.
- [20] Ursell, F. Mass transport in gravity waves *Proc. Cambridge Phil. Soc.*, (1953), **40**, 145–150.
- [21] Vasan, V. and Oliveras, K. Pressure beneath a traveling wave with constant vorticity *Discrete Contin. Dyn. Syst.*, (2014) **34**, 3219–3239.
- [22] Yaosong, C., Guocan, L. and Tao, J. Non-linear water waves on shearing flows. *Acta Mechanica Sinica*, 1994, **10** (2), 97–102.

## Paper D

# Wave Breaking in the KdV Equation in a Flow with Constant Vorticity

# Wave Breaking in the KdV Equation in a Flow with Constant Vorticity

Henrik Kalisch and Amutha Senthilkumar

Department of Mathematics, University of Bergen

Postbox 7803, 5020 Bergen, Norway

January 9, 2017

## Abstract

The paper describes a critical breaking wave height for long surface water waves with constant vorticity moving over a linear shear flow. Long surface gravity waves of small amplitude over a flow with non-zero vorticity are considered by using an asymptotic model derived under the assumption that there is an approximate balance between nonlinear steepening effects and dispersive spreading. The resulting system of Boussinesq equations reduced into the Korteweg-de Vries (KdV) equation with constant vorticity. The solutions treated here comprise the solitary wave and periodic travelling waves for any amplitude. It is shown that for both the solitary wave and the periodic travelling waves, there are critical wave heights where the horizontal component of the particle velocity matches the phase velocity of the wave.

## 1 Introduction

The conditions causing a breaking wave have been discussed from different view points by many researchers for more than a century. The kinematic breaking criterion is used often to predict wave breaking and simply assigns the onset for the breaking when the horizontal particle velocity at the crest  $U$  exceeds the wave phase speed  $C$ . Favorable measures of the nonlinearity are the wave steepness  $ak$ , where  $a$  is the wave amplitude and  $k$  is the wavenumber, or equivalently,  $U/C$ , thus, breaking is a strongly nonlinear process.

The experimental study of [9, 13] suggested that the kinematic criterion is the most potent while the other two classes are affected readily by wave directionality even for the three-dimensional case. In this paper, we describe the incipient wave breaking phenomenon for the KdV equation with constant vorticity. However, it does not accommodate the phenomenon of wave breaking as physical water waves do, and it will be shown here that the KdV equation features a different kind of wave breaking which is more closely related to spilling at the wave crest.

Let us briefly recall the governing equations for two dimensional water waves with constant vorticity. Recently, several authors [1, 2, 5, 7, 11, 12, 14] have introduced the influence of horizontal vorticity on the waves in their works. The starting point for the mathematical formulation is Euler's equations in two dimensions with no-flow conditions at the bottom and kinematic and dynamic boundary conditions at the free surface. Let the spatial coordinates be  $(x, z)$  and the  $x$ -axis be oriented in the horizontal direction. Assume that the motion is uniform in the direction perpendicular to the  $xz$ -plane (long-crested waves). The gravitational acceleration  $g$  is in the negative  $z$ -direction. Let  $\eta(x, t)$  denote the surface elevation.

Assuming the vorticity of the flow is  $\omega = v_x - u_y$ . Here we treat waves with constant  $\omega$ . A shear flow with constant vorticity is described by a velocity field  $\mathbf{u} = (U, W) = (u + z\Gamma, w) =$

$(\frac{\partial \phi}{\partial x} + z\Gamma, \frac{\partial \phi}{\partial z})$ , where  $\phi(x, z, t)$  be the velocity potential of the disturbances. For  $\Gamma > 0$  we have a current in the opposite wave-propagation direction, while for  $\Gamma < 0$  it is in a favorable direction.

We write down the following system of Euler equations for potential flow theory in the presence of a vorticity:

$$\Delta\phi = 0, \quad -h_0 < z < \eta \quad (1)$$

$$\phi_z = 0, \quad z = -h_0 \quad (2)$$

$$\mathbf{u}_t + \frac{1}{2}\nabla|\mathbf{u}|^2 - \mathbf{u} \times (\nabla \times \mathbf{u}) + ge_z = 0, \quad z = \eta \quad (3)$$

$$\eta_t + U\eta_x - \phi_z = 0, \quad z = \eta \quad (4)$$

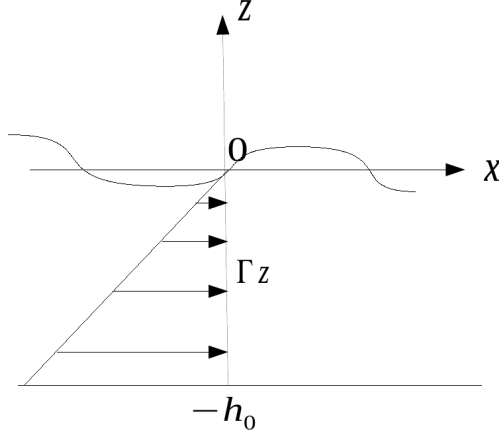


Figure 1: The background uniform shear flow  $U = z\Gamma$ . In the figure  $\Gamma$  is negative, the waves which are superposed onto this background current propagate to the right.

Non-dimensional variables are used as follows:

$$\tilde{x} = \frac{x}{l}, \quad \tilde{z} = \frac{z}{h_0}, \quad \tilde{t} = \frac{\sqrt{gh_0}t}{l}, \quad (5a)$$

$$\text{and } \tilde{\Gamma} = \frac{\Gamma h_0}{\sqrt{gh_0}}, \quad \tilde{\eta} = \frac{\eta}{a}, \quad \tilde{\phi} = \frac{h_0}{al\sqrt{gh_0}}\phi, \quad (5b)$$

where tilde  $\sim$  denotes non-dimensional variables and  $h_0$ ,  $l$  and  $a$  denote a characteristic. The parameter  $\alpha = a/h_0$  represents a waveheight to depth ratio, and the parameter  $\beta = h_0^2/l^2$  represents a water depth to wavelength ratio. As a result of the scaling the governing equations and boundary conditions for the irrotational wave problem read

$$\beta\tilde{\phi}_{\tilde{x}\tilde{x}} + \tilde{\phi}_{\tilde{z}\tilde{z}} = 0 \quad -1 < \tilde{z} < \alpha\tilde{\eta} \quad (6)$$

$$\tilde{\phi}_{\tilde{z}} = 0 \quad \text{at } \tilde{z} = -1 \quad (7)$$

$$\beta \left\{ \frac{\partial \tilde{\eta}}{\partial \tilde{t}} + \left[ \alpha\tilde{\eta}\tilde{\Gamma} + \alpha \frac{\partial \tilde{\phi}}{\partial \tilde{x}} \right] \frac{\partial \tilde{\eta}}{\partial \tilde{x}} \right\} = \tilde{\phi}_{\tilde{z}} \quad \text{at } \tilde{z} = \alpha\tilde{\eta} \quad (8)$$

$$\beta(\tilde{\phi}_{\tilde{t}} + \tilde{\eta}) + \frac{\alpha\beta}{2} \left[ \tilde{\phi}_{\tilde{x}} + \frac{\tilde{\Gamma}}{\alpha}(\alpha\tilde{\eta}) \right]^2 + \frac{\alpha}{2} \left[ \frac{\partial \tilde{\phi}}{\partial \tilde{z}} \right]^2 + \frac{\beta}{ag} G = 0 \quad \text{at } \tilde{z} = \alpha\tilde{\eta} \quad (9)$$

where

$$G = -\Gamma \int_{-h_0}^z \frac{\partial \phi}{\partial x} dz - \frac{\Gamma^2}{2} z^2. \quad (10)$$

Now we expand the velocity potential  $\tilde{\phi}$  as a power series in the vertical coordinate. We choose the expansion

$$\tilde{\phi} = \sum_{n=0}^{\infty} (1 + \tilde{z})^n \phi_n. \quad (11)$$

From Eq. (6), Eq. (7) and Eq. (11), we have

$$\tilde{\phi} = \phi_0 - \frac{\beta}{2} (1 + \tilde{z})^2 \frac{\partial^2 \phi_0}{\partial \tilde{x}^2} + \frac{\beta^2}{24} (1 + \tilde{z})^4 \frac{\partial^4 \phi_0}{\partial \tilde{x}^4} + \mathcal{O}(\beta^3), \quad (12)$$

which is a series solution with only one unknown function  $\phi_0$ . We use the following procedure to find a Boussinesq system of two evolution equations. We first substitute the asymptotic expression for  $\tilde{\phi}$  in the boundary conditions Eq. (8) and Eq. (9), and then collect all terms of zeroth and first order in  $\alpha$  and  $\beta$ . We finally differentiate dynamic bottom boundary with respect to  $\tilde{x}$  and expressed the boundary conditions in terms of the non-dimensional horizontal velocity at the bottom  $\frac{\partial \phi_0}{\partial \tilde{x}} = \tilde{v}$ .

$$\begin{aligned} \tilde{\eta}_{\tilde{t}} + \tilde{v}_{\tilde{x}} + \alpha \tilde{\Gamma} \tilde{\eta} \tilde{\eta}_{\tilde{x}} + \alpha (\tilde{\eta} \tilde{v})_{\tilde{x}} - \frac{\beta}{6} \frac{\partial^3 \tilde{v}}{\partial \tilde{x}^3} &= \mathcal{O}(\alpha \beta, \beta^2), \\ \tilde{v}_{\tilde{t}} + \tilde{\eta}_{\tilde{x}} + \alpha \tilde{v} \tilde{v}_{\tilde{x}} - \tilde{\Gamma} \tilde{v}_{\tilde{x}} - \frac{\beta}{2} \frac{\partial^3 \tilde{v}}{\partial \tilde{x}^2 \partial \tilde{t}} + \frac{\beta}{6} \tilde{\Gamma} \frac{\partial^3 \tilde{v}}{\partial \tilde{x}^3} &= \mathcal{O}(\alpha \beta, \beta^2). \end{aligned} \quad (13)$$

The Korteweg-de Vries equation is derived from the system (13) by specializing to a wave moving to the right. To lowest order, neglecting the terms of order  $\alpha$  and  $\beta$ , such a solution of system (13) is

$$\tilde{\eta}_{\tilde{t}} + \tilde{v}_{\tilde{x}} = 0, \quad \tilde{v}_{\tilde{t}} + \tilde{\eta}_{\tilde{x}} - \tilde{\Gamma} \tilde{v}_{\tilde{x}} = 0. \quad (14)$$

The system can be diagonalized by introducing characteristic coordinates. Introduce new variables  $r$  and  $s$  defined by  $(r, s) = P^{-1}(\tilde{\eta}, \tilde{v})$  where

$$P^{-1} = \frac{1}{1 + \tilde{c}_+^2} \begin{pmatrix} 1 & \tilde{c}_+ \\ \tilde{c}_+ & -1 \end{pmatrix}. \quad (15)$$

With  $\tilde{c}_+ = \frac{-\tilde{\Gamma}}{2} + \sqrt{\frac{\tilde{\Gamma}^2}{4} + 1}$ , and  $\tilde{c}_- = \frac{-\tilde{\Gamma}}{2} - \sqrt{\frac{\tilde{\Gamma}^2}{4} + 1}$  as the conjugate of  $\tilde{c}_+$ , the solutions of system (14) are

$$\begin{aligned} \tilde{v}(x, t) &= \frac{1}{1 + \tilde{c}_+^2} [\tilde{c}_+ \tilde{\eta}_0(x - \tilde{c}_+ t) + \tilde{c}_+^2 \tilde{v}_0(x - \tilde{c}_+ t) - \tilde{c}_+ \tilde{\eta}_0(x - \tilde{c}_- t) + \tilde{v}_0(x - \tilde{c}_- t)], \\ \tilde{\eta}(x, t) &= \frac{1}{1 + \tilde{c}_+^2} [\tilde{\eta}_0(x - \tilde{c}_+ t) + \tilde{c}_+ \tilde{v}_0(x - \tilde{c}_+ t) + \tilde{c}_+^2 \tilde{\eta}_0(x - \tilde{c}_- t) - \tilde{c}_+ \tilde{v}_0(x - \tilde{c}_- t)] \end{aligned} \quad (16)$$

The unidirectional KdV equation is derived from the system (13) by specializing to a wave moving to the right with speed  $c_0$ . We look for a solution, corrected to first order in  $\alpha$  and  $\beta$ , in the form

$$\tilde{v} = \tilde{c}_+ \tilde{\eta} + \alpha A + \beta B + \mathcal{O}(\alpha \beta, \beta^2), \quad (17)$$

where  $A$  and  $B$  are functions of  $\tilde{\eta}$  and its  $\tilde{x}$  derivatives. Then the system (13) becomes

$$\begin{aligned}\tilde{c}_+\tilde{\eta}_{\tilde{t}} + \tilde{c}_+^2\tilde{\eta}_{\tilde{x}} + \alpha(\tilde{c}_+A_x + 2\tilde{c}_+^2\tilde{\eta}\tilde{\eta}_{\tilde{x}} + \tilde{\Gamma}\tilde{c}_+\tilde{\eta}\tilde{\eta}_{\tilde{x}}) + \beta(\tilde{c}_+B_{\tilde{x}} - \frac{1}{6}\tilde{c}_+^2\tilde{\eta}_{\tilde{x}\tilde{x}\tilde{x}}) &= \mathcal{O}(\alpha\beta, \beta^2), \\ \tilde{c}_+\tilde{\eta}_{\tilde{t}} + \tilde{c}_+^2\tilde{\eta}_{\tilde{x}} + \alpha(A_{\tilde{t}} + \tilde{c}_+^2\tilde{\eta}\tilde{\eta}_{\tilde{x}} - \tilde{\Gamma}A_{\tilde{x}}) + \beta(B_{\tilde{t}} - \frac{1}{2}\tilde{c}_+\tilde{\eta}_{\tilde{x}\tilde{x}\tilde{t}} + \frac{\tilde{\Gamma}}{6}\tilde{c}_+\tilde{\eta}_{\tilde{x}\tilde{x}\tilde{x}}) &= \mathcal{O}(\alpha\beta, \beta^2).\end{aligned}\quad (18)$$

Since  $\tilde{\eta}_{\tilde{t}} = -\tilde{c}_+\tilde{\eta}_{\tilde{x}}$ , all derivatives in the first order terms may be replaced by  $-\tilde{c}_+$  times the  $x$  derivatives. Then the two equations are consistent if

$$A = \frac{-1}{2(2\tilde{c}_+ + \tilde{\Gamma})}\tilde{\eta}^2, \quad B = \frac{1 + 3\tilde{c}_+^2}{6(2\tilde{c}_+ + \tilde{\Gamma})}\tilde{\eta}_{\tilde{x}\tilde{x}} \quad (19)$$

Hence we have

$$\tilde{v} = \tilde{c}_+\tilde{\eta} + \alpha \frac{-1}{2(2\tilde{c}_+ + \tilde{\Gamma})}\tilde{\eta}^2 + \beta \frac{1 + 3\tilde{c}_+^2}{6(2\tilde{c}_+ + \tilde{\Gamma})}\tilde{\eta}_{\tilde{x}\tilde{x}} + \mathcal{O}(\alpha\beta, \beta^2), \quad (20)$$

$$\tilde{\eta}_{\tilde{t}} + \tilde{c}_+\tilde{\eta}_{\tilde{x}} + \alpha \frac{\tilde{c}_+(3 + \tilde{\Gamma}^2)}{(1 + \tilde{c}_+^2)}\tilde{\eta}\tilde{\eta}_{\tilde{x}} + \beta \frac{\tilde{c}_+^3}{3(1 + \tilde{c}_+^2)}\tilde{\eta}_{\tilde{x}\tilde{x}\tilde{x}} = \mathcal{O}(\alpha\beta, \beta^2). \quad (21)$$

From Eq. (12), the non-dimensional horizontal velocity becomes

$$\tilde{u} = \tilde{v} - \frac{\beta}{2}(1 + \tilde{z})^2 \frac{\partial^2 \tilde{v}}{\partial \tilde{x}^2} + \mathcal{O}(\beta^2). \quad (22)$$

From Eq. (21) and Eq. (22), we have

$$\tilde{u} = \tilde{c}_+\tilde{\eta} + \alpha \frac{-1}{2(2\tilde{c}_+ + \tilde{\Gamma})}\tilde{\eta}^2 + \beta \frac{1 + 3\tilde{c}_+^2}{6(2\tilde{c}_+ + \tilde{\Gamma})}\tilde{\eta}_{\tilde{x}\tilde{x}} - \tilde{c}_+ \frac{\beta}{2}(1 + \tilde{z})^2 \tilde{\eta}_{\tilde{x}\tilde{x}} + \mathcal{O}(\alpha\beta, \beta^2). \quad (23)$$

After neglecting the second-order term, the dimensional form of the velocity is given by

$$u = \frac{\sqrt{gh_0}}{h_0} \left\{ \tilde{c}_+\eta + \frac{-1}{2(2\tilde{c}_+ + \tilde{\Gamma})} \frac{\eta^2}{h_0} + \frac{1 + 3\tilde{c}_+^2}{6(2\tilde{c}_+ + \tilde{\Gamma})} h_0^2 \eta_{xx} - \frac{\tilde{c}_+}{2} h_0^2 (1 + \frac{z}{h_0})^2 \eta_{xx} \right\}. \quad (24)$$

The new non-dimensional variables are defined by

$$x = h_0x, \quad z = h_0z, \quad \eta = h_0\eta, \quad t = \frac{h_0}{\sqrt{gh_0}}t, \quad u = \sqrt{gh_0}u \quad \text{and} \quad \Gamma = \frac{\Gamma\sqrt{gh_0}}{h_0}. \quad (25a)$$

Then Eq. (24) and Eq. (21) can be rewritten in terms of new variables as

$$u = c_+\eta + \frac{-1}{2(2c_+ + \Gamma)}\eta^2 + \frac{1 + 3c_+^2}{6(2c_+ + \Gamma)}\eta_{xx} - c_+ \frac{1}{2}(1 + z)^2 \eta_{xx}, \quad (26)$$

$$\eta_t + c_+\eta_x + \frac{c_+(3 + \Gamma^2)}{(1 + c_+^2)}\eta\eta_x + \frac{c_+^3}{3(1 + c_+^2)}\eta_{xxx} = 0. \quad (27)$$

Here  $c_+ = \frac{-\Gamma}{2} + \sqrt{\frac{\Gamma^2}{4} + 1}$ .

The expression for the horizontal velocity of a fluid particle in the presence of the shear flow is given in non-dimensional variables as

$$U(x, z, t) = c_+\eta + \frac{-1}{2(2c_+ + \Gamma)}\eta^2 + \frac{1 + 3c_+^2}{6(2c_+ + \Gamma)}\eta_{xx} - c_+ \frac{1}{2}(1 + z)^2 \eta_{xx} + z\Gamma. \quad (28)$$

Since the horizontal component of the particle velocity has been found approximately, it may be

compared to the local phase velocity of the wave. As we mentioned already, this leads to one of the most fundamental breaking criteria used in the literature, the kinematic breaking criterion. Sections 2 and 3 are dedicated to the application of this convective breaking criterion to the solitary and periodic travelling waves, respectively.

## 2 Maximum wave height for solitary waves

We now apply this convective breaking criterion to the solitary wave solution of the KdV equation (27). The solitary-wave solution of the KdV equation (27) is given by

$$\eta = H \operatorname{sech}^2 \left( \sqrt{\frac{(3 + \Gamma^2)H}{4(1 - c_+ \Gamma)}} (x - x_0 - ct) \right). \quad (29)$$

Letting the argument  $\mathcal{B}(x, t) = \sqrt{\frac{(3 + \Gamma^2)H}{4(1 - c_+ \Gamma)}} (x - x_0 - ct)$ ,  $\eta_{xx}$  is given by

$$\eta_{xx} = H^2 \frac{(3 + \Gamma^2)}{4(1 - c_+ \Gamma)} (-6 \operatorname{sech}^2(\mathcal{B}) + 4) \operatorname{sech}^2(\mathcal{B}), \quad (30)$$

where  $H$  is the wave amplitude,  $x_0$  is the initial location of the wave crest, and  $c = c_+ + \frac{(3 + \Gamma^2)H}{3(\Gamma + 2c_+)}$  is the phase velocity. Since the solitary wave retains its shape for all time, we may evaluate at  $(x - x_0 - ct) = 0$  in which case we obtain  $\eta = H$  and  $\eta_{xx} = \frac{-H^2}{2} \frac{(3 + \Gamma^2)}{(1 - c_+ \Gamma)}$ . Substituting these values into horizontal velocity of the fluid particle (28) and evaluating at the surface yields the breaking criterion

$$\begin{aligned} c_+ H + \frac{-H^2}{2(2c_+ + \Gamma)} + \frac{H^2}{2} \frac{(3 + \Gamma^2)}{(1 - c_+ \Gamma)} \left\{ -\frac{1 + 3c_+^2}{6(2c_+ + \Gamma)} + c_+ \frac{1}{2}(1 + H)^2 \right\} + z\Gamma \\ \geq c_+ + \frac{(3 + \Gamma^2)H}{3(\Gamma + 2c_+)}. \end{aligned} \quad (31)$$

To find the critical value of the wave height, set the left-hand side equal to the right-hand side and rearrange terms to obtain

$$\begin{aligned} \mathbb{P}(H) = \frac{H^4}{4} \frac{(3 + \Gamma^2)}{(1 - c_+ \Gamma)} c_+ + \frac{H^3}{2} \frac{(3 + \Gamma^2)}{(1 - c_+ \Gamma)} c_+ + H^2 \left( \frac{-1}{2(2c_+ + \Gamma)} \right. \\ \left. - \frac{3 + \Gamma^2}{12(1 - \Gamma c_+)} \frac{3c_+^2 + 1}{2c_+ + \Gamma} + \frac{3 + \Gamma^2}{1 - \Gamma c_+} \right) + H \left( c_+ - \frac{3 + \Gamma^2}{3(2c_+ + \Gamma)} + \Gamma \right) - c_+ = 0. \end{aligned} \quad (32)$$

The above equation  $\mathbb{P}(H)$  is a fourth order polynomial in  $H$ , and since the derivative of the polynomial  $\mathbb{P}(H)$  is positive for  $H \geq 0$  and  $\mathbb{P}(0) < 0$  while  $\mathbb{P}(1) > 0$ ,  $\mathbb{P}(H)$  can have only one positive root which lies in  $[0, 1]$ . For various values of the vorticity  $\Gamma$ , this root can be found numerically to obtain the following values of the maximum admissible waveheight for the solitary wave:

$\Gamma$	$H_{\max \text{ solitary}}$
-0.4	0.8229
-0.3	0.7911
-0.2	0.7578
-0.1	0.7233
-0.02	0.6950
-0.01	0.6914
0	0.6879
0.01	0.6843
0.02	0.6807
0.1	0.6519
0.2	0.6157
0.3	0.5798
0.4	0.5444

Table 1: Critical waveheight for the solitary solution of the KdV-equation, calculated for various values of the vorticity parameter  $\Gamma$ .

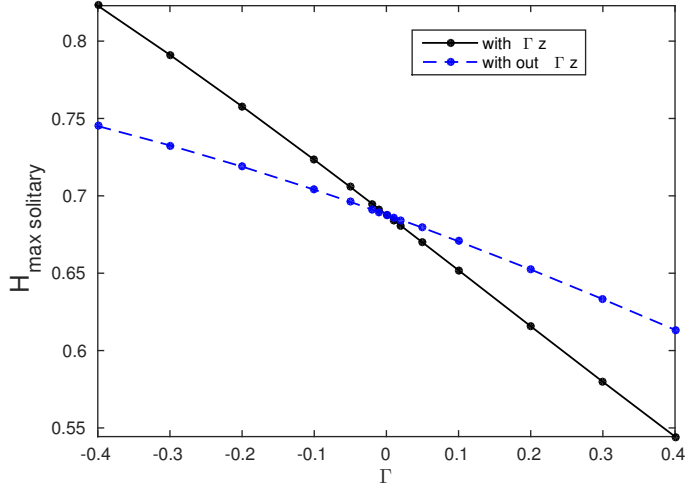


Figure 2: Plots of maximum admissible waveheight for the solitary solution as a function of  $\Gamma$  for two different case of breaking criterion (31). The dashed curve shows the maximum allowable wave height in which the breaking criterion (31) does not include the linear term  $\Gamma z$ . While the solid curve shows the maximum allowable wave height for solitary waves in which the breaking criterion (31) includes the linear term  $\Gamma z$ .

It can be clearly seen from Table 1 that the critical waveheights for the solitary waves are reasonably large for the considered vorticity constants  $\Gamma$ . The maximum admissible waveheight for the solitary wave solution is increasing for larger favorable direction of shear flow ( $\Gamma < 0$ ). It is noteworthy to mention that even though the KdV equation admits solutions with any waveheight, solitary waves with a waveheight larger than  $H_{\max \text{ solitary}}$  do not describe actual surface waves since these waves already feature incipient wave breaking. It can be noticed from the Figure 2 that the curve of  $H_{\max \text{ solitary}}$  is a nice straight line as a function of the vorticity parameter  $\Gamma$ .

### 3 Maximum wave height for cnoidal waves

The cnoidal wave solutions of the KdV equation (27) are given by

$$\eta = f_2 + (f_1 - f_2)cn^2(\mathcal{B}), \quad (33)$$

where the solution is defined by the three constants  $f_1$ ,  $f_2$  and  $f_3$  which are arranged in the order  $f_3 < f_2 < f_1$ ,  $\text{cn}$  is one of the Jacobian elliptic functions defined by the incomplete elliptic integral of the first kind [8], and the modulus of  $\text{cn}$  is given by  $m = (f_1 - f_2)/(f_1 - f_3)$ . The argument  $\mathcal{B} = \sqrt{\frac{(3+\Gamma^2)}{4(1-c_+\Gamma)}}(f_1 - f_3)^{1/2}(x - ct)$ . The phase speed of the wave is  $c = c_+ + \frac{(3+\Gamma^2)}{3(2c_++\Gamma)}(f_1 + f_2 + f_3)$ , and the wavelength is given by  $\lambda = 4\sqrt{\frac{(1-c_+\Gamma)}{(3+\Gamma^2)}}K(m)\frac{1}{\sqrt{f_1-f_3}}$ , where  $K(m)$  is the complete elliptic integral of the first kind.

As shown in [8], the parameters  $f_1$ ,  $f_2$  and  $f_3$  can be expressed in terms of wave height  $H = f_1 - f_2$  and the elliptic parameter  $m$  as follows:

$$\begin{aligned} f_1 &= \frac{H}{m} \left( 1 - \frac{E(m)}{k(m)} \right), \\ f_2 &= \frac{H}{m} \left( 1 - m - \frac{E(m)}{k(m)} \right), \\ f_3 &= \frac{H}{m} \left( -\frac{E(m)}{k(m)} \right). \end{aligned} \quad (34)$$

Therefore, fixing  $H$  and  $m$  is sufficient to specify any cnoidal wave as long as the undisturbed water level is set to zero. We now test the kinematic breaking criterion to determine whether a given cnoidal wave is a reasonable description of a water wave in the KdV approximation with presence of the shear flow. Differentiating (33) twice with respect  $x$  yields  $\eta_{xx}$

$$\eta_{xx} = (f_1 - f_2)(f_1 - f_3) \frac{(3 + \Gamma^2)}{2c_+^2} (sn^2(\mathcal{B})dn^2(\mathcal{B}) - cn^2(\mathcal{B})dn^2(\mathcal{B}) + msn^2(\mathcal{B})cn^2(\mathcal{B})). \quad (35)$$

Evaluating at  $(x - ct) = 0$  yields  $\eta = f_1$  and  $\eta_{xx} = -(f_1 - f_2)(f_1 - f_3) \frac{(3 + \Gamma^2)}{2c_+^2}$  and the breaking criterion can be written as

$$\begin{aligned} c_+f_1 - \frac{f_1^2}{2(2c_+ + \Gamma)} + (f_1 - f_2)(f_1 - f_3) \frac{(3 + \Gamma^2)}{(1 - c_+\Gamma)} \left\{ -\frac{1 + 3c_+^2}{6(2c_+ + \Gamma)} + c_+ \frac{1}{2}(1 + H)^2 \right\} + z\Gamma \\ \geq c_+ + \frac{(3 + \Gamma^2)(f_1 + f_2 + f_3)}{3(\Gamma + 2c_+)}. \end{aligned} \quad (36)$$

In the following, the constants are defined by

$$a = \frac{1}{m} \left( 1 - \frac{E(m)}{k(m)} \right), b = \frac{1}{m} \left( 1 - m - \frac{E(m)}{k(m)} \right) \text{ and } c = \frac{1}{m} \left( \frac{E(m)}{k(m)} \right). \quad (37)$$

Substituting these definitions into equation (36) and setting the left and right hand sides equal yield

$$\begin{aligned} \mathbb{Q}(H) = H^4(a^4 + a^3c - a^3b - a^2bc) \frac{(3 + \Gamma^2)}{(2c_+)} + H^3(a^3 + a^2c - a^2b - abc) \frac{(3 + \Gamma^2)}{2c_+} \\ + H^2 \left( \frac{-1}{2(2c_+ + \Gamma)} - \frac{3 + \Gamma^2}{12c_+^2} \frac{3c_+^2 + 1}{2c_+ + \Gamma} + \frac{3 + \Gamma^2}{1 - \Gamma c_+} \right) (a^2 + ac - ab - bc) \\ H \left( c_+a - \frac{3 + \Gamma^2}{3(2c_+ + \Gamma)} + \Gamma \right) - c_+ = 0. \end{aligned} \quad (38)$$

Here  $\mathbb{Q}(H)$  is a fourth-order polynomial in  $H$ , and by fixing a value of  $m$  and  $\Gamma$  it can be solved numerically to obtain the maximum admissible waveheight for the cnoidal wave,  $H_{\max \text{ cnoidal}}(m, \Gamma)$ . After all in the nonlinear limit ( $m \rightarrow 1$ ), the cnoidal wave reduces to the solitary wave, and

$(m \rightarrow 0^+)$  is the linear limit, we search real roots of (38) in the interval  $[0, 1]$ .

$m$	$H_{\max}$ cnoidal	wavelength ( $\lambda$ )	$\alpha$	$\beta$	S
0.01	0.0196	2.591	0.0098	0.1489	0.0661
0.1	0.1698	2.857	0.0849	0.1224	0.6933
0.2	0.2909	3.178	0.1454	0.0990	1.4689
0.3	0.3820	3.507	0.1910	0.0812	2.3499
0.4	0.4548	3.849	0.2274	0.0674	3.3702
0.5	0.5152	4.218	0.2575	0.0562	4.5834
0.6	0.5667	4.632	0.2833	0.0465	6.0813
0.7	0.6114	5.128	0.3056	0.0380	8.0399
0.8	0.6504	5.781	0.3252	0.0299	10.869
0.9	0.6841	6.829	0.3420	0.0214	15.952

Table 2: Critical waveheight for the cnoidal solution of the KdV-equation, calculated for various values of the elliptic parameter  $m$  and the vorticity  $\Gamma = 0$ .

$m$	$H_{\max}$ cnoidal	$\lambda$	$\alpha$	$\beta$	S
0.01	0.0207	2.4015	0.0103	0.1734	0.0596
0.1	0.1791	2.6424	0.0896	0.1432	0.6253
0.2	0.3070	2.9379	0.1535	0.1159	1.3248
0.3	0.4031	3.2426	0.2016	0.0951	2.1193
0.4	0.4796	3.5601	0.2398	0.0789	3.0395
0.5	0.5431	3.9018	0.2715	0.0657	4.1337
0.6	0.5971	4.2861	0.2986	0.0544	5.4845
0.7	0.6440	4.7454	0.3220	0.0444	7.2510
0.8	0.6849	5.3501	0.3425	0.0349	9.8027
0.9	0.7201	6.3210	0.3601	0.0250	14.3864

Table 3: Critical waveheight for the cnoidal solution of the KdV-equation, calculated for various values of the elliptic parameter  $m$  and the vorticity  $\Gamma = -0.1$ .

$m$	$H_{\max}$ cnoidal	$\lambda$	$\alpha$	$\beta$	S
0.01	0.0187	2.7926	0.0093	0.1282	0.0728
0.1	0.1604	3.0859	0.0802	0.1050	0.7637
0.2	0.2746	3.4329	0.1373	0.0849	1.6180
0.3	0.3609	3.7875	0.1804	0.0697	2.5883
0.4	0.4298	4.1563	0.2149	0.0579	3.7121
0.5	0.4870	4.5531	0.2435	0.0482	5.0485
0.6	0.5359	4.9996	0.2680	0.0400	6.6983
0.7	0.5784	5.5337	0.2892	0.0327	8.8557
0.8	0.6155	6.2370	0.3078	0.0257	11.972
0.9	0.6475	7.3667	0.3238	0.0184	17.5701

Table 4: Critical waveheight for the cnoidal solution of the KdV-equation, calculated for various values of the elliptic parameter  $m$  and the vorticity  $\Gamma = 0.1$ .

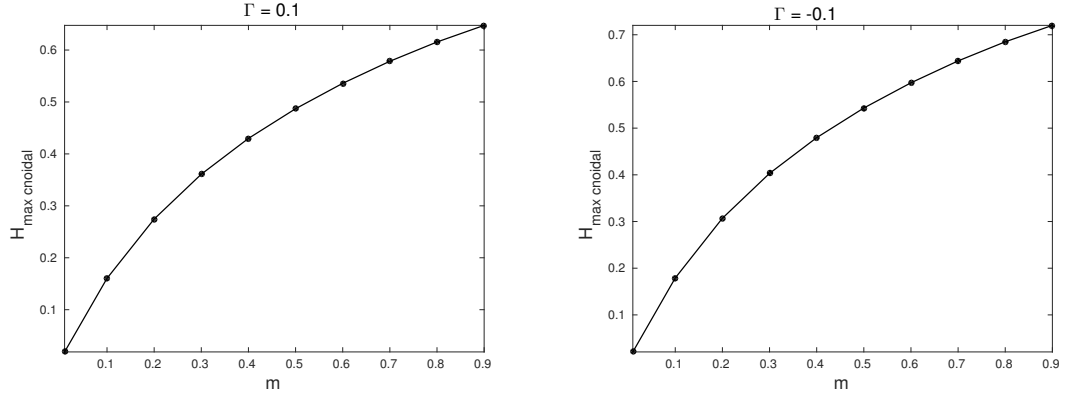


Figure 3: The left panel shows the maximum allowable wave height for the cnoidal solution as a function of  $m$  for  $\Gamma = 0.1$ . The right panel shows the maximum allowable wave height for the cnoidal solution as a function of  $m$  for  $\Gamma = -0.1$ .

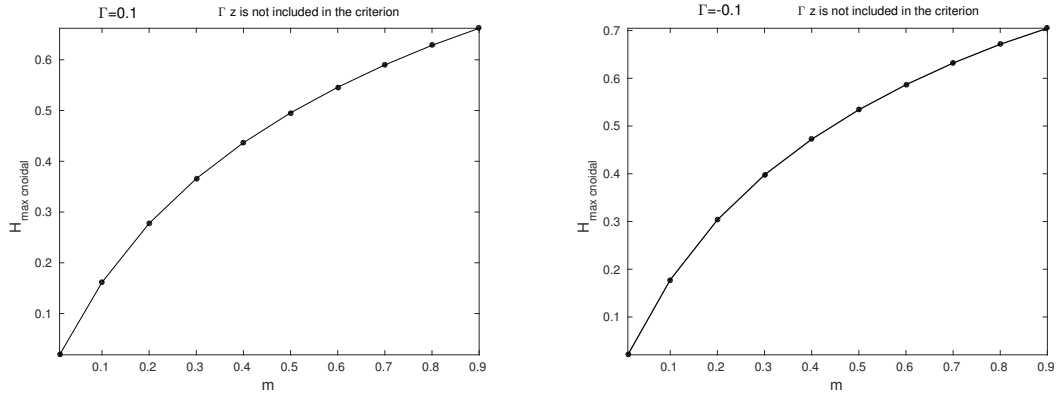


Figure 4: The left panel shows the maximum allowable wave height for the cnoidal solution as a function of  $m$  for  $\Gamma = 0.1$ . The right panel shows the maximum allowable wave height for the cnoidal solution as a function of  $m$  for  $\Gamma = -0.1$ . Here the breaking criterion (36) does not include the linear term  $\Gamma z$ .

Tables 2, 3 and 4 list the values of  $m$  and the corresponding  $H_{\max \text{ cnoidal}}$  for three different vorticity values  $\Gamma = 0, -0.1$  and  $0.1$ . This is in agreement with the results of [4] in the absence of shear flow. These tables also list the corresponding values of  $\lambda$ ,  $\alpha$ ,  $\beta$  and Stokes number  $S$ , defined by the ratio  $\alpha/\beta$ . Figure 3 shows a plot of maximum allowable waveheight of the cnoidal wave as a function of elliptic parameter  $m$  for different vorticity constants  $\Gamma = 0.1$  and  $-0.1$ . It can be seen that  $H_{\max \text{ cnoidal}}$  approaches zero as  $m$  approaches zero, since it is not in line with the Boussinesq approximation, where  $\alpha$  and  $\beta$  are assumed to be of the same order of magnitude. And the maximum allowable waveheight of the cnoidal wave as a function of wavelength ( $\lambda$ ) for different vorticity constants  $\Gamma = 0.1$  and  $-0.1$  are shown in Figure 5.

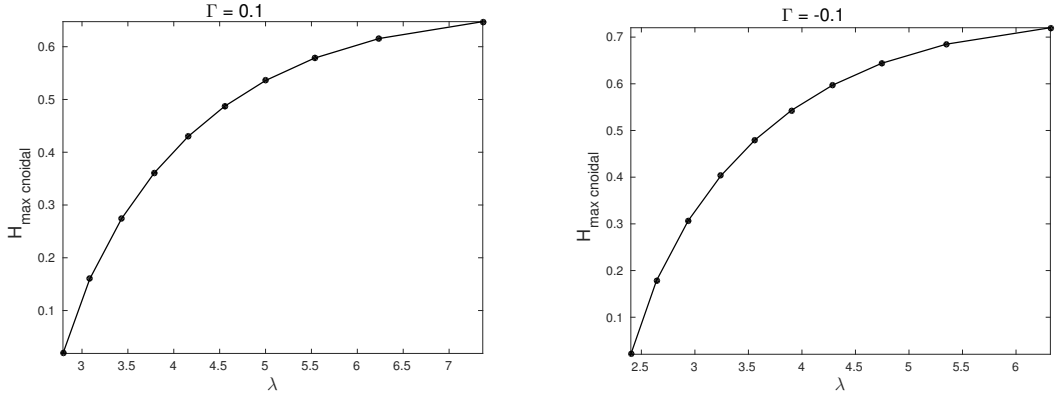


Figure 5: The left panel shows the maximum allowable wave height for the cnoidal solution as a function of wavelength  $\lambda$  for  $\Gamma = 0.1$ . The right panel shows the maximum allowable wave height for the cnoidal solution as a function of wavelength  $\lambda$  for  $\Gamma = -0.1$ .

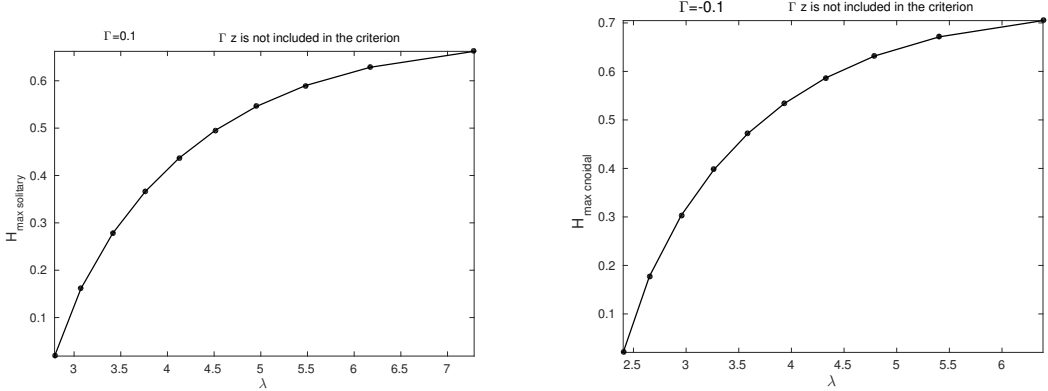


Figure 6: The left panel shows the maximum allowable wave height for the cnoidal solution as a function of wavelength  $\lambda$  for  $\Gamma = 0.1$ . The right panel shows the maximum allowable wave height for the cnoidal solution as a function of wavelength  $\lambda$  for  $\Gamma = -0.1$ . The breaking criterion (36) does not include the linear term  $\Gamma z$ .

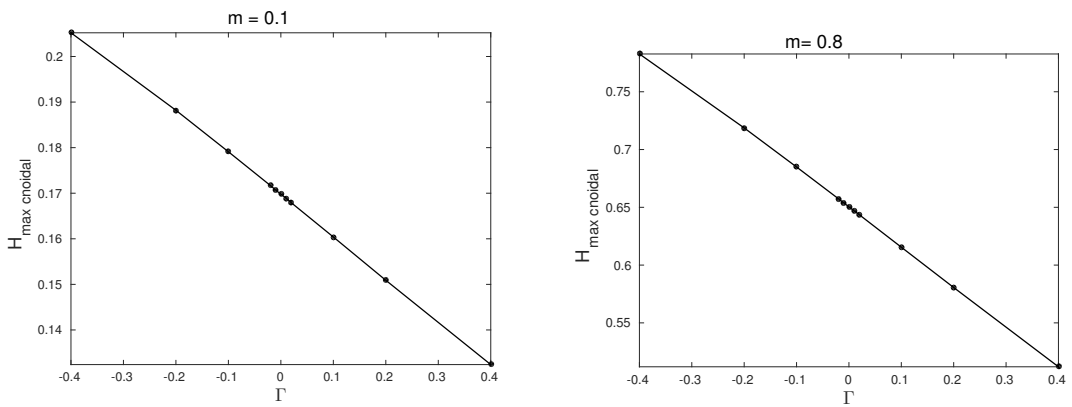


Figure 7: The left panel shows the maximum allowable wave height for the cnoidal solution as a function of  $\Gamma$  for  $m = 0.1$ . The right panel shows the maximum allowable wave height for the cnoidal solution as a function of  $\Gamma$  for  $m = 0.8$ .

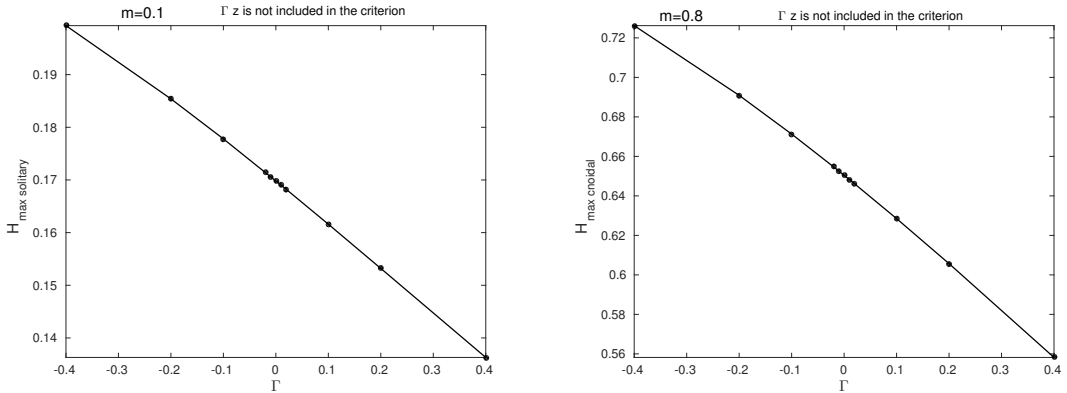


Figure 8: The left panel shows the maximum allowable wave height for the cnoidal solution as a function of  $\Gamma$  for  $m = 0.1$ . The right panel shows the maximum allowable wave height for the cnoidal solution as a function of  $\Gamma$  for  $m = 0.8$ . Note that the breaking criterion (36) does not include the linear term  $\Gamma z$ .

Figure 7 shows a plot of maximum allowable waveheight of the cnoidal wave as a function of  $\Gamma$  for different elliptic parameters  $m = 0.1$  and  $m = 0.8$ . It can be seen from Figure 7 that for favorable case of shear flow ( $\Gamma \leq 0$ ) the maximum allowable wave height for the cnoidal solution is increasing with larger values of vorticity. And they follow the same pattern for all elliptic parameters  $m$  lies between 0 and 1, and the variation is a straight line.

## 4 Conclusion

In this article, it has been found that the derivation of the KdV equation in the presence of the shear flow as a model for surface water waves admits the definition of a local particle velocity field and also possible to reconstruct the horizontal particle velocity. The solutions evaluated here contain the solitary waves and the cnoidal waves. Concerning the solitary wave solutions, the computations have been performed for different values of vorticity constant, and the critical waveheight for solitary waves are tabulated in Table 1. It is seen from Figure 2 that the critical waveheights are quite large, and it is not surprise that the waves do not represent reasonable approximations to real surface waves. For all vorticity constants in the range ( $-\infty < \Gamma < 0.6$ ) and waves near stokes number 1, it can be seen that the maximum allowable waveheight for cnoidal waves according to the breaking criterion is in the range 0.1 to 0.3. While for larger positive values of ( $\Gamma \geq 0$ ) and stokes number greater than 1, the critical waveheight tends to 0. On the other hand, for the linear case ( $m \rightarrow 0$ ), the cnoidal waves have negligible waveheight, and the critical waveheight in this case is indeed 0 for all vorticity constants.

## References

- [1] Ali, A. and Kalisch, H. Reconstruction of the pressure in long-wave models with constant vorticity. *Eur. J. Mech. B Fluids*, 2013, **37**, 187–194.
- [2] Benjamin, T. B. The solitary wave on a stream with an arbitrary distribution of vorticity, *J. Fluid Mech.*, 1962, **12** (1), 97–116.
- [3] Bjørkavåg, M. and Kalisch, H. Wave breaking in Boussinesq models for undular bores, *Phys. Lett. A*, 2011, **375** (14), 1570–1578.
- [4] Brun, M. K. and Kalisch, H. Convective wave breaking in the KdV equation, *arkiv: 1603.09104v1. physics.flu-dyn*, 2016.

- [5] Choi, W. Strongly nonlinear long gravity waves in uniform shear flows, *Physical review E*, 2003, **68**.
- [6] Curtis, C. W., Oliveras, K. L. and Morrison, T. Shallow waves in density stratified shear currents, *European Journal of Mechanics-B/Fluids*, 2016, **61 (1)**, 100-111.
- [7] Freeman, N. C. and Johnson, R.S. Shallow water waves on shear flow, *J. Fluid Mech.*, 1970, **42 (2)**, 401–409.
- [8] Lawden, D. F. Elliptic functions and applications, *Springer, New York*, 1989.
- [9] Nepf, H. M., Wu, C. H. and Chan, E. S. A comparison of two- and three-dimensional wave breaking, *J. Phys. Oceanogr.*, 1998, **28 (7)**, 1496-1510
- [10] Thomas, R., Kharif, C. and Manna, M. A nonlinear Schroedinger equation for water waves on finite depth with constant vorticity *Phys. Fluids*, 2012, **24 (12)**, doi: 10.1063/1.4768530.
- [11] Vasan, V. and Oliveras, K. Pressure beneath a traveling wave with constant vorticity *Discrete Contin. Dyn. Syst.*, (2014) **34**, 3219–3239.
- [12] Wahlén, E. Hamiltonian long-wave approximations of water waves with constant vorticity, *Physics Letters A*, 2008, **372(15)**, 2597–2602.
- [13] Wu, C. H. and Nepf, H. M. Breaking criteria and energy losses for three-dimensional wave breaking, *J. Geophys. Res.*, 2002, **107**, 3177–3195.
- [14] Yaosong, C., Guocan, L. and Tao, J. Non-linear water waves on shearing flows, *Acta mechanics sinica*, 1994, **10 (2)**, 97–102.